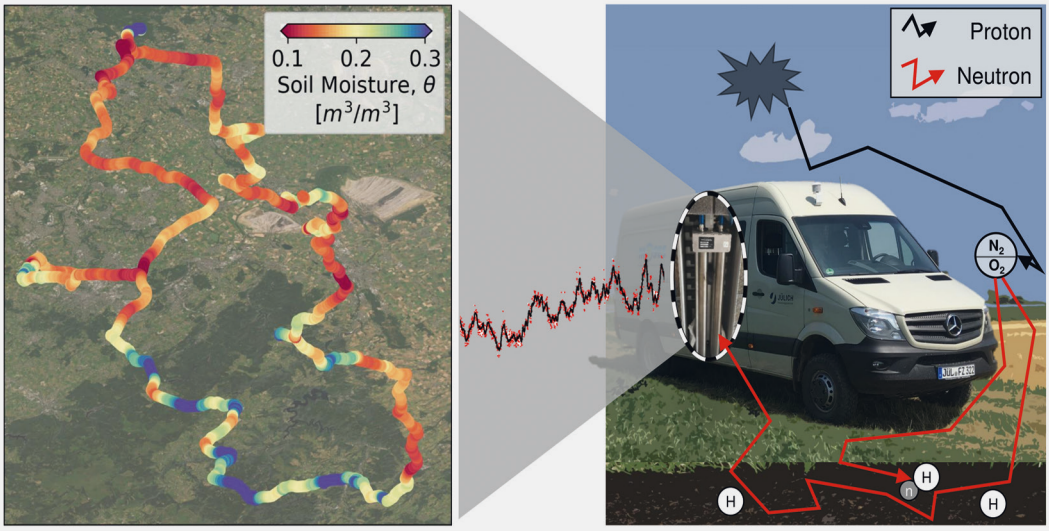

Improving stationary and mobile cosmic ray neutron soil moisture measurements

Assessment of the cosmic ray neutron uncertainty and the potential of the thermal neutron signal

Jannis Christoph Jakobi

Energie & Umwelt / Energy & Environment
Band / Volume 578
ISBN 978-3-95806-628-1

Mitglied der Helmholtz-Gemeinschaft

JÜLICH
Forschungszentrum

Schriften des Forschungszentrums Jülich
Reihe Energie & Umwelt / Energy & Environment Band / Volume 578

Forschungszentrum Jülich GmbH
Institut für Bio- und Geowissenschaften
Agrosphäre (IBG-3)

Improving stationary and mobile cosmic ray neutron soil moisture measurements

Assessment of the cosmic ray neutron uncertainty and the potential of the thermal neutron signal

Jannis Christoph Jakobi

Schriften des Forschungszentrums Jülich
Reihe Energie & Umwelt / Energy & Environment Band / Volume 578

ISSN 1866-1793 ISBN 978-3-95806-628-1

Bibliografische Information der Deutschen Nationalbibliothek.
Die Deutsche Nationalbibliothek verzeichnet diese Publikation in der
Deutschen Nationalbibliografie; detaillierte Bibliografische Daten
sind im Internet über http://dnb.d-nb.de abrufbar.

Herausgeber und Vertrieb:	Forschungszentrum Jülich GmbH Zentralbibliothek, Verlag 52425 Jülich Tel.: +49 2461 61-5368 Fax: +49 2461 61-6103 zb-publikation@fz-juelich.de www.fz-juelich.de/zb
Umschlaggestaltung:	Grafische Medien, Forschungszentrum Jülich GmbH
Druck:	Grafische Medien, Forschungszentrum Jülich GmbH
Copyright:	Forschungszentrum Jülich 2022

Schriften des Forschungszentrums Jülich
Reihe Energie & Umwelt / Energy & Environment, Band / Volume 578

D 5 (Diss. Bonn, Univ., 2022)

ISSN 1866-1793
ISBN 978-3-95806-628-1

Vollständig frei verfügbar über das Publikationsportal des Forschungszentrums Jülich (JuSER)
unter www.fz-juelich.de/zb/openaccess.

Abstract

Soil moisture has a major influence on the partitioning between infiltration and runoff, and thus affects groundwater recharge, floodings, and the susceptibility of hillslopes to landslides. In addition, soil moisture can influence weather and climate, and the availability of water for plant growth directly affects agricultural productivity and food supply. Soil moisture varies in time and space and on multiple scales, which leads to nonlinear environmental interactions and scaling problems. Thus, timely information on multiple scales is required to accurately characterize soil moisture dependent processes.

Depending on the measurement technique, soil moisture content is representative of the point scale (e.g., in situ sensors) to the global scale (i.e., satellite observations). Satellite borne soil moisture content estimates have tremendous advantages in terms of spatial coverage, but they are less accurate compared to in-situ measurements. Furthermore, they only represent soil moisture content at shallow soil depths (~5 cm) and they have either low spatial resolution (> ~25 km) or low temporal resolution (> ~daily). Thus, intermediate scale soil moisture content measurements are of interest, which can also serve as reference for improving the accuracy and extent of satellite borne datasets via calibration and validation. Among other techniques for measuring soil moisture content, cosmic ray neutron (CRN) sensing is considered promising for this purpose.

Cosmic ray neutron sensors (CRNS) measure the epithermal neutron intensity (~0.5 eV – 100 keV) in 1 – 2 m above the ground, which inversely depends on the amount of hydrogen in 130 to 240 m radius and soil depths of 15 to 83 cm. In terrestrial environments and in the absence of snow, most hydrogen is usually stored as soil water. Therefore, soil moisture content can be measured with CRNS, which is possible stationary and in mobile mode (e.g., CRNS mounted on cars - “CRN rover”).

However, soil moisture content measurements with CRNS are susceptible to a variety of errors. Amongst these, is the statistical measurement uncertainty, which depends on the number of neutrons counted, and therefore increases with increasing soil moisture content. For stationary soil moisture content measurements with CRNS this is usually considered by aggregation for time intervals ≥ 12 hours. However, in case of mobile observations, such long aggregation times are impractical since a trade-off must be made between aggregation time and the associated spatial resolution and accuracy of a soil moisture product. To analyze these influencing variables and better plan CRN rover campaigns, a new approach

was introduced in this thesis for the propagation of the uncertainty from raw epithermal neutron counts in soil moisture content measurements with CRNS, based on a 3rd order Taylor expansion approach. The new approach was validated using theoretic examples and experimental measurements. In addition, the combined uncertainty from raw epithermal neutron counts and soil bulk density was investigated, and CRN rover measurements were used in two examples to illustrate the added value of an explicit consideration of the uncertainty from raw epithermal neutron counts.

Another key error is the influence of additional hydrogen in the environment, e.g., biomass. Earlier studies have shown that biomass can be measured by additionally considering thermal neutron intensity (≤ 0.5 eV) in the ratio of thermal-to-epithermal neutrons (N_r). However, basic features of thermal neutrons such as the area of influence (i.e., the footprint) or the sensitivity to soil moisture content were unknown, which hampered the interpretation of these results. For this thesis, the footprint of thermal neutrons was investigated experimentally with a river crossing experiment and with neutron transport simulations. It was found that thermal neutrons have a horizontal footprint between 43 and 48 m and that the vertical footprint ranges between 10 and 65 cm soil depth, both dependent on soil moisture content. In addition, analytical expressions were fitted to the distant- and depth-dependent thermal neutron intensities and an existing approach for considering the influence of pressure was recommended. Moreover, selected examples of the influences of soil chemistry and detector height above ground on the footprint of thermal neutrons were investigated.

Finally, the influence of time-varying biomass on soil moisture content measurements with CRNS was investigated based on three experiments with different crops. Four approaches for the consideration of the biomass influence on the accuracy of soil moisture content measurement with CRNS were adopted and compared. The best results were obtained when site-specific functions based on in-situ measured biomass were used for correction. Consideration of thermal neutron intensity for correction was similarly accurate. Correction with N_r also improved the soil moisture content measurement accuracy, but to a lesser extent. The use of a generic approach for correction did not generally improve the soil moisture content measurement accuracy with CRNS. Further, the possibility of biomass measurements with N_r was investigated, but this proved successful for only one of the crops. On the contrary, thermal neutron intensity allowed for the measurement of biomass for all three crops.

Overall, it was concluded that for accurate stationary and mobile measurements of soil moisture content with CRNS, errors introduced by uncertain neutron counts and by hydrogen stored in biomass must be considered. In addition, it was shown that the local and plant specific calibration of the thermal neutron intensity allows for the measurement of biomass.

Zusammenfassung

Bodenfeuchte hat einen großen Einfluss auf die Aufteilung zwischen Infiltration und Abfluss und wirkt sich dadurch auf die Grundwasserneubildung, Überschwemmungen und die Anfälligkeit von Hängen für Erdrutsche aus. Darüber hinaus kann die Bodenfeuchte das Wetter und das Klima beeinflussen, und die Verfügbarkeit von Wasser für das Pflanzenwachstum wirkt sich direkt auf die landwirtschaftliche Produktivität und die Nahrungsmittelversorgung aus. Die Bodenfeuchte variiert in Zeit und Raum, was zu nichtlinearen Umweltinteraktionen und Skalierungsproblemen führt. Für die Charakterisierung von Prozessen, die von der Bodenfeuchte abhängen, sind daher zeitnahe Informationen auf verschiedenen Skalen erforderlich.

Je nach Messverfahren ist der Bodenfeuchtegehalt repräsentativ für die Punktskala (z.B. In-situ Sensoren) bis hin zur globalen Skala (d.h. Satellitenbeobachtungen). Satellitengestützte Messungen des Bodenfeuchtegehalts haben enorme Vorteile in Bezug auf die räumliche Abdeckung, sind aber im Vergleich zu In-situ-Messungen weniger genau. Außerdem repräsentieren sie den Bodenfeuchtegehalt nur in geringen Bodentiefen (~5 cm) und haben entweder eine geringe räumliche (> ~25 km) oder zeitliche Auflösung (> ~ täglich). Daher sind Messungen des Bodenfeuchtegehalts auf mittlerer Skala von Interesse, die auch als Referenz für die Verbesserung der Genauigkeit und des Umfangs satellitengestützter Datensätze durch Kalibrierung und Validierung dienen können. Neben anderen Techniken zur Messung des Bodenfeuchtegehalts gilt die Messung mittels kosmischer Neutronen (CRN) als vielversprechend für diesen Zweck.

Sensoren zur Messung von kosmischen Neutronen (CRNS) messen die epithermische Neutronenintensität (~0,5 eV - 100 keV) in 1 - 2 m über dem Boden, die umgekehrt von der Wasserstoffmenge in einem Radius von 130 bis 240 m und einer Bodentiefe von 15 bis 83 cm abhängt. In terrestrischen Umgebungen und ohne Schnee ist der meiste Wasserstoff normalerweise als Bodenwasser gespeichert. Daher kann der Bodenfeuchtegehalt mit CRNS gemessen werden, was sowohl stationär als auch mobil (z.B. mit auf Autos montierten CRNS - „CRN Rover“) möglich ist.

Die Messung des Bodenfeuchtegehalts mit CRNS ist jedoch anfällig für eine Reihe von Fehlern. Dazu gehört die statistische Messunsicherheit, die von der Anzahl der gezählten Neutronen abhängt und daher mit steigendem Bodenfeuchtegehalt zunimmt. Bei stationären Bodenfeuchtgehaltsmessungen mit CRNS wird dies üblicherweise durch

Aggregation für Zeitintervalle ≥ 12 Stunden berücksichtigt. Für mobile Beobachtungen sind solch lange Aggregationszeiten jedoch nicht praktikabel, da ein Kompromiss zwischen der Aggregationszeit und der damit verbundenen räumlichen Auflösung und der Genauigkeit eines Bodenfeuchteprodukts gefunden werden muss. Zur Analyse dieser Einflussgrößen und zur besseren Planung von CRN Rover Kampagnen, wurde in dieser Arbeit ein neuer Ansatz für die Fortpflanzung der Messunsicherheit von epithermischen Neutronen auf die Bodenfeuchtgehaltsmessung mit CRNS eingeführt, der auf einer Taylorentwicklung 3. Ordnung basiert. Der neue Ansatz wurde anhand von theoretischen Beispielen und experimentellen Messungen validiert. Darüber hinaus wurde die kombinierte Messunsicherheit von epithermischen Neutronen und der Lagerungsdichte des Bodens untersucht, und CRN Rover Messungen wurden in zwei Beispielen verwendet, die den zusätzlichen Nutzen einer expliziten Berücksichtigung der Messunsicherheit von epithermischen Neutronen verdeutlichen.

Ein weiterer wichtiger Fehler ist der Einfluss von zusätzlichem Wasserstoff in der Umgebung, z.B. Biomasse. Frühere Studien haben gezeigt, dass Biomasse gemessen werden kann, indem zusätzlich die Intensität thermischer Neutronen (≤ 0,5 eV) im Verhältnis von thermischen zu epithermischen Neutronen (N_r) berücksichtigt wird. Grundlegende Eigenschaften der thermischen Neutronen, wie z.B. der Einflussbereich (d.h. der Footprint) oder die Abhängigkeit von der Bodenfeuchte, waren jedoch unbekannt, was die Interpretation dieser Ergebnisse erschwerte. In dieser Arbeit wurde der Footprint thermischer Neutronen mit einem Flussdurchquerungsexperiment und mit Neutronentransportsimulationen untersucht. Es wurde festgestellt, dass der horizontale Footprint thermischer Neutronen zwischen 43 und 48 m und der vertikale Footprint zwischen 10 und 65 cm Bodentiefe liegt, beides in Abhängigkeit vom Bodenfeuchtegehalt. Darüber hinaus wurde die von der Entfernung und Bodentiefe abhängige Intensität der thermischen Neutronen analytisch beschrieben und ein bestehender Ansatz zur Berücksichtigung des Druckeinflusses empfohlen. Weiterhin wurden ausgewählte Beispiele für den Einfluss der Bodenchemie und der Detektorhöhe über dem Boden auf den Footprint thermischer Neutronen untersucht.

Zuletzt wurde der Einfluss von zeitlich variierender Biomasse auf die Bodenfeuchtegehaltsmessung mit CRNS anhand von drei Experimenten mit verschiedenen Kulturpflanzen untersucht. Es wurden vier Ansätze für die Berücksichtigung des Einflusses der Biomasse auf die Genauigkeit der Bodenfeuchtegehaltsmessung mit CRNS angewandt

und verglichen. Die besten Ergebnisse wurden erzielt, wenn standortspezifische Funktionen auf Grundlage der lokal gemessenen Biomasse für die Korrektur verwendet wurden. Die Berücksichtigung der Intensität thermischer Neutronen für die Korrektur war ähnlich genau. Auch die Korrektur mit N_r verbesserte die Genauigkeit der Bodenfeuchtemessung, allerdings in geringerem Maße. Ein generischer Korrekturansatz führte nicht generell zu besseren Bodenfeuchtegehaltsmessungen mit CRNS. Darüber hinaus wurde die Möglichkeit von Biomassemessungen mit N_r untersucht, was jedoch nur bei einer der Kulturpflanzen möglich war. Mit der thermischen Neutronenintensität hingegen konnte die Biomasse aller drei Kulturpflanzen gemessen werden.

Zusammenfassend kann geschlussfolgert werden, dass für genaue stationäre und mobile Messungen des Bodenfeuchtegehalts mit CRNS Fehler aufgrund unsicherer Neutronenzählraten und des in Biomasse gespeicherten Wasserstoff berücksichtigt werden müssen. Darüber hinaus konnte gezeigt werden, dass die lokal und pflanzenspezifisch kalibrierte Intensität thermischer Neutronen die Messung von Biomasse ermöglicht.

Contents

List of Figures

List of Tables

List of Abbreviations

a.s.l.	Above Sea Level
CRN	Cosmic Ray Neutron
CRNS	Cosmic Ray Neutron Sensor
DFG	Deutsche Forschungsgemeinschaft
GNSS	Global Navigation Satellite System
GPS	Global Positioning System
HDPE	High Density Polyethylene
JUNG	neutron monitor at Jungfraujoch
LiDAR	Light Detection And Ranging
MOSES	Modular Observation Solutions for Earth Systems
NDVI	Normalized Difference Vegetation Index
NMDB	Neutron Monitor DataBase
NMR	Nuclear Magnetic Resonance
RMSE	Root Mean Square Error
SMAP	Soil Moisture Active Passive
TDR	Time Domain reflectometry
TDT	Time Domain Transmission
TERENO	TERrestrial ENvironmental Observatories
URANOS	Ultra Rapid Adaptable Neutron-Only Simulations (KÖHLI ET AL., 2015)

List of Symbols

Symbol	Name / Explanation	Dimension
A	total number of measurements	-
a_1	parameter to obain BWE from LAI (Equation (4.2))	mm
a_2	slope to obtain BWE_a from N_r (Equation (4.7))	-
a_3	slope to obtain BWE_{tot} from T (Equation (4.8))	-
$a_4 - a_7$	empirical factors, that represent the change in N_0 per mm BWE_a, mm BWE_{tot}, N_r or T (Equations (4.10) - (4.13))	cts/time
BM_d	dry biomass weight per m row	kg
BM_f	fresh biomass weight per m row	kg
$BWE_{(a, b, tot)}$	water equivalent contained in biomass (aboveground, belowground, total)	mm
BWE_{LAI}	aboveground ($BWE_{a,LAI}$), belowground ($BWE_{b,LAI}$) or total ($BWE_{tot,LAI}$) water equivalent contained in biomass obtained from LAI	mm
c	number of aggregated measurements	-
d	soil depth	cm
D_{86}	vertical footprint; i.e., 86 % of the depth of all scattering interactions in soil before detection	cm
E	epithermal neutron intensity corrected for additional influences (see Appendix I)	cts/time
E_{out}	synthetically generated draw from poissoin distribution; represent uncorrected epithermal neutron counts	cts/time
$E_{poisson}$	E_{out} corrected with f_i, f_p and f_h	cts/time
E_{raw}	uncorrected epithermal neutron intensity	cts/time
E_s	epithermal neutron intensity adjusted for data gaps	cts/time
f	temporally variable correction factor	-
$F_1 - F_{12}$	parametric functions derived in Chapter 3, to analytically describe W_r and W_d	-
f_{BWEa}	correction factor to account for the influence of aboveground biomass	-
$f_{BWEa,Baatz}$	correction factor to account for the influence of aboveground biomass according to BAATZ ET AL. (2015)	-
f_{BWEtot}	correction factor to account for the influence of total biomass	-
$f_{BWEtot,Baatz}$	correction factor to account for the influence of total biomass; modified from BAATZ ET AL. (2015)	-

Symbol	Name / Explanation	Dimension
f_{ew}	water equivalent contained in cellulose	weight %
f_h	correction factor for the influence of air humidity	-
f_i	correction factor for the influence of the incoming cosmic ray neutron intensity	-
f_{Nr}	correction factor to account for the influence of N_r	-
f_p	correction factor for the influence of pressure	-
f_T	correction factor to account for the influence of thermal neutron intensity	-
h	air humidity	g/m^3
h_0	reference air humidity	g/m^3
I	neutron monitor count rate	cts/time
I_{ref}	reference neutron monitor count rate	cts/time
L	local mass attenuation length	g/cm^3
LAI	Leaf Area Index	m/m
N	neutron intensity, irrespective of kinetic energy and corrected for additional influences (see Appendix I)	cts/time
N_0	calibration parameter for the conversion of epithermal neutrons to soil moisture content (DESILETS ET AL., 2010)	cts/time
$N_{0,\,BWEa}$	N_0 when BWE_a equals 0	cts/time
$N_{0,\,BWEtot}$	N_0 when BWE_{tot} equals 0	cts/time
$N_{0,\,Nr}$	N_0 when Nr equals 0	cts/time
$N_{0,\,T}$	N_0 when T equals 0	cts/time
N_c	uncorrected neutron intensity, irrespective of kinetic energy, filtered for outliers with N_{c24m} relative to $\sqrt{N_{c24s}}$	cts/time
N_{c1}	uncorrected neutron intensity, irrespective of kinetic energy, filtered for extreme outliers	cts/time
N_{c24m}	24 hours moving average of N_{c1}	cts/time
N_{c24s}	24 hours moving sum of N_{c1}	cts/time
N_r	thermal-to-epithermal neutron ratio	-
N_{raw}	uncorrected neutron intensity; irrespective of kinetic energy	cts/time
P	air pressure	mbar
P_0	reference air pressure	mbar
$p_0 - p_2$	fitting parameters determined by DESILETS ET AL. (2010) (= 0.0808, 0.372, 0.115)	-
p_3, p_4	fitting parameters determined in Chapter 3, to analytically describe W_r and W_d	-

Symbol	Name / Explanation	Dimension
p_d	distance between planting rows	m
r	radial distance from the detector	m
r^*	radial distance from the detector; rescaled for pressure influence	m
R_{86}	horizontal footprint; i.e., lateral distance that 86 % of the neutrons travelled from their first soil contact until detection	m
s	product of the correction factors for pressure (f_p), humidity (f_h) and incoming cosmic radiation (f_i)	-
s_f	scaling factor for a detector relative to the cumulative average countrate – relevant when multiple detectors are used for the measurement of CRN	-
T	thermal neutron intensity corrected for additional influences (see Appendix I)	cts/time
T_{raw}	uncorrected thermal neutron intensity	cts/time
T_s	thermal neutron intensity adjusted for data gaps	cts/time
W_d	vertical weighting function	contribution %
W_r	radial weighting function	kcts/r
x	value of a measurement	-
x_2	reference value of a measurement	-
Z_1	gravel content	weight %
Z_2	volume of rock fragments estimated according BRAKENSIEK AND RAWLS (1994)	cm^3
θ	soil moisture content, usually volumetric	m^3/m^3
θ_g	gravimetric soil moisture content	g/g
θ_{off}	hydrogen stored in lattice water and soil organic matter	g/g
θ_v	volumetric soil moisture content	m^3/m^3
ϱ_{bd}	soil bulk density	g/cm^3
$\varrho_{bd<2}$	bulk density of soil < 2 mm	g/cm^3
$\varrho_{bd>2}$	bulk density of rock fragments according BRAKENSIEK AND RAWLS (1994) (= 2.65 g/cm^3)	g/cm^3
ϱ_w	density of liquid water (=1 g/cm^3)	g/cm^3
σ	standard deviation	-

1 Motivation and general introduction

1.1 The relevance of soil moisture content

Water stored in soils only amounts to ~0.05 % (SHIKLOMANOV, 1993) to 0.15 % (DINGMAN, 1994) of the total fresh water on Earth. Nonetheless, soil moisture plays a vital role in controlling the energy fluxes in the continuum of soil, vegetation, and atmosphere. For instance, 58 % of the net radiation that reaches the land surface is consumed by evapotranspiration processes which drive the soil moisture uptake towards the atmosphere (OHMURA AND RASCHKE, 2005). Consequently, soil moisture affects atmospheric processes, including precipitation patterns, air temperature, and evapotranspiration, and has an influence on weather and climate (ENTEKHABI ET AL., 1996; KOSTER ET AL., 2004; SENEVIRATNE ET AL., 2010). The soil moisture status is of importance in the generation of runoff processes (DUNNE ET AL., 1975) from the hillslope to the catchment scale (e.g., ZEHE AND BLÖSCHL, 2004). It controls infiltration and groundwater recharge (GRAY AND NORUM, 1967) with pre-storm soil moisture content being key in the prediction of runoff and flood events (WANDERS ET AL., 2014). Similarly, soil moisture content strongly influences the susceptibility of slopes to landslides (e.g., RAY ET AL., 2010). Plant growth is thightly linked to soil moisture content, as this water is not only needed for evapotranspiration, but also controls the mobilization and availability of nutrients (RODRIGUEZ-ITURBE, 2000). Thus, especially in (semi-)arid regions, soil moisture content is considered a driving force of ecological responses (SCHWINNING AND SALA, 2004) and agricultural productivity, with irrigation being often essential to sustain food production (SIEBERT ET AL., 2005). This also underlines the necessity for accurate soil moisture content information in monitoring agricultural droughts (e.g., MARTÍNEZ-FERNÁNDEZ ET AL., 2016; ZINK ET AL., 2016).

1.2 The measurement of soil moisture content

1.2.1 Scales of soil moisture content measurements

The characteristic temporal and spatial scales of soil moisture are highly variable and range from minutes to years and from centimeters to kilometers (ROBINSON ET AL., 2008; VEREECKEN ET AL., 2008; VEREECKEN ET AL., 2014), which leads to nonlinear environmental interactions (WESTERN ET AL., 2002). Consequently, information on soil moisture content is required on multiple scales. The scale of soil moisture content data can be described by its support (i.e., the integration volume or time of a single measurement),

spacing (i.e., the spatial or temporal resolution of measurements) and extent (i.e., the area or time over which measurements are available) (BLÖSCHL AND SIVAPALAN, 1995). To compare soil moisture content products obtained with different measurement techniques a change of scale is typically required (e.g., for calibration and validation). For this, multiple measurements of the same type can be combined, which does not necessarily produce an equal increase in support, spacing, and extent (VEREECKEN ET AL., 2014). For example, the spatial extent of a soil moisture product can be increased by performing additional measurements outside the previously sampled area. For a comprehensible two-dimensional representation of the scales of soil moisture content measurement techniques, simplifications are necessary, and the support, spacing, and extent are mixed. Figure 1.1 presents a non-exhaustive overview of popular soil moisture content measurement techniques (or groups of measurement techniques). These are briefly described below, focusing on the spatial and temporal capabilities of each measurement technique.

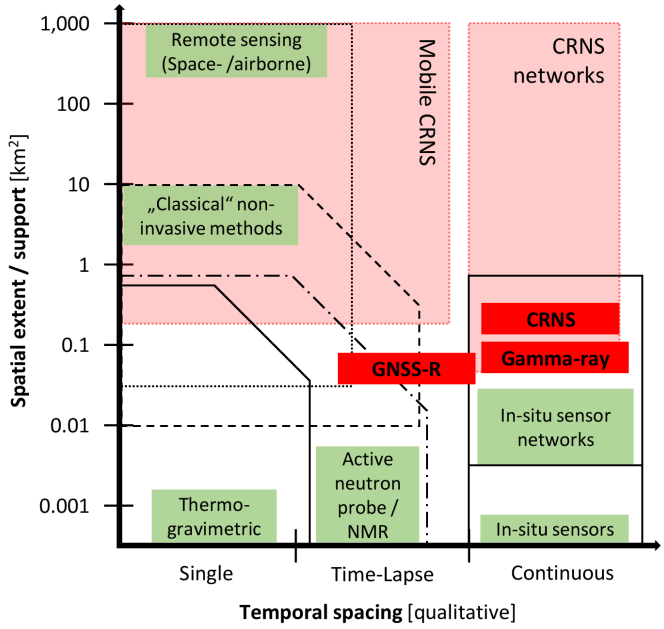

Figure 1.1: Scales of various soil moisture content measurement techniques. Modified and extended after ROBINSON ET AL. (2008) and BOGENA ET AL. (2015).

1.2.2 **Point scale soil moisture content measurements**

The reference standard for soil moisture content measurements is the point-specific thermogravimetric method, i.e., the weight loss from drying a soil sample to constant weight at 105 °C (e.g., ROBINSON ET AL., 2008; MARSHALL ET AL., 2012; Figure 1.1). Such determination is laborious, and generally inconvenient for deep soil (WESTERN ET AL., 2002), which limits both the temporal and spatial resolution of observations. Moreover, the thermogravimetric determination of soil moisture content is destructive, which prevents repetitive sampling (MARSHALL ET AL., 2012) and thus increases the interest towards alternative measurement techniques.

A range of in-situ point-scale sensor types based on various electromagnetic techniques can be used to continuousily measure soil moisture content, e.g., time domain reflectometry, time domain transmission, impedance or capacitance sensors (BOGENA ET AL., 2017; see "in-situ sensors" in Figure 1.1). These techniques measure the soil permittivity, which is higher in water as compared to soil minerals and therefore a function of soil moisture content (TOPP ET AL., 1980). In-situ sensors typically have measurement volumes in the order of ~10 – 1000 cm^3, which strongly depends on the length of the measurement rod (e.g., WEITZ ET AL., 1997; SAKAKI ET AL., 2008). Due to recent declining costs, it is now possible to integrate newer generation in-situ soil moisture content sensors into networks where multiple sensors are distributed in space. Geostatistical methods can be used to combine these measurements for appropriate comparison with other soil moisture content measurement techniques or for the preparation of soil moisture maps. Hence, continuous soil moisture content observations on the sub-km scale (e.g., BOGENA ET AL., 2010, see Figure 1.1) and thereby on the typical correlation lengths of soil moisture content (~30 – 60 m; WESTERN ET AL., 2004) and beyond, has become possible.

Alternative, non-invasive, point scale soil moisture content measurement techniques are, e.g., active neutron probes (ANP) and nuclear magnetic resonance (NMR; see Figure 1.1). ANP rely on the ratio of neutrons detected and emitted from a an active source, which depends on the hydrogen content of the probed soil (HIGNETT AND EVETT, 2002). In most countries however, the operation of an active neutron source requires the permission of the local authorities. Also, such probes must be inserted in the ground and thus measurements are not fully non-invasive. Nonetheless, because of the large support volume of ANP in comparison to in-situ sensors (~30 cm radius and thus > 100,000 cm^3) almost only

undisturbed soil is sampled (EVETT ET AL., 2003). NMR is based on external magnetic fields that are induced in the ground and influence the spin of hydrogen nuclei. The orientation of the hydrogen atoms modifies the field attenuation, which can be measured (e.g., WALSH ET AL., 2011). NMR allows for the non-destructive measurement of soil moisture content in great depths (e.g., WALSH ET AL. (2011) derive soil moisture content in depths up to 20 m) and in multiple depths, but the measurement accuracy is questionable (pers. communication Benjamin Fersch). ANP and NMR measurements can be used for time-lapse measurements, but due to their high operating costs, they are not suitable for integration into continuous measurement networks on spatial scales comparable to in situ sensors.

1.2.3 **Air- and spaceborne remote sensing of soil moisture content**

Soil moisture content can also be determined from a wide variety of air– and spaceborne remote sensors. These can be grouped by the measurement principle: optical near infrared and optical shortwave infrared sensors, thermal sensors, active microwave sensors, and passive microwave sensors (BABAEIAN ET AL., 2019). Air- and spaceborne soil moisture content measurements rely on similar instruments. Airborne surveys require dedicated flight campaigns. Consequently, surveys must be coordinated with local authorities, and local weather forecasts are usually taken into account (e.g., MENGEN ET AL., 2021). Airborne campaigns are either single or time-lapse observations that cover relatively short periods of time. Nevertheless, airborne surveys of soil moisture content have been conducted regularly in the recent past, especially in the preparation and testing of candidate and planned satellite missions (BABAEIAN ET AL., 2019; MENGEN ET AL., 2021). Because of the lower measurement altitude, airborne soil moisture content surveys generally have better spatial support (~1 - 100 m compared to > ~25 km) but smaller spatial extent (≤ 100 km compared to up to global observations) than spaceborne observations (MONTZKA ET AL., 2017; BABAEIAN ET AL., 2019, see Figure 1.1). Operational systems for spaceborne soil moisture content monitoring on the global scale mostly rely on microwave sensors (BABAEIAN ET AL., 2019), typically integrate soil moisture content up to ~5 cm soil depth and, have a > daily spacing, depending on the type of the measurement system (MONTZKA ET AL., 2017). With satellite based synthetic aperture radar measurements also spatial supports of ~4 – 50 m are possible. However, such fine spatial support comes with the drawback of increased temporal spacing (~3 - 6 days; PATHE ET AL., 2009; MENGEN ET AL.,

2021) and less accurate estimates of soil moisture content (GRUBER ET AL., 2020). Spaceborne soil moisture content measurements generally suffer from inteferences with clouds, atmosphere, and surface conditions. Typically, relatively low measurement accuracies are targeted, i.e., root mean square error (RMSE) ≥ 0.04 m^3/m^3 compared to reference measurements (e.g., CHAN ET AL., 2014; GRUBER ET AL., 2020 and references given therein). In addition, in-situ reference measurements on comparable scales are required for calibration and validation of spaceborne soil moisture content products (ROBINSON ET AL., 2008). This can been done by using in-situ sensor networks (e.g., JACKSON ET AL., 2012) or by using alternative methods for measuring soil moisture content at intermediate scales (e.g., MONTZKA ET AL., 2017, in this case cosmic ray neutron sensing).

1.2.4 "Classical" non-invasive soil moisture content measurement techniques

A variety of long-established non- or minimal-invasive techniques to measure soil moisture content are available ("classical" methods in Figure 1.1). For instance, electromagnetic induction (EMI; e.g., SHEETS AND HENDRICKX, 1995) and electrical resistivity tomography (ERT; e.g., BRUNET ET AL., 2010) rely on the good conducting properties of water. However, EMI and ERT are also sensitive to water salinity and to a number of soil properties such as soil texture, soil bulk density, porosity, and soil organic carbon; (CALLEGARY ET AL., 2007; BRUNET ET AL., 2010; BRINDT ET AL., 2019; BROGI ET AL., 2019). Thus, for the accurate measurement of soil moisture content the signal must be disentagled. For this, time lapse observations can be used, given that certain soil properties are unchanged (ROBINSON ET AL., 2009; NIJLAND ET AL., 2010; DE JONG ET AL., 2020). EMI instruments can be carried by operators or towed by all-terrain vehicles and thus allow time-lapse measurements of soil moisture dynamics at the field scale and beyond (e.g., ROBINSON ET AL., 2009). Depending on the transmitter and receiver orientation and separation, the penetration depth in the soil can represent an integrated signal of a few tens of centimeters to several meters (CALLEGARY ET AL., 2007) and newer devices allow for the simultaneous observation of multiple depths (e.g., BROGI ET AL., 2019). ERT measurements are obtained from electrode transects (DE JONG ET AL., 2020), and three dimensional imaging is also possible if transects intersect (CHAMBERS ET AL., 2014). Depending on the instrument used, ERT transects can be several tens of meters long. The

measured signal corresponds to a three dimensional space along the ERT transect (because the electrical current flows in sphere-like patterns) and the measurement depth is a function of the distance between the electrodes. Thus, a long array will reach several meters below the ground surface (e.g., NIJLAND ET AL., 2010), although this generally comes at the cost of a lower resolution.

For measuring soil moisture content with ground penetrating radar (GPR), electromagnetic microwave pulses are transmitted through the soil. Because the transit time of the microwave pulses depends on the dielectric permittivity of the soil (LUNT ET AL., 2005), soil moisture content can be inferred (TOPP ET AL., 1980). GPR instruments can be operated from boreholes, on the soil surface or off-ground (e.g., drone based; WU ET AL., 2019). For borehole observations, the lateral extent is generally < 10 m. From on- or off-ground GPR observations, accurate soil moisture content estimates (RMSE ≤ 0.025 m^3/m^3 compared to TDR measurements) are representative for a maximum soil depth of ~20 cm (LUNT ET AL., 2005). With a horizontal resolution of decimeters (LUNT ET AL., 2005), areas up to 500 x 500 m can be mapped daily (HUISMAN ET AL., 2001). However, GPR signal interpretation is complex, which hampers the use by non-experts (e.g., HUISMAN ET AL., 2003; KLOTZSCHE ET AL., 2018).

1.2.5 Emerging non-invasive soil moisture content measurement techniques

In most cases, the spatial and temporal capabilities of soil moisture content measurement techniques are related on a linear trajectory: increasing spatial measurement scales are associated with increasing temporal measurement scales (see Figure 4 in BOGENA ET AL., 2015). Some proximal sensing techniques have the potential to overcome this caveat (see BOGENA ET AL., 2015 for a review). Amongst others, promising techniques for retrieving soil moisture content on intermediate spatial and temporal scales are global navigation satellite system (GNSS) reflectometry, gamma ray intensity monitoring, and cosmic ray neutron (CRN) sensing (for the latter see Chapter 1.3). In the following, these soil moisture content measurement techniques are presented in more detail as they have similar measurement accuracy and costs (BOGENA ET AL., 2015).

GNSS (i.e., GPS – global positioning system) was originally a military development for positioning and navigation purposes (PARKINSON AND SPILKER, 1996). To measure soil

moisture content, the interference patterns of direct and ground reflected GNSS signals received at ground stations are inspected. Depending on the soil permittivity, which is related to soil moisture content, the signal amplitude and phase are modified (LARSON ET AL., 2008). GNSS reflections are representative for two – five cm soil depth, depending on soil moisture content (LARSON ET AL., 2008; LARSON ET AL., 2010). In obstacle free (e.g., no vegetation or buildings) and flat areas, a 1.8 m above ground installed GNSS antenna allows for the derivation of soil moisture content along a satellite ground track in an ellipsoidal area with maximal extents of ~4 by 50 m (LARSON ET AL., 2010; see Figure 1.1). A sub-daily time resolution is realistic when considering the numerous satellite constellations that are available (i.e., systems with global coverage are operated by the United States, Russia, China, and the European Union and additionally regional coverage systems are operated by Japan and India). Moreover, if the overpasses of several satellites are inspected the information may be spatially discretized allowing for the production of soil moisture maps (e.g., RODRIGUEZ-ALVAREZ ET AL., 2009). Worldwide more than 5000 GNSS ground stations are operated (LARSON ET AL., 2008). However, these often cluster in urban areas, where a meaningful soil moisture content retrieval is not possible (BOGENA ET AL., 2015).

Gamma ray intensity monitoring relies on the radionuclides ^{232}Th, ^{238}U or ^{40}K, which naturally occur in soils. In their decay chains, gamma rays are emitted and as the attenuation in water is much more efficient than in soil minerals or in air, the above ground measurement of the gamma ray intensity enables the derivation of soil moisture content (STRATI ET AL., 2018). A gamma ray detector mounted in 2.25 m above ground is sensitive to soil moisture content in ~25 m radius and depths up to ~30 cm (see Figure 1.1), dependent on soil bulk density (BALDONCINI ET AL., 2018) and soil moisture content (BOGENA ET AL., 2015). Furthermore, gammy ray intensity monitoring allows for the quasi continuous measurement of soil moisture content (BALDONCINI ET AL., 2018). Airborne gamma ray intensity monitoring was applied for soil moisture content retrieval on medium spatial scales (< 100 km^2) with good agreement (RMSE of ~0.025 m^3/m^3) to in-situ reference data of the first 10 cm soil depth (JONES AND CARROLL, 1983). However, the costs of such surveys are nowadays considered excessive. More promising for soil moisture content measurements on large spatial scales is the utilization of the gamma ray stations that are already operational in many European countries (e.g., alone in Germany ~1800 stations are operative) and elsewhere (BOGENA ET AL., 2015).

1.3 **Cosmic ray neutron sensing**

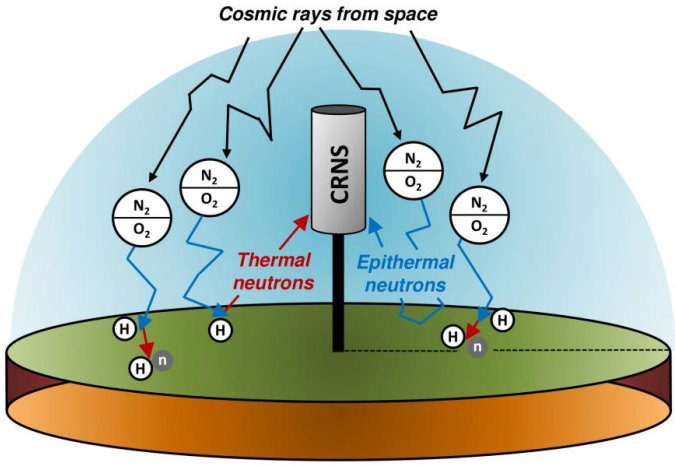

Figure 1.2: Simplified representation of the energy-dependent evolution of cosmic ray neutrons. Modified from BROGI ET AL. (2021).

Primary ionized particles (in the order of 1 GeV) from space constantly penetrate the Earth's atmosphere and generate secondary particle showers that cascade towards the ground surface. HESS (1912), observed an increased intensity of secondary ionized particles with altitude from balloon observations up to approximately 5000 m height. The secondary particle showers also include neutrons that are mostly generated from protons by the splitting of nitrogen and oxygen (i.e., via spallation; Figure 1.2 - black arrows; KÖHLI ET AL., 2015). Thereby created high-energy neutrons are further propagated towards the earth surface and constantly loose kinetic energy from collisions with atmospheric nuclei. With the progressing loss of kinetic energy (≤ ~10 MeV) the neutron interactions are dominated by elastic scattering and also the absorption and the subsequent release of new neutrons (i.e., via evaporation) becomes more likely (ZREDA ET AL., 2012; KÖHLI ET AL., 2015).

Due to its low mass and high elastic scattering cross section, the moderation of neutrons in the epithermal energy regime (~0.5 eV – 100 keV) is dominated by hydrogen (Figure 1.2 - blue arrows; ZREDA ET AL., 2012). Thus, the density of epithermal neutrons measured close to the soil surface inversely depends on the amount of hydrogen in the environment (ZREDA ET AL., 2008). However, the intensity of epithermal neutrons also depends on air pressure (DESILETS AND ZREDA, 2003), incoming CRN intensity (DESILETS AND ZREDA, 2001) and air humidity (ROSOLEM ET AL., 2013), which must be taken into account for an accurate derivation of changes in ambient hydrogen storage (see Appendix I).

First field applications identified a relation between epithermal neutron intensity and snow water equivalent (BISSELL AND BURSON, 1974; KODAMA ET AL., 1979; KODAMA, 1980), which is still of interest today as highlighted by numerous recent studies (e.g., ZWECK ET AL., 2013; SIGOUIN AND SI, 2016; SCHATTAN ET AL., 2017; GUGERLI ET AL., 2019; SCHATTAN ET AL., 2019; BOGENA ET AL., 2020). In the absence of snow, most of the near-surface hydrogen in terrestrial environments is stored in soil water. Therefore, the measurement of epithermal neutrons (i.e., the counting of epithermal neutrons) allows for the measurement of soil moisture content (ZREDA ET AL., 2008; DESILETS ET AL., 2010; KÖHLI ET AL., 2021). KODAMA ET AL. (1985) were the first to attempt measurements of soil moisture content with cosmic ray neutron sensors (CRNS). For this purpose, they used epithermal neutron intensities measured at different depths in the soil, which resulted in measurements that were representative for relatively small volumes. In contrast, for the measurement of soil moisture content, CRNS are nowadays operated above the ground surface, at ~1 - 2 m height (e.g., ZREDA ET AL., 2008; DESILETS ET AL., 2010; RIVERA VILLARREYES ET AL., 2011; ZREDA ET AL., 2012; BOGENA ET AL., 2013). In this configuration, the derived signal is representative for 130 to 240 m radius and soil depths of 15 to 83 cm. Both radius and depth strongly depend on soil moisture content (KÖHLI ET AL., 2015; SCHRÖN ET AL., 2017; see Figure 1.1).

Commercially available CRNS are typically proportional counter tubes filled with ^{3}He-gas or $^{10}BF_3$-enriched gas as neutron converter (ZREDA ET AL., 2012; BOGENA ET AL., 2018; KÖHLI ET AL., 2018; WEIMAR ET AL., 2020). Unfortunately, ^{3}He is costly while $^{10}BF_3$ is toxic. Therefore, newer measurement concepts avoid the use of these gases and neutron conversion is based on solid ^{6}Li (FERSCH ET AL., 2020), solid ^{10}B (WEIMAR ET AL., 2020) or scintillator technology (STEVANATO ET AL., 2019). All of these sensor types are most sensitive to thermal neutrons ($\leq$ ~0.5 eV; e.g., ZREDA ET AL., 2012; WEIMAR ET AL., 2020). To measure epithermal neutrons, and thus soil moisture content, the bare neutron sensors are shielded with high density polyethylene (HDPE), which contains large amounts of hydrogen and is very efficient in moderating CRN to lower energy levels (KODAMA, 1980; ZREDA ET AL., 2012). CRNS can also be operated in mobile mode. For this, the CRNS are mounted on cars (i.e. CRN rover – compare Figure 1.1; e.g., CHRISMAN AND ZREDA, 2013; DONG ET AL., 2014; SCHRÖN ET AL., 2018a), carried as backpacks (IAEA, 2018), transported in trains (SCHRÖN ET AL., 2021) or operated on flying devices (e.g., on gyrocopters or blimps; SCHRÖN, 2017; HEISTERMANN ET AL., 2021a).

In mobile observations especially, the statistical uncertainty of CRNS measurements is of great interest. Such uncertainty greatly depends on soil moisture content with wet soils yielding less detectable neutrons and thus increasing statistical uncertainty (ZREDA ET AL., 2012; BOGENA ET AL., 2013; GUGERLI ET AL., 2019). Measurements of epithermal neutrons are thus usually aggregated to intervals ≥ 12 hours, to reduce the soil moisture content measurement uncertainty for stationary CRNS (e.g., ZREDA ET AL., 2012; BOGENA ET AL., 2013). However, for mobile observations this is undesirable, as a trade-off must be made between measurement speed and the accuracy of the final soil moisture product. On one hand, higher speed will result in a larger measured area while on the other hand spatial resolution will be reduced and statistical uncertainty will be increased since shorter measurement time generally results in a reduction of detected neutrons. Mobile observations can also make use of larger and/or multiple detectors but spatial aggregation of neutron counts remains necessary despite the use of such high sensitivity devices (e.g., CHRISMAN AND ZREDA, 2013; DONG ET AL., 2014; SCHRÖN ET AL., 2021). Overall, the relation between spatial aggregation and statistical uncertainty of mobile soil moisture content measurements with CRNS is of key importance but it was not yet investigated in detail due to the novelty of this technology.

Stationary CRNS are nowadays operated in networks of varying spatial extent (compare Figure 1.1). For instance, several regional and national networks are operated in Germany (e.g., BAATZ ET AL., 2014; KIESE ET AL., 2018), the US (ZREDA ET AL., 2012), the UK (COOPER ET AL., 2021), Australia (HAWDON ET AL., 2014), and India (UPADHYAYA ET AL., 2021). In Europe, a continent-wide network is currently in development (BOGENA ET AL., 2021). In total, more than 200 CRNS locations are operated around the world (BOGENA ET AL., 2015; ANDREASEN ET AL., 2017b) and in many of these locations thermal neutrons are measured as well (i.e., CRNS without HDPE moderator; see Figure 1.2). However, these measurements are rarely used since basic properties of thermal neutrons are not fully understood yet. For instance, the dependency of the thermal neutron intensity on pressure, humidity and incoming CRN is still under debate. Here, different approaches are found in literature with TIAN ET AL. (2016) and DESILETS ET AL. (2010) not correcting the thermal neutron intensity, ANDREASEN ET AL. (2016) useing the corrections for pressure and incoming CRN and JAKOBI ET AL. (2018) useing the corrections for pressure and humidity. Moreover, the footprint of thermal neutrons is not well defined (BOGENA ET AL., 2020 assumed a radial footprint of ~35 m), and due to the absorption of thermal neutrons on

(mostly) soil nuclei (see Figure 1.2) the thermal neutron intensity is site-specific (ZREDA ET AL., 2008). However, it is unclear if soil moisture content or other hydrogen pools (e.g., snow, biomass, interception) predominantly define the thermal neutron intensity. In the case of snow, it was found that the thermal neutron intensity increases with increasing snow thickness up to a specific threshold, followed by an abrupt decrease (DESILETS ET AL., 2010; BOGENA ET AL., 2020). This was confirmed by neutron transport simulations and a threshold value of approximately 30 mm of snow water equivalent or liquid water based on the bedrock was identified (see Figure 4 in ZWECK ET AL., 2013 and Table 5 in HUBERT ET AL., 2016). This can be explained by the counterplay of thermalization (i.e., the moderation of epithermal neutrons to thermal energies) and absorption. Here, when the hydrogen content of the environment increases more neutrons are thermalized, but thermal neutrons will also lose more kinetic energy, which in turns facilitates absorption (RASCHE ET AL., 2021).

The combined analysis of thermal and epithermal neutrons was proposed to allow the discretization of aboveground hydrogen pools (RIVERA VILLARREYES ET AL., 2011). For instance, it was shown that the ratio of thermal-to-epithermal neutrons (N_r) allows the distinction between snow and rain events (DESILETS ET AL., 2010). N_r was also shown to be sensitive to changes in aboveground biomass of crops (TIAN ET AL., 2016; JAKOBI ET AL., 2018), which was confirmed from neutron transport simulations of a forested site (ANDREASEN ET AL., 2017a) and from a good correspondence with remote sensing derived vegetation indices (i.e., normalized difference vegetation index (NDVI) and leaf area index (LAI); VATHER ET AL., 2020). However, the general applicability of N_r for the measurement of biomass was not yet confirmed for other crops than maize, soybean (TIAN ET AL., 2016), and sugar beet (JAKOBI ET AL., 2018).

The epithermal neutron intensity is sensitive to all pools of hydrogen at the land surface (e.g., biomass, interception; BOGENA ET AL., 2013; BAATZ ET AL., 2015) with especially large and abrupt changes in biomass having a strong impact on the accuracy of soil moisture content measurements with CRNS. When the amount of biomass is known, this can be considered with local linear models (e.g., FRANZ ET AL., 2013b) or with generalized models (e.g., HAWDON ET AL., 2014; BAATZ ET AL., 2015). Alternatively, the dependency of N_r on biomass can be used for the correction of biomass effects on soil moisture content measurements with CRNS (TIAN ET AL., 2016; JAKOBI ET AL., 2018; VATHER ET AL., 2020).

However, available methods that consider the effects of biomass on soil moisture content measurements with CRNS have not been yet compared in detail.

1.4 **Objectives and outline**

This dissertation was written as sub-project of the research unit FOR 2694 “Cosmic Sense” funded by the Deutsche Forschungsgemeinschaft (DFG, German Research Foundation, project-no. 357874777). The aim of Cosmic Sense is the improved characterization of scale dependent water fluxes for a better understanding of hydrologic changes at the land surface. As outlined in Chapters 1.2 and 1.3, CRNS bear great potential for filling previously existing scale gaps in soil moisture content measurements (see also Figure 1.1). However, CRNS are also susceptible to statistical measurement uncertainties and to other pools of hydrogen (i.e., biomass) than soil moisture content. Within such context, the aim of this thesis is to improve the CRN sensing method for mobile and stationary soil moisture content measurements. To this end, the following three sub-objectives were defined.

First, an easy-to-apply method for the estimation of neutron count related measurement uncertainties should be developed. This method should allow for an improved planning and evaluation of mobile CRN measurements. More specifically, users should be enabled to balance the inherent trade-off between spatial resolution, determined by driving (or walking, or flying) speed, and measurement uncertainty according to their requirements (and instrument capabilities). Additionally, the interpretation of soil moisture content measurements with CRNS should be facilitated. The development of such a method is presented in Chapter 2 of this thesis, where a 3rd order Taylor expansion approach is introduced for propagation of the uncertainty from raw epithermal neutron counts to soil moisture content measurements with CRNS. The new method is compared to Monte Carlo simulations and to the measurement uncertainty determined in an experiment. In addition, CRN rover measurements from two experiments are used as examples to characterize the influence of aggregation on the spatial resolution and on the measurement uncertainty of the resulting soil moisture product.

Second, the footprint of thermal neutrons should be investigated. To this end, measured thermal neutron intensities should be reproduced to confirm the ability of the neutron transport code URANOS (Ultra Rapid Adaptable Neutron-Only Simulations; KÖHLI ET AL., 2015) to model thermal neutrons. In a next step, the horizontal and vertical footprint of

thermal neutrons should be investigated and weighting functions that represent the modeled distance and depth dependent thermal neutron intensities should be developed. Such footprint investigations are presented in Chapter 3, where a river-crossing experiment is used to gain initial understanding of the horizontal thermal neutron footprint and to test whether URANOS is able to reproduce thermal neutron transport correctly. The horizontal and vertical thermal neutron footprints are derived from simulations and analytical expressions of the distance and depth dependent thermal neutron intensity are developed. For this, the influence of soil moisture content is considered. In addition, an existing approach is recommended to account for the influence of pressure, and the influences of soil chemistry and detector height above the soil surface on the thermal neutron footprint are investigated.

Third, the understanding of available methods for the correction of biomass effects on soil moisture content estimates with CRNS should be improved. For this, available biomass correction methods should be compared with respect to their requirements for application and to their performance for the correction of biomass effects of three different crops. Additionally, it should be evaluated if N_r is generally suited for the measurement of aboveground biomass and in which contexts it can be applied. Such investigations are presented in Chapter 4, where four methods for the consideration of biomass effects on soil moisture content measurements with CRNS are compared based on data from three experiments with different crops. For this, I) site-specific functions based on in-situ measured biomass, II) thermal neutron intensity, III) N_r, and IV) a generic approach are considered. In addition, the possibility of measuring biomass with N_r or thermal neutron intensity alone are investigated.

The final Chapter 5 provides the overall conclusions of this work and an outlook where possible future developments are discussed. Here, two preliminary examples are presented. In the first example, thermal neutron intensity and plant height measurements from seven cropping periods are used to investigate the possibility of stationary long-term vegetation monitoring with CRNS. In the second example, the value and limits of CRN rover measurements at the catchment scale are discussed and obstacles for calibration to soil moisture content are elaborated.

2 Error estimation for soil moisture measurements with cosmic ray neutron sensing and implications for rover surveys

Abstract

Cosmic ray neutron (CRN) sensing allows for non-invasive soil moisture content measurements at the field scale and relies on the inverse correlation between aboveground measured epithermal neutron intensity (1 eV − 100 keV) and environmental water content. The measurement uncertainty follows Poisson statistics and thus increases with decreasing neutron intensity, which corresponds to increasing soil moisture content. In order to reduce measurement uncertainty, the neutron count rate is usually aggregated over 12 or 24 h time windows for stationary CRN probes. To obtain accurate soil moisture content estimates with mobile CRN rover applications, the aggregation of neutron measurements is also necessary and should consider soil wetness and driving speed. To date, the optimization of spatial aggregation of mobile CRN observations in order to balance measurement accuracy and spatial resolution of soil moisture patterns has not been investigated in detail. In this work, we present and apply an easy-to-use method based on Gaussian error propagation theory for uncertainty quantification of soil moisture content measurements obtained with CRN sensing. We used a 3rd order Taylor expansion for estimating the soil moisture content uncertainty from uncertainty in neutron counts and compared the results to a Monte Carlo approach with excellent agreement. Furthermore, we applied our method with selected aggregation times to investigate how CRN rover survey design affects soil moisture content estimation uncertainty. We anticipate that the new approach can be used to improve the strategic planning and evaluation of CRN rover surveys based on uncertainty requirements.

This chapter is based on a journal article published as:

JAKOBI, J., HUISMAN, J. A., SCHRÖN, M., FIEDLER, J., BROGI, C., VEREECKEN, H., AND BOGENA, H. R. (2020), Error Estimation for Soil Moisture Measurements with Cosmic Ray Neutron Sensing and Implications for Rover Surveys, *Front. Water*, 2:10, doi: 10.3389/frwa.2020.00010.

2.1 **Introduction**

Soil moisture is an essential variable of the terrestrial system as it governs the transfer of both water and energy between the land surface and the atmosphere (VEREECKEN ET AL., 2015). Accurate information on soil moisture dynamics is vital for a better understanding of processes in the vadose zone, because it controls major subsurface processes, such as ground water recharge, runoff and infiltration. Furthermore, soil moisture dynamics are important for the optimization of agricultural management because they determine crop growth, leaching processes and the fate of fertilizers applied to soils. Soil moisture is highly variable in both space and time, with typical length and time scales ranging from a few centimeters to several kilometers and from minutes to years, respectively (ROBINSON ET AL., 2008; VEREECKEN ET AL., 2008).

Recent advances in non-invasive monitoring techniques enable continuous and contactless measurements of soil moisture dynamics at the field scale (BOGENA ET AL., 2015). Among other methods, the cosmic ray neutron sensing (CRNS) method has become increasingly popular for soil moisture content estimation since its introduction by ZREDA ET AL. (2008). The CRNS method relies on the inverse relationship between soil moisture content and the amount of aboveground epithermal neutrons (energy range from ~0.2 eV to 100 keV) (KÖHLI ET AL., 2018). The measurement footprint ranges from 130 to 240 m radius around the neutron detector with a penetration depth ranging between 15 and 80 cm depending on soil moisture content and other parameters (KÖHLI ET AL., 2015). Typically, stationary CRNS are used to obtain continuous information on field scale soil moisture dynamics (ZREDA ET AL., 2012; ANDREASEN ET AL., 2017b; SCHRÖN ET AL., 2018b). More recently, mobile applications of CRNS (i.e. CRN roving) have been introduced, which enable to measure spatial soil moisture variability at the larger catchment scale (CHRISMAN AND ZREDA, 2013; DONG ET AL., 2014; FRANZ ET AL., 2015; AVERY ET AL., 2016; MCJANNET ET AL., 2017; SCHRÖN ET AL., 2018a).

Measurement uncertainty is an important quantity that should accompany every geophysical dataset. The systematic uncertainty has been analyzed by BARONI ET AL. (2018), who quantified the influence of environmental factors, such as vegetation or soil properties, on the CRNS product. The present study investigates the statistical uncertainty of CRNS soil moisture content estimates, which depends on the detector configuration, i.e., the number of counts in a given period of time. This count rate, however, is inversely related

to soil moisture content, such that dryer soil leads to more precise measurements (cf. DESILETS ET AL., 2010; BOGENA ET AL., 2013). In CRN rover applications, this translates to the number of detected neutrons in a specific spatial unit that is passed during the record period of the detector. Hence, the travelling speed determines the spatial resolution and is an important factor for the quantification of measurement uncertainty.

Various neutron detectors exist of different size and efficiency. Typically, a larger detector volume improves the counting statistics, and thus reduces the uncertainty of the soil moisture product. The record period of most mobile neutron detectors is between 10 sec and 1 min, while typical driving speeds range from 2 - 10 km/h on agricultural fields (SCHRÖN ET AL., 2018a; FENTANES ET AL., 2020) to ~50 km/h for large-scale surveys (e.g., CHRISMAN AND ZREDA, 2013; DONG ET AL., 2014; MCJANNET ET AL., 2017; DONG AND OCHSNER, 2018). In most studies, additional spatial smoothing was applied to the CRN rover measurements by using a temporal moving window filter in order to reduce the uncertainty in the soil moisture content estimates (e.g., SCHRÖN ET AL., 2018a: window size of 3 measurements; CHRISMAN AND ZREDA, 2013: window size of 7 measurements). However, long record periods as well as large averaging window sizes lead to elongated measurement footprints in the direction of data acquisition and thus to a decrease in spatial resolution (CHRISMAN AND ZREDA, 2013; FERSCH ET AL., 2018; SCHRÖN ET AL., 2018a). For instance, aggregated neutron counts for 1, 3, 5, and 7 minute time periods acquired with an average driving speed of 50 km/h correspond to elongated footprints where the longer axis is 0.8, 2.5, 4.2, and 5.8 km long, respectively. More advanced approaches for data aggregation have also been proposed. Some studies assigned the average of all raw neutron measurements within a fixed radius to a grid (e.g., DONG AND OCHSNER, 2018; GIBSON AND FRANZ, 2018; FINKENBINER ET AL., 2019). In a further processing step, inverse distance weighting was used to further sharpen the image and to increase resolution (GIBSON AND FRANZ, 2018; FINKENBINER ET AL., 2019).

BOGENA ET AL. (2013) and SCHRÖN ET AL. (2018b) have already analyzed the dependence of the accuracy of CRN-based soil moisture content measurements on the time integration for a stationary CRNS. In principle, this method can also be applied to mobile CRN rovers by taking spatial aggregation into account. Nevertheless, the effects of the spatial aggregation of neutron counts on the soil moisture content measurement accuracy have not yet been investigated in detail. A comprehensive method to determine uncertainty in soil moisture content from uncertainty in neutron counts would allow for the discrimination of

statistical effects from the effects of environmental water. In earlier CRN rover studies, such undetermined features could not be assessed in full detail (e.g., DONG ET AL., 2014; FRANZ ET AL., 2015; DONG AND OCHSNER, 2018; SCHRÖN ET AL., 2018a).

In this study, we aim to analyze how temporal and spatial aggregation of neutron counts affects the accuracy of soil moisture content measurements with CRNS technology with a focus on mobile CRN roving. To this end, analytical expressions for error propagation are introduced that allow to assess the accuracy of soil moisture content estimates from uncertain neutron count rates. The appropriateness of the analytical expressions is evaluated using Monte Carlo simulations. The applicability of the analytical expressions is tested using experimental data from three different CRN rover campaigns with different spatial scales in Germany and in Oklahoma (USA).

2.2 **Material and Methods**

2.2.1 **Jülich CRN rover**

The Jülich CRN rover consists of an array of nine neutron detector units (Hydroinnova LLC, Albuquerque, NM, USA) each holding four $_{10}BF^3$-filled tubes, which amounts to a total number of 36 neutron detector tubes located in 9 detector housings. The housing of the detector tubes was designed such that the moderating High Density Polyethylene (HDPE) can be removed on demand. This allows to convert the neutron detector tubes from epithermal (with HDPE) to thermal neutron sensitive (without HDPE) and back. During the presented measurement campaigns, the Jülich CRN rover was configured to measure epithermal neutrons (E_{raw}) with five detector units. Three of these units were mounted in vertical orientation, while the other two units were oriented horizontally (Figure 2.1). The remaining four detector units measured thermal neutrons during the experiments to calculate the thermal-to-epithermal neutron ratio (N_r). The N_r ratio has already been successfully used in previous studies to estimate surface biomass and to correct the influence of surface biomass on soil moisture content from cosmic ray neutrons (TIAN ET AL., 2016; JAKOBI ET AL., 2018). The driving speed during the presented measurement campaigns with the Jülich CRN rover was 4 - 5 km/h, and the time interval of the raw neutron count measurements was 10 sec.

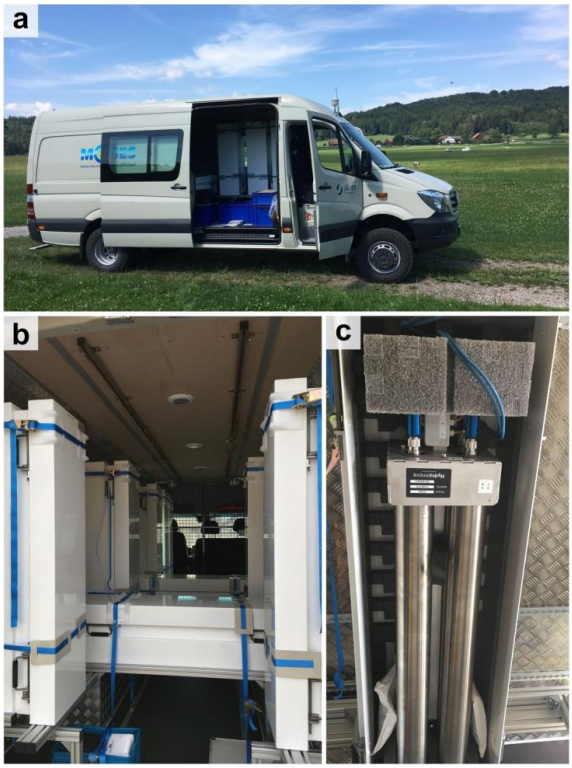

Figure 2.1: a) Jülich Cosmic rover in the field at the TERENO research site Fendt. b) Setup of the nine detector units inside the car. c) Example of one detector unit consisting of four detector tubes – here shown without the moderating HDPE..

2.2.2 **Experimental sites**

Fendt site (Germany, Experiment A)

The long-term research site Fendt (47°50'N, 11°3.6'E) belongs to the Pre-Alpine observatory (WOLF ET AL., 2017; KIESE ET AL., 2018) of the TERENO (TERrestrial ENvironmental Observatories) network (ZACHARIAS ET AL., 2011; BOGENA ET AL., 2012). The Fendt site is located at the south-eastern tip of the Rott catchment (55 km^2) at about 595 m a.s.l.. The soils are dominated by Cambrian stagnosols and land use consists mainly of pasture and forest. The Fendt site has a temperate marine climate with an average annual rainfall of 1033 mm and temperature of 8.6 °C (FU ET AL., 2017). For more detailed information on site characteristics, we refer to KIESE ET AL. (2018).

The CRN rover measurements on the Fendt research site were carried out as part of a joint field campaign of the CosmicSense project (for more information please visit the project

webpage: https://www.uni-potsdam.de/en/cosmicsense.html). We drove back and forth along a ~350 m long grass road for 4 h at the lowest possible speed of 4 - 5 km/h on 14 April 2019. For reference, shallow soil moisture content (0 – 7 cm depth) was measured at 155 locations a few meters off the road using HydraProbe soil moisture content sensors (Hydra Go Field Version, Stevens Water Monitoring Systems, Inc., Portland, USA). The measurement transect was bordered by a road in the west and a small stream in the east.

Selhausen site (Germany, Experiment B)

The research site Selhausen (50°52'N, 6°27'E) covers an area of ~1 x 1 km and is part of the Lower Rhine Valley/Eifel Observatory of the TERENO network (BOGENA ET AL., 2018). The Selhausen site is located in the eastern part of the Rur catchment (2354 km^2) and is characterized by an eastern upper terrace composed of Pleistocene sand and gravel sediments that are buried in loess sediments and by a western lower terrace that is generally dominated by Pleistocene/Holocene loess sediments (WEIHERMÜLLER ET AL., 2007). The soils in the area consist of Cambisols, Luvisols, Planosols, and Stagnosols (RUDOLPH ET AL., 2015). Generally, all fields within the study area are used for agriculture. The crops that are most commonly grown are winter cereals, sugar beet, and silage maize (REICHENAU ET AL., 2016). The site has a temperate maritime climate with a mean annual precipitation and temperature of 714 mm and 10.2 °C, respectively (KORRES ET AL., 2015). Detailed information on the Selhausen research site can be found in BOGENA ET AL. (2018) and BROGI ET AL. (2019).

The CRN rover measurements at the Selhausen site were collected as part of a MOSES (Modular Observation Solutions for Earth Systems) test campaign. MOSES is an infrastructure program funded by the Helmholtz Association (https://www.ufz.de/moses/). The campaign was carried out on 11 July 2018 and we mostly drove on the roads in the research area. Whenever it was possible, we also drove on the agricultural fields. Some of the fields in the northwest and southeast of the area were irrigated during the CRN rover measurements. Reference soil moisture content measurements were again made with HydraProbe sensors as in the Fendt experiment at 738 locations distributed over a large fraction of the experimental area with a focus on sites where earlier studies were based (e.g., RUDOLPH ET AL., 2015; JAKOBI ET AL., 2018; BROGI ET AL., 2019). This was done to limit the amount of work associated with taking reference measurements (4 people were measuring for ~4 hours).

For this site, the bulk density of the fine fraction ($\varrho_{bd<2}$) was estimated to be 1.32 g/cm^3 from literature values (EHLERS ET AL., 1983; UNGER AND JONES, 1998) and from previous sampling campaigns conducted within the study area. These values were modified using gravel content as successfully done by BROGI ET AL. (2020) for the simulation of crop growth in this study area. For this, a high-resolution soil map produced from a combination of electromagnetic induction measurements and direct soil sampling (BROGI ET AL., 2019) was used to retrieve spatially distributed gravel content. This map divides the study area in 18 soil units, each provided with information on gravel content for each horizon. To obtain bulk density (ϱ_{bd}) values considering gravel content, the method proposed by BRAKENSIEK AND RAWLS (1994)was used:

$$\varrho_{bd} = \varrho_{bd_{<2}} + Z2\,(\varrho_{bd_{>2}} - \varrho_{bd_{<2}}) \tag{2.1}$$

where $\varrho_{bd>2}$ is the bulk density of rock fragments (2.65 g/cm^3, BRAKENSIEK AND RAWLS, 1994) and $Z2$ [cm^3] is the volume of rock fragments (FLINT AND CHILDS, 1984), which was approximated according to BRAKENSIEK AND RAWLS (1994) with:

$$Z2 = Z1/(2 - Z1) \tag{2.2}$$

where $Z1$ is the gravel content in % of weight relative to the total weight of dry samples. The same map was used to determine the sum of lattice water and organic matter θ_{off} for the Selhausen site with the loss-on-ignition method by heating mixed samples of the 18 soil units to 1000 °C for 12 hours (ZREDA ET AL., 2012; BAATZ ET AL., 2015). The samples were obtained from mixed top soil material (30 - 40 cm depth) from a total of 200 measurement locations in the area. The reference soil moisture content, ϱ_{bd} and θ_{off} were horizontally weighted to match the CRN rover measurement locations (SCHRÖN ET AL., 2017).

Oklahoma site (USA, Experiment C)

The Oklahoma site is located in the Cimarron River catchment in the central north of Oklahoma, USA. The soil is dominated by Mollisols, Alfisols, and Inzeptisols with loamy texture in the central part of the transect and sandy texture in the western part of the transect (SSURGO database, https://websoilsurvey.sc.egov.usda.gov/). The land use consists mainly of warm seasonal grasses, winter wheat, and small patches of deciduous forests. The average annual precipitation ranges from 880 mm in the east to 732 mm in the west (DONG AND OCHSNER, 2018).

CRN rover measurements were performed 18 times on a ~150 km long unpaved road. The resulting dataset was analyzed by DONG AND OCHSNER (2018) to determine controlling factors for mesoscale soil moisture patterns. The CRN rover used at this site consists of two epithermal neutron detectors, each holding two ^{3}He-filled detector tubes (Hydroinnova LLC, Albuquerque, NM, USA). The aggregation interval of the raw neutron count measurements was 1 minute and the driving speed varied according to the local conditions. The average speed was 48 km/h (DONG AND OCHSNER, 2018).

For the Oklahoma study area, we extracted ϱ_{bd} and clay content of the top soil from the SSURGO database and converted it to a 200 x 200 m resolution grid as described by DONG AND OCHSNER (2018). In a further step, we used their linear relation to derive lattice water (θ_{off}) from clay content. The hydrogen pool of the soil organic matter was not considered by DONG AND OCHSNER (2018). Next, average values of ϱ_{bd} and θ_{off} in a 200 m radius were assigned to the CRN rover measurement locations.

2.2.3 **Data acquisition and standard processing**

Both CRN rovers recorded GPS locations at the end of each aggregation interval. These were set to half the distance travelled between two recordings so that the location better reflected the origin of the accumulated neutron counts (DONG AND OCHSNER, 2018; SCHRÖN ET AL., 2018a). In addition, absolute humidity (calculated from measured air temperature and relative humidity) and atmospheric pressure were recorded with both CRN rovers. The corrected epithermal neutron counts (E) for the Jülich CRN rover were obtained by applying standard correction procedures for atmospheric pressure (DESILETS AND ZREDA, 2003), absolute humidity (ROSOLEM ET AL., 2013), and variation in incoming cosmic radiation (DESILETS AND ZREDA, 2001) (see Appendix I). The reference incoming cosmic radiation was obtained from the neutron monitor at Jungfraujoch (JUNG, available via the NMDB neutron monitor database at www.nmdb.eu). The hourly incoming cosmic ray data were interpolated linearly to the respective time stamps of the measurements with the Jülich CRN rover. For the Oklahoma CRN rover, we used the raw and corrected neutron counts as published by DONG AND OCHSNER (2018).

2.2.4 **Conversion of neutron counts to soil moisture content**

We converted the corrected neutron count rates to gravimetric soil moisture content (θ_g [g/g]) with the approach of DESILETS ET AL. (2010):

$$\theta_g = p_0 \left(\frac{E}{N_0} - p_1 \right)^{-1} - p_2 - \theta_{off} \tag{2.3}$$

where N_0 is a free parameter that is usually calibrated with independent in-situ soil moisture content reference measurements, and p_i = (0.0808, 0.372, 0.115) are fitting parameters determined by DESILETS ET AL. (2010) and validated in many publications thereafter. Estimated hydrogen content within the CRNS footprint stored in pools other than soil moisture content (θ_{off} [g/g], i.e. lattice water and organic matter) is subtracted from the CRN soil moisture content estimate (FRANZ ET AL., 2012a). As in previous CRN rover studies, we only considered lattice water and organic matter here (e.g., AVERY ET AL., 2016; MCJANNET ET AL., 2017). The conversion from gravimetric to volumetric soil moisture content (θ_v [m^3/m^3]) is known as:

$$\theta_v = \varrho_{bd}\, \theta_g \tag{2.4}$$

For the Fendt site, we used a constant ϱ_{bd} = 1.028 g/m^3 and θ_{off} = 0.072 g/g, which were sampled ~150 m northeast of the measurement transect by FERSCH ET AL. (2018). The in-situ soil moisture content measurements were used to calibrate N_0 in Equation (2.3), which resulted in a value of 753 cts/min for the Fendt site. For the N_0 calibration of the CRN rover application at the Selhausen site, all reference in-situ soil moisture content were used with four different aggregation methods (moving window and nearest neighbor aggregation of 3 and 9 measurements, respectively). Subsequently, the four aggregated N_0 values were averaged, resulting in a mean N_0 value of 720 cts/min for the Selhausen site. In this way, we did not favor any of the aggregation strategies used in this study. For the conversion of measured neutron counts to soil moisture content at the Oklahoma site, we used N_0 = 556 cts/min. This value was obtained by DONG AND OCHSNER (2018) using calibration against reference data from four stations of the Oklahoma Mesonet.

2.2.5 **Quantification of measurement accuracy**

The measurement accuracy of CRN rover measurements was quantified using the standard deviation (σ) and the root mean squared error (RMSE). Both have a similar meaning and are therefore directly comparable. The standard deviation σ is given by:

$$\sigma(c) = \sqrt{\frac{1}{A(c)-1}\sum_{i=1}^{A(c)}\left|x(c)_i - \overline{x(c)}\right|^2} \tag{2.5}$$

where x and $\bar{x}$ are the measurements and their mean, respectively, and A is the total number of measurements, which scales with the aggregation size c. The RMSE is given by:

$$\mathrm{RMSE(c)} = \sqrt{\frac{1}{A(c)}\sum_{i=1}^{A(c)}|x(c)_i - x_2(c)_i|^2} \tag{2.6}$$

where x_2 are the reference measurements for a given level of aggregation.

2.2.6 **Expected measurement accuracy due to uncertain neutron count rates**

Measurements of a proportional neutron detector system are governed by counting statistics that follow a Poissonian probability distribution (ZREDA ET AL., 2012). For a large number of events per unit time, the Poisson distribution converges to a normal distribution. Therefore, the expected uncertainty in the neutron count rate E_{raw} is defined by the standard deviation $\sqrt{E_{raw}}$. Consequently, increasing neutron count rates lead to decreasing relative measurement uncertainty as well as decreasing absolute soil moisture content uncertainty (SCHRÖN, 2017). It is important to realize that the basic uncertainty is introduced by the raw count rate rather than the processed neutron counts after correction. Therefore, the uncertainty analysis must be based on the raw measurement E_{raw} and propagated to the corrected neutron counts with the factor s, the product of the correction factors for pressure, humidity, and incoming cosmic radiation:

$$\sigma_E = s\sqrt{E_{raw}} \tag{2.7}$$

In order to obtain the expected standard deviation of soil moisture content, the uncertainty of the neutron count rates must be propagated through Equation (2.3). One possible

approach is the approximation by an analytical Taylor expansion. We used the method presented by MEKID AND VAJA (2008), which develops the Taylor expansion up to the 3rd polynomial order and considers six central moments in the uncertainty distribution. Since the random detection of neutron counts follow a symmetric Gaussian normal distribution, only the 2nd, 4th, and 6th moments are relevant in this calculation. The 1st, 2nd, and 3rd order approximation of the propagated uncertainty of θ_g ($\sigma_{\theta g}$ [g/g]) are given by:

$$\sigma_{\theta_g}(E_{raw}) = \sqrt{\begin{array}{l}\boxed{\theta'(E)^2{\sigma_E}^2} + \dfrac{1}{2}\theta''(E)^2{\sigma_E}^4 \\ +\theta'(E)\theta'''(E){\sigma_E}^4 + \dfrac{15}{36}\theta'''(E)^2{\sigma_E}^6\end{array}} \tag{2.8}$$

where the rectangles from small to large denote increasing order of approximation (MEKID AND VAJA, 2008). Equation (2.8) requires the 1st, 2nd, and 3rd derivatives of Equation (2.3), which are given by:

$$\theta'(E) = -\frac{p_0}{N_0\left(\frac{E}{N_0} - p_1\right)^2}$$

$$\theta''(E) = \frac{2p_0}{{N_0}^2\left(\frac{E}{N_0} - p_1\right)^3} \tag{2.9}$$

$$\theta'''(E) = -\frac{6p_0}{{N_0}^3\left(\frac{E}{N_0} - p_1\right)^4}$$

For easier implementation of the 3rd order uncertainty approximation, the expressions given in Equations (2.8) and (2.9) can be simplified to:

$$\sigma_{\theta_g}(E_{raw}) = \sigma_E \frac{p_0 N_0}{(E - p_1 N_0)^4}\sqrt{(E - p_1 N_0)^4 + 8{\sigma_E}^2(E - p_1 N_0)^2 + 15{\sigma_E}^4} \tag{2.10}$$

To convert the expected standard deviation from gravimetric to volumetric units ($\sigma_{\theta v}$ [m^3/m^3]) we used:

$$\sigma_{\theta_v}(E_{raw}) = \varrho_{bd}\,\sigma_{\theta_g} \tag{2.11}$$

To validate the proposed Taylor expansion approach, we used a more computationally intensive Monte Carlo uncertainty analysis (e.g., BOGENA ET AL., 2013; BARONI ET AL., 2018). For this, we calculated neutron count rates representative for volumetric soil

moisture content ranging from 0.0 to 0.7 m^3/m^3. This was done using Equations (2.3) and (2.4) by assuming Fendt site conditions (i.e., ϱ_{bd}, θ_{off}, and s) and N_0 values ranging from 0 to 45000 cts. These values were chosen since they cover typical N_0 values for the counting periods of CRN rovers (e.g., AVERY ET AL., 2016: 518 cts/min; DONG AND OCHSNER, 2018: 556 cts/min; VATHER ET AL., 2019: 133 cts/min) aggregated up to 1 h (e.g., DONG AND OCHSNER, 2018: 33360 cts/h), as well as typical N_0 values for long aggregation periods of stationary cosmic ray probes (e.g., BAATZ ET AL., 2014: 936 – 1242 cts/h; BARONI ET AL., 2018: 1438 and 1531 cts/h) aggregated up to 24 h. Subsequently, the synthetic mean neutron count rates were recalculated to raw neutron count rates with $E_{raw} = \frac{1}{s}E$ assuming the average conditions of the Fendt experiment and used to generate large sets of draws from the appropriate Poisson distribution (E_{out}). These were rescaled again with $E_{poisson} = sE_{out}$ and converted to soil moisture content. The standard deviation of the resulting soil moisture content distributions was used to obtain the measurement accuracy as a function of soil moisture content, aggregation time, and N_0.

It should be noted that the non-linear behavior of Equation (2.3) transforms the Gaussian probability distribution of E_{raw} to a skewed distribution of θ_g. Consequently, the uncertainty of θ_g is asymmetric, which cannot be expressed by a single standard deviation as obtained from the uncertainty approximation methods used in this study. However, since the focus is the optimization of CRN rover surveys, we are confident that the presented approaches represent the uncertainty in soil moisture content estimates from uncertain neutron count rates sufficiently well.

Since uncertainties of rover measurements are often more prone to areal than to temporal variation in soil moisture content, we also converted aggregation time to aggregation length for 5, 10, 50, and 100 km/h driving speed using:

$$Aggregation\ length\ [km] = Speed\ \left[\frac{km}{h}\right] \cdot Aggregation\ time\ [h] \tag{2.12}$$

2.2.7 **Other sources of uncertainty**

Additional uncertainties for the estimation of soil moisture content with the CRNS method, such as the uncertainties in the amount of biomass (AVERY ET AL., 2016), N_0, the incoming cosmic ray flux (BARONI ET AL., 2018), air pressure (GUGERLI ET AL., 2019), and humidity are not investigated in this manuscript. However, due to the linear dependency of $\sigma_{\theta v}$ and

soil bulk density (Equation (2.11)), the uncertainty in soil bulk density ($\sigma_{\varrho bd}$) is known to have a particularly strong influence on the volumetric soil moisture product (AVERY ET AL., 2016; BARONI ET AL., 2018). According to error propagation theory, the relative uncertainty of soil bulk density and gravimetric soil moisture content in Equation (2.11) sum up, which leads to the following calculation of volumetric soil moisture content uncertainty:

$$\sigma_{\theta_v}(E_{raw}, \varrho_{bd}) = \varrho_{bd}\sigma_{\theta_g} + \sigma_{\varrho_{bd}}\,\theta_g \tag{2.13}$$

2.2.8 **Neutron aggregation strategies**

For the Fendt experiment, we subdivided the measurement transect into equally long sections while assuring that each section contained at least 100 neutron count measurements. This resulted in ten sections, for which we assumed constant soil moisture content during the four hour measurement campaign. Within each of the sections, we defined a central location using the respective means of the east-west distance and the north-south distance. Subsequently, we selected the ten measurements nearest to the central location and calculated the standard deviation of the first aggregation step using Equation (2.5). In the next aggregation step, the twenty nearest measurements were selected. Then, the first and 11th, second and 12th measurement, etc., were added to obtain 10 aggregated neutron count rates, and the standard deviation was calculated again. This process was continued until less than ten measurement were left. Finally, we used Equations (2.3) and (2.4) to convert the corrected neutron counts to volumetric soil moisture content.

As mentioned above, the neutron count statistics of CRN rover measurements are usually improved by using a moving window filter. However, in many locations more local information is available where streets are intersecting. Therefore, using a nearest neighbor average should improve the measurement accuracy in these locations. We used the Selhausen experiment to compare a moving window aggregation strategy with a nearest neighbor aggregation strategy. We used a moving average filter with a window size of three and nine measurements along the driven route. Analogously, we averaged the neutron counts at each location with the nearest neighbor measurements in a way that the same number of measurements can be compared (e.g., a moving window of nine subsequent measurements is compared to the average of the location and the eight nearest neighbors).

For the Oklahoma experiment, we followed the strategy described by DONG AND OCHSNER (2018). From the average driving speed during data collection (~50 km/h), an average

measurement interval of ~800 m was derived. This was used to generate an ideal route with 800 m spacing between the end, start, and turning points of the transect driven on 7 August 2015. Next, the neutron measurements within different radii from the generated location were averaged for each transect driven. For a more detailed explanation on the averaging strategy, we refer to DONG AND OCHSNER (2018). GIBSON AND FRANZ (2018) and FINKENBINER ET AL. (2019) applied a similar aggregation strategy, but extended it by inverse distance weighting of the averaged neutron measurements. We did not test the potential benefits of this interpolation method as our primary focus was to establish an analytical approach for soil moisture content uncertainty assessment. However, we suggest that the effects of different interpolation methods should be investigated in a separate study.

2.3 **Results and Discussion**

2.3.1 **Expected accuracy – Analytical vs. Monte Carlo approach**

Figure 2.2 shows the standard deviation of soil moisture content as a function of soil moisture content for synthetic neutron count rates using the Fendt site characteristics and N_0 values of 500, 1000, 2000, and 5000 cts, respectively. It is important to note that the presented results are site-specific and depend on soil bulk density, θ_{off}, and s. As expected, the uncertainty in soil moisture content estimation increased with increasing soil moisture content (BOGENA ET AL., 2013). An increase in N_0 (i.e. more aggregation or more efficient detectors) and therefore an increase in the count rate E_{raw} led to substantially lower errors in soil moisture content estimation (Figure 2.2).

In addition, four error estimation methods are compared in Figure 2.2, namely the Monte Carlo approach and the Taylor expansions of 1st, 2nd, and 3rd order. We found that the analytical expressions for measurement uncertainty underestimated the standard deviation for high soil moisture content (> ~0.3 m^3/m^3) when the 1st and 2nd order Taylor expansions were used. For N_0 values larger than 1000, the 3rd order approximation matched the results of the Monte Carlo analysis very well. For low N_0, the 3rd order approximation still deviated from the Monte Carlo simulations (Figure 2.2) with high water content (i.e. low neutron counts). This can be explained by the increasing steepness of Equation (2.3) towards the asymptote present at a neutron count rate of $p_1 N_0$. Overall, we found only minor differences

between Monte Carlo simulations and the 3rd order Taylor expansion to estimate measurement accuracy of soil moisture content due to uncertainty of neutron count rates. Therefore, the 3rd order approximation was used in the remainder of this study.

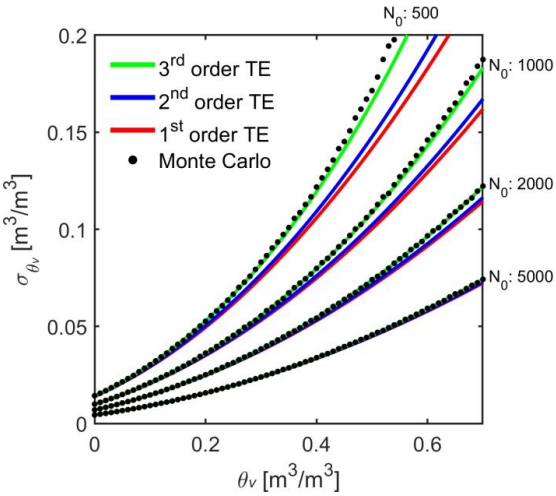

Figure 2.2: Standard deviation of soil moisture content from raw neutron counts ($\sigma_{\theta v}$ [m^3/m^3]) as a function of soil moisture content (θ_v [m^3/m^3]) using N_0 = 500, 1000, 2000, and 5000 cts with Fendt site conditions and soil properties (ϱ_{bd} = 1.028 g/m^3, θ_{off} = 0.072 g/g, and s = 0.6136). The standard deviations were obtained from a Monte Carlo approach and Taylor expansions (TE) of 1st, 2nd, and 3rd polynomial order with Equations (2.8), (2.9), and (2.11).

Figure 2.2 clearly shows that higher count rates will result in lower soil moisture content uncertainty. For this reason, aggregation periods of 12 or 24 h are often used with stationary probes and multiple CRN rover measurements along the same track are averaged. Figure 2.3 shows the aggregation time required to obtain soil moisture content estimates of a specified measurement uncertainty with the Jülich CRN rover and Fendt site conditions. The aggregation time was obtained using the Monte Carlo approach and the 3rd order Taylor expansion approach. In addition, the aggregation time was converted to aggregation length using Equation (2.12). For soil moisture contents below 0.4 m^3/m^3, an aggregation time of 10 min is necessary to achieve a measurement uncertainty below 0.03 m^3/m^3 with the Jülich CRN rover and Fendt site conditions. Correspondingly, this measurement uncertainty can be achieved with increasing spatial aggregation depending on the driving speed. For instance, aggregation lengths of ~1, ~2, ~10, and ~20 km are needed for driving speeds of 5, 10, 50, and 100 km/h, respectively (Figure 2.3).

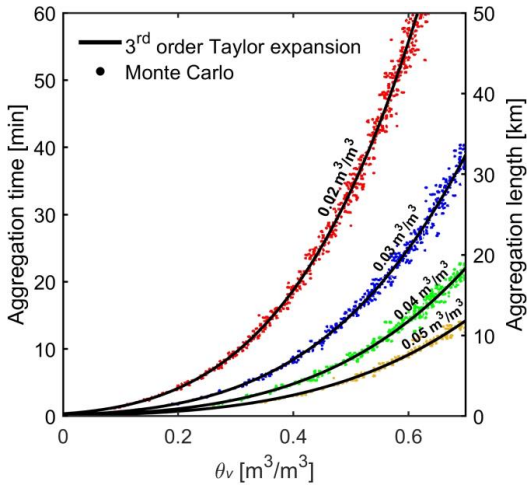

Figure 2.3: Aggregation time / aggregation length with 50 km/h travelling speed required to obtain soil moisture content estimates (θ_v [m^3/m^3]) with 0.02, 0.03, 0.04, and 0.05 m^3/m^3 measurement uncertainty expressed as standard deviation from raw neutron counts ($\sigma_{\theta v}$ [m^3/m^3]) as function of soil moisture content. The standard deviation was obtained from a Monte Carlo approach and a Taylor expansion approach of 3rd polynomial order with Equations (2.8), (2.9), and (2.11) and the presented estimates are valid for neutron measurements with the Jülich CRN rover and Fendt site conditions (N_0 = 753 cts/min, ϱ_{bd} = 1.028 g/m^3, θ_{off} = 0.072 g/g, and s = 0.6136). The aggregation length can be converted linearly to other aggregations lengths and corresponding travelling speeds with Equation (2.12) (e.g., for 100 km/h multiply tick marks with 2, for 10 km/h divide the tick marks by 5, and for 5 km/h divide tick marks by 10).

It is important to note that the measurement uncertainty presented in Figure 2.2 and Figure 2.3 only considered uncertainty in neutron count rate, and thus does not include other sources of uncertainty in CRN soil moisture content estimates, such as the uncertainty in soil bulk density (AVERY ET AL., 2016; BARONI ET AL., 2018). Figure 2.2 suggests that a soil moisture content of 0.3 m^3/m^3 is associated with an uncertainty of 0.056 m^3/m^3 for N_0 = 1000 cts due to uncertain neutron counts. An uncertainty of 20 % in bulk density would add an additional uncertainty of 0.06 m^3/m^3 according to Equation (2.13). Thus, the combined uncertainty due to uncertain soil bulk density and raw neutron counts would be 0.116 m^3/m^3. It is clear that above a minimum threshold of raw neutron counts, the greatest absolute uncertainty in volumetric soil moisture content estimates using CRNS technology can be attributed to soil bulk density (AVERY ET AL., 2016). The framework presented here can be used to determine such a minimum threshold for a particular site, which is shown exemplary in Figure 2.4 for the Fendt site. For this, we obtained the uncertainty in soil moisture content estimation with fixed neutron count rates E_{raw} for different values of N_0 using Equations (2.10) and (2.11). If we assume a 20 % uncertainty in soil bulk density and a soil moisture content range from 0.2 to 0.4 m^3/m^3, the uncertainties in soil bulk density

and raw neutron counts are approximately equal, when there are 500 cts/unit area. For a soil moisture content of 0.4 m^3/m^3 the combined uncertainties (Equation (2.13)) from 20 % uncertainty in soil bulk density and 1000 cts/unit area is ~0.13 m^3/m^3. As we lack estimates of the uncertainty in bulk density for the case studies presented here, we focus on the uncertainty from raw neutron counts in the remainder of this manuscript.

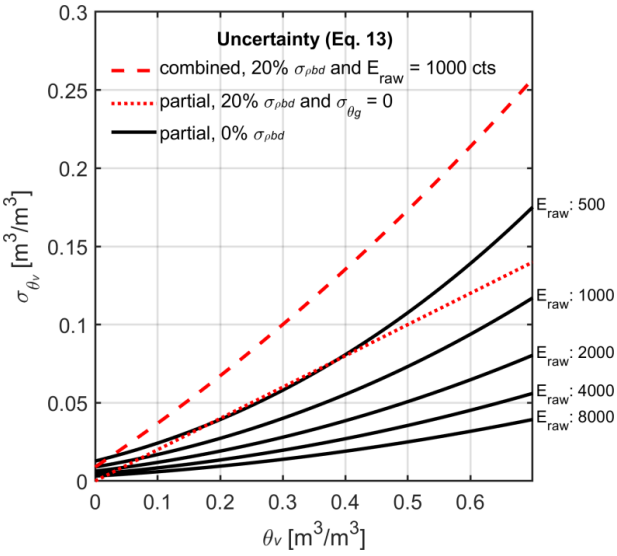

Figure 2.4: Standard deviation from raw neutron counts ($\sigma_{\theta v}$ [m^3/m^3]) as a function of soil moisture content (θ_v [m^3/m^3]) using fixed E_{raw} = 500, 1000, 2000, 4000, and 8000 cts and variable N_0s representative for soil moisture contents between 0 and 0.7 m^3/m^3 at the Fendt site (ϱ_{bd} = 1.028 g/m^3, θ_{off} = 0.072 g/g, and s = 0.6136) obtained with Equation (2.11). For comparison, the standard deviation from soil bulk density ($\sigma_{\varrho bd}$) in units of soil moisture content as a function of soil moisture content, assuming 20 % uncertainty in bulk density and the combined uncertainty from soil bulk density and raw neutron counts in units of soil moisture content as a function of soil moisture content, assuming E_{raw} = 1000 and 20 % uncertainty in bulk density (Equation (2.13)), is shown.

2.3.2 **Experiment A (Fendt site)**

The measurements at the Fendt site (Experiment A) were acquired to illustrate the accuracy of the 3rd order approximation to estimate measurement uncertainty of actual CRN roving measurements. The minimum, average, and maximum count rates were 402, 606, and 810 cts/min, respectively, before correction (E_{raw}). After correction, we observed a distinct reduction in neutron count rates, which is mostly attributed to the atmospheric pressure correction (responsible for an average reduction of ~35 %). It is important to note that the large reduction due to the pressure correction occurred because we normalized to standard pressure (1023.25 hPa). The use of a different reference value (e.g., the average pressure

during the measurement campaign) would reduce this effect. Minimum, average, and maximum count rates after correction (E) were 246, 372, and 504 cts/min, respectively. The measurement transect showed a distinct gradient in epithermal neutron count rates, with increasing environmental water content towards the east and corresponding decreasing epithermal neutron count rates (Figure 2.5a). The gradient in neutron counts was dominated by the road at the western end and the small stream at the eastern end of the transect (Figure 2.5a-b). These additional influences were considered during calibration and validation by adding artificial measurement points along the road and the stream (see Figure 2.5b). It is perhaps possible to correct neutron counts for the road influence with the approach from SCHRÖN ET AL. (2018a), but this was not tested here because this correction would not have influenced the error estimation because it is based on raw neutron counts. To our knowledge, there is currently no correction approach for nearby water bodies available. Here, we assumed homogeneous soil moisture equivalent values of 0.07 m^3/m^3 for the road (SCHRÖN ET AL., 2018a) and 1.0 m^3/m^3 for the stream, respectively, and the density of the artificially added points to consider roads and water bodies corresponded to the in-situ measurements.

To guide the visual analysis of the results, we divided the measurement transect into 10 sections. The expected and measured uncertainty of E_{raw} with increasing aggregation is shown in Figure 2.5c. Both showed very similar behavior with increasing aggregation in most sections. Exceptions were sections 5 and 9, where the measured standard deviation of the counts was lower than expected. Figure 2.5d shows the standard deviation of measured soil moisture content calculated with Equations (2.3) and (2.4) and the expected standard deviation calculated with Equations (2.10) and (2.11) (3^{rd} order Taylor expansion) as a function of spatial aggregation. With the exception of sections 5, 9, and 10, all sections showed a good agreement between the expected and measured uncertainty of soil moisture content. Generally, the standard deviation of measured soil moisture content was relatively high (> 0.05 m^3/m^3) even after aggregation. This can be explained by the relatively short maximum aggregation time per section, which varied between 1.5 and 2.5 min. Such short aggregation times lead to a high measurement uncertainty as shown in Figure 2.3. To achieve a measurement accuracy of 0.05 m^3/m^3 at a soil moisture content of 0.60 m^3/m^3 (e.g., section 10), it would be required to aggregate for more than 10 minutes (cf. Figure 2.3). To achieve the same measurement accuracy for a soil moisture content of 0.3 m^3/m^3 (e.g., section 1), an aggregation time of 2.5 min would have been sufficient.

Figure 2.5e shows the CRN rover derived soil moisture content with increasing aggregation time as well as the mean reference in-situ soil moisture content of each section. In most sections, the mean reference soil moisture content fell within the range of the standard deviation of soil moisture content. We found the largest deviations between the reference in-situ soil moisture content and CRN rover derived soil moisture content in sections 5 and 10 (Figure 2.5e). A possible explanation is that within these two sections the environmental moisture conditions were not constant as assumed in the analysis approach. This is consistent with earlier results of SCHRÖN ET AL. (2018b), who found that small differences in position can significantly influence soil moisture content estimates from CRN probes in complex environments.

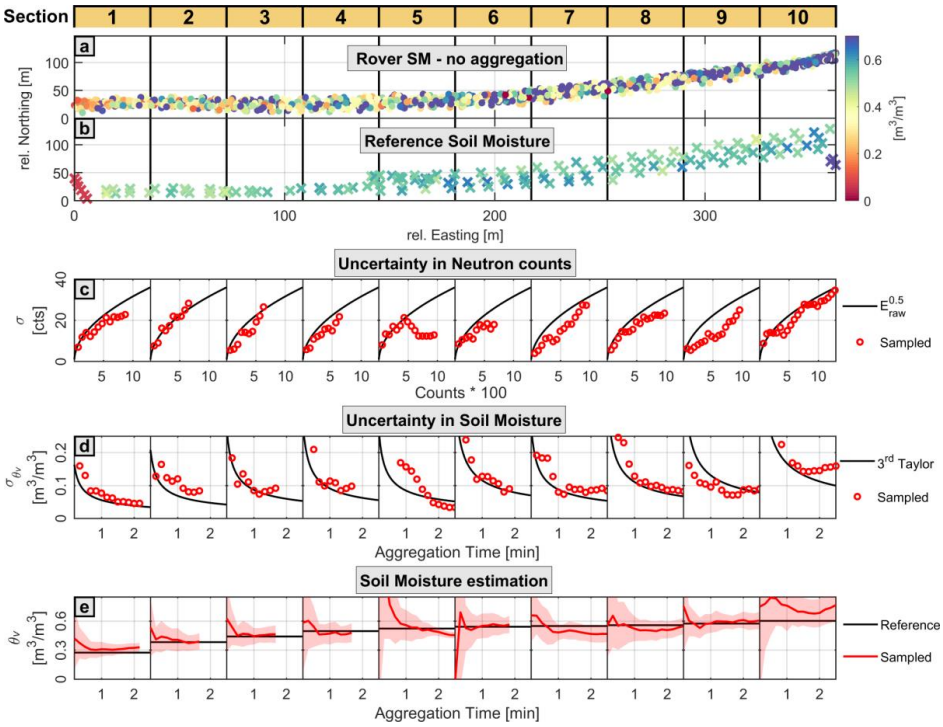

Figure 2.5: Overview of the results from the Fendt experiment for each of the ten analyzed sections. a) CRN rover soil moisture content without aggregation. b) In-situ reference soil moisture content. The relative coordinates in subplots a) and b) were calculated from UTM coordinates. c) Expected standard deviation of raw neutron counts (σ). d) 3rd order approximation of standard deviation of soil moisture content from raw neutron counts ($\sigma_{\theta v}$) in comparison to measured standard deviation with the CRN rover. e) Soil moisture content (θ_v) estimated with the CRN rover in comparison with mean reference soil moisture content for each section. Red area indicates ± one measured standard deviation of the mean.

2.3.3 **Experiment B (Selhausen site)**

The measurements from the Selhausen experiment were used to compare different aggregation scales and strategies. Minimum, average, and maximum count rates were 450, 654, and 888 cts/min, respectively, before correction (E_{raw}). After correction, we observed a moderate reduction in neutron count rates and the incoming neutron correction had the greatest influence (responsible for an average reduction of ~10 %). Minimum, average, and maximum count rates after correction (E) were 408, 588, and 798 cts/min, respectively.

The estimated soil moisture content was very low (< 0.15 m^3/m^3, Figure 2.6) due to the extended drought period before and during the campaign. The soil moisture content estimates of the CRN rover showed low values in the northeast and high values in the southwest, which reflects differences in soil texture (RUDOLPH ET AL., 2015; BROGI ET AL., 2019; Figure 2.6). Reference soil moisture content measurements were even lower (< 0.1 m^3/m^3) than the soil moisture content estimates from CRN roving.

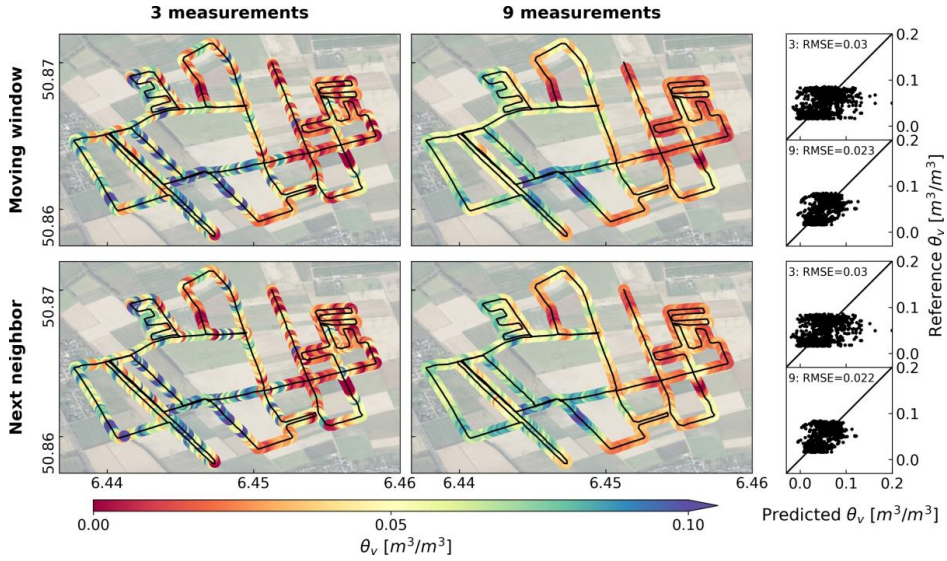

Figure 2.6: Comparison of four aggregation strategies with the Jülich CRN rover at the Selhausen site with data measured on 11 July 2018. Top panels: moving window aggregation for three and nine following measurements, respectively. Bottom panels: nearest neighbor aggregation with the nearest two and eight neighbors, respectively. The scatter plots show the reference soil moisture content (θ_v) measurements (horizontally averaged according to SCHRÖN ET AL. 2017) as a function of the predicted soil moisture content from the CRN rover. Base maps: ESRI World Imagery and Contributors.

A correction for the effect of biomass on the soil moisture content estimates was attempted using two approaches: 1) a linear regression between N_0 and in-situ measured biomass (e.g., BAATZ ET AL., 2015), and 2) the thermal-to-epithermal neutron ratio method (JAKOBI ET AL., 2018). Both correction methods did not result in substantial improvements of the soil moisture content estimates. We also attempted to remove road effects on the measured neutron count rate using the approach of SCHRÖN ET AL. (2018a). However, this also did not result in an improvement, which was perhaps related to the dry conditions. Soil moisture content was lower than or equal to the soil moisture equivalents of different road types (grassy pathways, dirt roads and asphalt), which is unusual and was not considered in the development of the correction approach (SCHRÖN ET AL., 2018a).

Aggregation clearly improved the accuracy of soil moisture content estimates as indicated by the lower RMSE, irrespective of aggregation strategy (Figure 2.6). Only minor differences were found for the aggregation approaches both in the case of three and nine measurements. In the case of the aggregation of nine measurements, the most pronounced differences occurred near crossroads or for closely separated tracks (Figure 2.7). If only three measurements were aggregated, the differences were more variable due to the high measurement uncertainty, but they occurred in the same locations for both cases. A drawback of the nearest neighbor aggregation approach is that the processing algorithm potentially also takes measurements into account that were taken on parallel roads, even though they may have different water contents (cf. Figure 2.7).

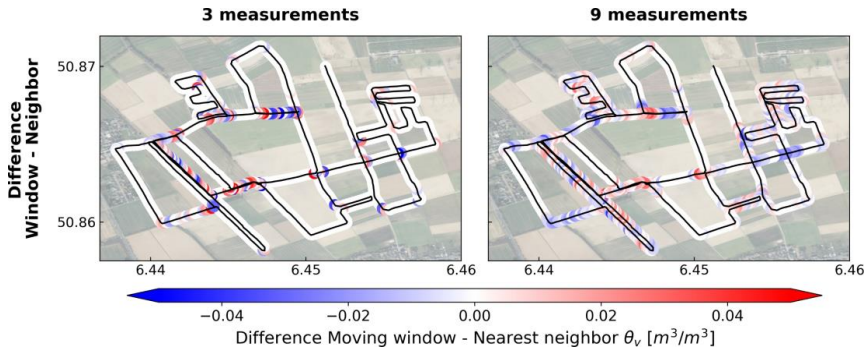

Figure 2.7: Difference in soil moisture content (θ_v) between moving window and nearest neighbor aggregation strategies for three and nine aggregated measurements. Base maps: ESRI World Imagery and Contributors.

At first sight, the results from this experiment looked satisfying because of the relatively low reported RMSEs. However, the expected soil moisture content estimation uncertainty

using Selhausen site conditions (Figure 2.8) were similar to the overall uncertainty as expressed by the RMSE when only 3 measurements were used (0.032 m^3/m^3). This is undesirable, and suggests the need for more aggregation. When nine measurements were aggregated, the average uncertainty due to uncertain neutron measurements decreased to 0.017 m^3/m^3 irrespective of aggregation strategy. Also, the patterns of soil moisture content uncertainty distribution varied minimally between the aggregation strategies (Figure 2.8).

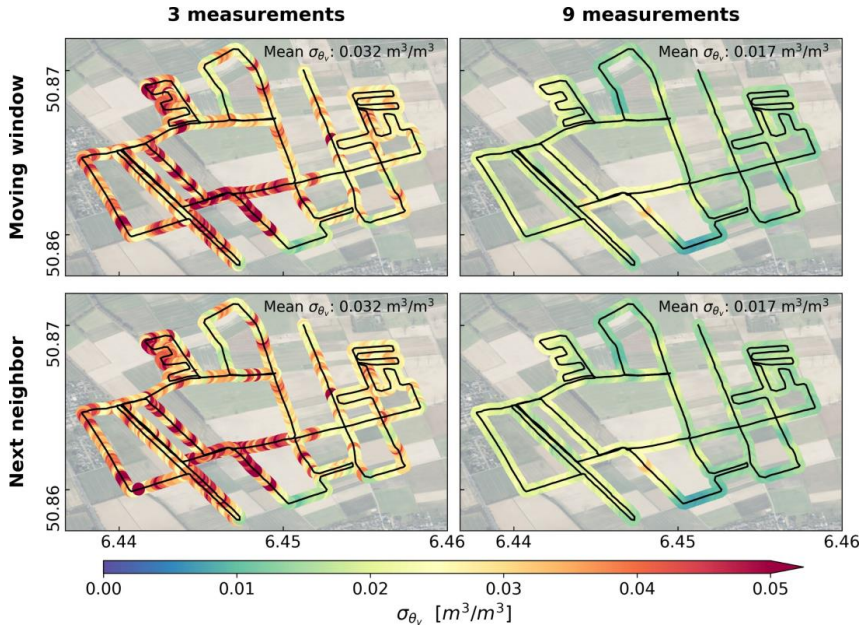

Figure 2.8: Comparison of soil moisture content uncertainty from neutron counts (σ_{θ_v}) estimation with four aggregation strategies with the Jülich CRN rover at the Selhausen site with data measured on 11 July 2018. Top panels: moving window aggregation for three and nine following measurements, respectively. Bottom panels: nearest neighbor aggregation with the nearest two and eight neighbors, respectively. Base maps: ESRI World Imagery and Contributors.

This measurement campaign illustrates the required compromise between aggregation time and spatial resolution that is sometimes necessary for CRN rover measurements. In order to achieve lower uncertainty, the driving speed would have to be much lower. However, the vehicle did not allow lower driving speeds. Alternatively, one can increase the aggregation scale, with the drawback of less spatial resolution of the resulting soil moisture map. However, this led only to a slight reduction in RMSE (e.g., aggregation of 36 measurements led to a RMSE of 0.018 m^3/m^3). Since further aggregation only had a minor influence on the RMSE, we attribute the remaining part of the RMSE to other influences. Important additional sources of error were the spatial variability in bulk density, the

heterogeneous vegetation, roads of different size and nature, as well as the inconsistency between in-situ and CRN rover measurements (both in time and depth).

2.3.4 **Experiment C (Oklahoma site)**

Figure 2.9 provides an overview of the data from DONG AND OCHSNER (2018) with 800, 1600, and 2400 m aggregation length for soil moisture content, expected standard deviation, as well as the relative standard deviation ($\frac{\sigma_{\theta_v}}{\theta_v}$). Using the original aggregation to 800 m, the mean soil moisture content was 0.19 m^3/m^3 and the estimated mean standard deviation for all CRN rover measurements was 0.039 m^3/m^3, which is still below the error benchmark of 0.04 m^3/m^3 defined for the soil moisture active passive (SMAP) satellite mission (CHAN ET AL., 2014). However, both soil moisture content and the estimated standard deviation were spatially and temporally variable (Figure 2.9, upper and middle panel). As expected, the soil moisture content and standard deviation of soil moisture content showed a very similar pattern (Figure 2.9, upper and middle panel), while the relative standard deviation showed a different pattern (Figure 2.9, lower panel). There were two reason for this difference. First, some high relative standard deviation values were related to locations with only a few measurements within one pixel, which appear as red stripes across most measurement days in the lower panel of Figure 2.9. Second, measurement days with low soil moisture content and relatively low standard deviation nevertheless showed high relative errors. This is in line with the high relative uncertainty we found for the Selhausen site (Experiment B). Measurement days with high soil moisture content and relatively high standard deviation nevertheless showed lower relative errors (Figure 2.9, compare driest and wettest measurement date). With increasing aggregation length, sharp transitions in soil moisture content estimates of neighboring pixels are reduced (Figure 2.9, top panel) and both the absolute (Figure 2.9, middle panel) and relative standard deviation of soil moisture content (Figure 2.9, lower panel) are reduced.

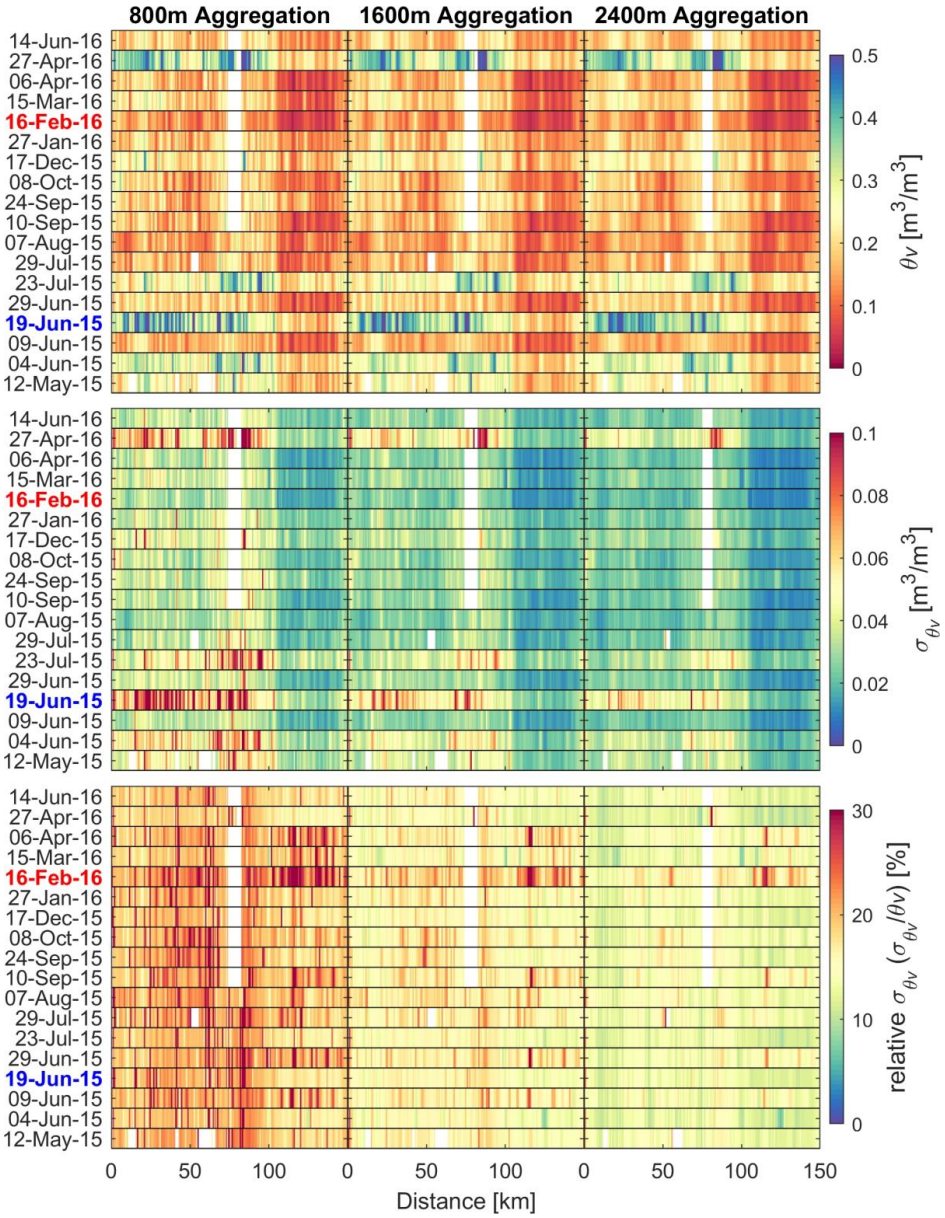

Figure 2.9: Soil moisture content (θ_v), uncertainty of soil moisture content from neutron counts ($\sigma_{\theta v}$) approximated using a 3rd order Taylor expansion approach and relative standard deviation ($\sigma_{\theta v}/\theta_v$) using 800, 1600, and 2400 m aggregation along the measurement transects in Oklahoma. White patches are areas not covered during a measurement date due to road closures (DONG AND OCHSNER, 2018). Blue and red dates indicate the wettest and driest measurement dates, respectively.

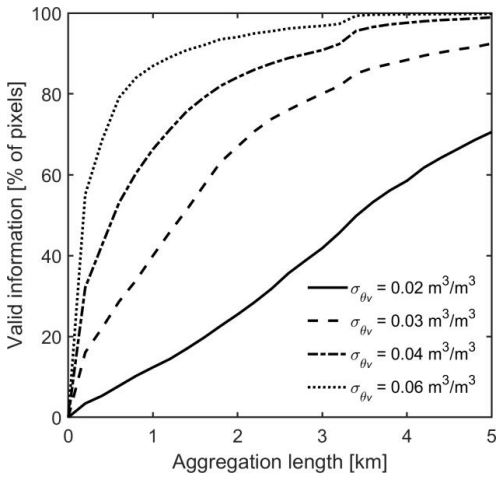

Figure 2.10: Percentage of pixels with soil moisture content uncertainty from neutron counts ($\sigma_{\theta v}$) ≤ 0.02, 0.03, 0.04, and 0.06 m^3/m^3 standard deviation as a function of aggregation length.

To evaluate the trade-off between aggregation length and expected standard deviation for the Oklahoma CRN rover data, we determined the proportion of pixels with an expected measurement uncertainty below 0.02, 0.03, 0.04, and 0.06 m^3/m^3 for different aggregation lengths (Figure 2.10). With increasing aggregation lengths, the number of pixels with valid information increased and this increase became stronger with increasing uncertainty thresholds. Less than 40 % of the pixels had a measurement uncertainty below 0.03 m^3/m^3 for the original aggregation length of 800 m solely due to the neutron count uncertainty. This is consistent with the analysis of DONG AND OCHSNER (2018), who estimated the average measurement uncertainty for 800 m aggregation length as 0.03 g/g, which corresponds to ~0.044 m^3/m^3. Only at locations with low soil moisture content (< ~0.14 m^3/m^3), the expected measurement uncertainty was lower than 0.02 m^3/m^3. If all CRN rover locations were required to have a measurement uncertainty below 0.04 m^3/m^3, an aggregation length of more than 5 km would be necessary. However, already with 2400 m aggregation length, the measurement uncertainty in the drier part of the measurement transect was lower than this (Figure 2.9, top and middle panel: km 110 – 150).

Although we cannot recommend a universal aggregation length, we believe that the presented uncertainty approximation approach can serve as a tool for assessing the best possible compromise between measurement accuracy and spatial resolution. It should be noted that it is not possible to determine the uncertainty without taking into account site conditions and rover specifications and that the presented uncertainties are best possible

estimates as other sources of uncertainty have not yet been taken into account. In general, the aggregation length should be carefully tailored to the needs of users, the capabilities of the CRN rover, and the site conditions. In addition to the uncertainty in the neutron count rate, further uncertainties in the soil moisture content estimation with the dataset from DONG AND OCHSNER (2018) are worthwhile mentioning. First, the influence of vegetation on soil moisture content estimates was not considered. Promising approaches for removing these influences are the use of airborne (e.g., FERSCH ET AL., 2018) or satellite (e.g., AVERY ET AL., 2016) derived biomass estimates. Second, the influence of roads was not considered, which most likely resulted in underestimation of soil moisture content in most measurement locations (SCHRÖN ET AL., 2018a). Third, the derivation of lattice water (θ_{off}) and soil bulk density from uncertain soil maps, such as the SSURGO database, will introduce uncertainty in soil moisture content estimation. However, this has been demonstrated in several other studies (e.g., AVERY ET AL., 2016; MCJANNET ET AL., 2017) and is challenging to overcome. Fourth, soil organic carbon is an additional hydrogen pool in soils that should be considered for accurate soil moisture content estimation (FRANZ ET AL., 2013b). Regarding the influence of some of those environmental factors and their uncertainty, the reader is referred to BARONI ET AL. (2018).

2.4 **Conclusion and Outlook**

In this study, we quantified the uncertainty in soil moisture content estimation with cosmic ray neutron measurements with an easy to use 3rd order Taylor expansion approach. The performance was evaluated using Monte Carlo simulations and experimentally determined measurement uncertainty and we found good agreement. Because of the typically short aggregation time and thus a low amount of neutron counts, soil moisture content estimates obtained with cosmic ray neutron rover measurements are typically more uncertain than those obtained using stationary measurements. The proposed approach to approximate measurement uncertainty in soil moisture content estimates has great potential for the planning and evaluation of rover experiments. It was shown that such uncertainty estimates can be used to find a suitable trade-off between measurement accuracy, aggregation, and the associated spatial resolution of the resulting soil moisture products.

The approach can also be used to design surveys with the cosmic ray neutron rover according to given accuracy requirements. We applied our error estimation approach to three cosmic ray neutron rover experiments and the major findings were:

- Measured and expected uncertainty matched well even with short aggregation periods.
- Uncertainty in soil moisture content estimation from uncertainty in cosmic ray neutron counts can be reduced to only a fraction of the total measurement uncertainty if appropriate aggregation is used.
- The aggregation length of an experiment needs to be carefully selected based on the needs of the user, taken into account the site characteristics and the cosmic ray neutron rover specifications.

3 The footprint characteristics of cosmic ray thermal neutrons

Abstract

The advance of the cosmic ray neutron (CRN) sensing method for estimating field scale soil moisture content relied largely on simulations of the footprint properties of epithermal neutrons (~0.5 eV – 100 keV). Commercially available CRN probes are usually additionally equipped with a thermal neutron (< 0.5 eV) detector. The potential of these measurements is rarely explored because relevant features of thermal neutrons, such as the footprint and the sensitivity to soil moisture content are unknown. Here, we used neutron transport modeling and a river crossing experiment to assess the thermal neutron footprint. We found that the horizontal thermal neutron footprint ranges between 43 and 48 m distance from the probe and that the vertical footprint extends to soil depths between 10 and 65 cm depending on soil moisture content. Furthermore, we derived weighting functions that quantify the footprint characteristics of thermal neutrons. These results will enable new applications of thermal neutrons.

Key Points

- The cosmic ray thermal neutron footprint was assessed with neutron transport simulations and a river-crossing experiment
- The thermal neutron footprint ranges between 43 and 48 m distance and 10 to 65 cm depth dependent on soil moisture content
- The dependency of the thermal neutron footprint on air humidity is small compared to its dependency on soil moisture content

---

This chapter is based on a journal article published as:

JAKOBI, J., HUISMAN, J. A., RASCHE, D., VEREECKEN, H., AND BOGENA, H. R. (2021), The footprint characteristics of cosmic ray thermal neutrons, *Geophys Res Lett*, 48(15), doi: 10.1029/2021GL094281.

3.1 **Introduction**

Cosmic ray neutron (CRN) sensing is a non-invasive method for intermediate scale soil moisture content measurements (ZREDA ET AL., 2008). This method relies on the inverse dependence of aboveground epithermal neutrons (energy range from ~0.5 eV to 100 keV) on the environmental hydrogen content in a footprint of 130 to 240 m radius and soil depths ranging from 15 to 83 cm (KÖHLI ET AL., 2015; SCHRÖN ET AL., 2017). In terrestrial environments, most hydrogen is stored in water in soils. Therefore, it is possible to infer soil moisture content from the amount of aboveground epithermal neutrons. Secondary hydrogen pools, such as biomass, have a large impact on the measurement accuracy, especially when they are not constant in time. For reliable soil moisture content estimation, these secondary pools thus need to be considered (BOGENA ET AL., 2013; FRANZ ET AL., 2013b; BAATZ ET AL., 2014). Recently, it was found that by additionally considering the thermal neutron intensity below ~0.5 eV, aboveground biomass can be inferred using the ratio of thermal-to-epithermal neutrons (TIAN ET AL., 2016; JAKOBI ET AL., 2018).

CRN sensors are currently installed in approximately 200 locations worldwide (ANDREASEN ET AL., 2017b). Many of these locations are also instrumented with thermal neutron detectors. However, these extensive data sets are rarely explored because key properties of the thermal neutron signal, such as the footprint of thermal neutrons, are not well defined. Preliminary investigations suggest that the thermal neutron footprint is smaller than the epithermal neutron footprint and in the order of tens of meters (BOGENA ET AL., 2020). For the improved interpretation of the epithermal neutron signal, horizontal and vertical weighting functions were of great importance. However, such weighting functions are still lacking for thermal neutrons. In addition, the dependence of the thermal neutron footprint on soil moisture content and chemical composition is still under debate (e.g., ZREDA ET AL., 2008; ANDREASEN ET AL., 2016; TIAN ET AL., 2016; JAKOBI ET AL., 2018).

In this study, we present CRN measurements as well as Monte Carlo simulations using the neutron transport model URANOS (Ultra Rapid Adaptable Neutron-Only Simulations, KÖHLI ET AL., 2015). In a first step, we show that URANOS can describe measured thermal neutron fluxes. In a second step, we derive horizontal and vertical weighting functions that describe the thermal neutron footprint from URANOS simulations.

3.2 **Material and Methods**

3.2.1 **River experiment**

According ZREDA ET AL. (2012), coastal transect experiments with mobile CRN detectors are useful to obtain a coarse understanding of CRN footprints and to evaluate neutron intensities simulated with neutron transport models. We measured the changes in neutron intensity along an approx. 1 km long transect with a ferry crossing over the approx. 400 m wide Rhine river near Cologne (central coordinates: 51.056, 6.918) on two days in 2020 (9 September with dry conditions and 21 November with moist conditions). For this, we used the Jülich CRN rover consisting of an array of nine detector units, each holding four $^{10}BF_3$ filled neutron probes (Hydroinnova LLC, Albuquerque, NM, USA). Commonly used neutron detectors are far more sensitive to thermal neutrons than to epithermal neutrons. To increase the sensitivity to epithermal neutrons, the detectors are surrounded with high-density polyethylene (HDPE) that moderates a large fraction of the arriving neutrons to lower energy levels. During the experiment we measured neutron intensities with five moderated (with HDPE) and four bare (without HDPE) detector units. To reduce the uncertainty associated to the number of neutron counts (Chapter 2), we crossed the river four and six times during the dry and moist conditions, respectively. The maximum driving speed during data acquisition was ~5 km/h. The time interval between two readings was set to 10 seconds. In addition to accumulated neutron counts, pressure, humidity, and GPS position were recorded. All measurements were assigned to half of the driven distance between two readings. We linearly interpolated hourly incoming neutron counts obtained from the neutron monitor located on the Jungfraujoch (JUNG, available via the NMDB neutron monitor database at www.nmdb.eu) to the measurement times and used these alongside the pressure and humidity measurements to obtain corrected moderated neutron counts (see Appendix I). Neutron counts measured with the bare detector were only corrected for pressure and humidity (cf. JAKOBI ET AL., 2018). We also measured soil moisture content in the top 6 cm of the soil on both sides of the river using HydraProbe sensors (Hydra Go Field Version, Stevens Water Monitoring Systems, Inc., Portland, USA). In total, ~300 measurements were made in dry conditions and ~200 measurements in moist conditions. Along the measuring transect, different amounts of biomass (i.e. bushes and trees) were present on both sides of the river at distances > ~70 m from the shores.

3.2.2 **Neutron transport modeling**

We used the URANOS Monte Carlo neutron interaction code for neutron transport modeling (KÖHLI ET AL., 2015). The neutron physics of URANOS is based on a ray-casting engine with a voxel geometry. It considers all relevant interaction processes between neutrons and atomic nuclei, such as absorption and evaporation as well as elastic and inelastic collisions in the fast, epithermal, and thermal neutron energy regime (KÖHLI ET AL., 2015). Several previous neutron modeling studies used simplified approaches where neutrons were launched from within the ground (e.g., ZREDA ET AL., 2008; DESILETS ET AL., 2010) or only secondary neutrons were launched (e.g., FRANZ ET AL., 2013a; ROSOLEM ET AL., 2013). Here, neutrons are launched from a horizontal layer above the soil surface using a realistic energy spectrum (SATO AND NIITA, 2006; SATO, 2015) for the given geographic location and height above ground (KÖHLI ET AL., 2015). The model domain used in this study represents an area of 2000 x 2000 m with the source layer having an edge length of 2600 m and a height that extends from 50 to 80 m. The cutoff rigidity was set to 10 GeV and for each model run, 10^6 source neutrons were simulated. The air medium extended to 1000 m height and consisted of 78 $\%_{vol}$ nitrogen, 21 $\%_{vol}$ oxygen, and 1 $\%_{vol}$ argon at a pressure of 1020 mbar. The soil extended to 5 m depth and was a homogeneous silica soil consisting of 50 $\%_{vol}$ solid material, of which 75 $\%_{vol}$ was SiO_2 and 25 $\%_{vol}$ was Al_2O_3. The soil bulk density was 1.43 g/cm^3 and the pore space of the soil was filled with H_2O and air with the same composition as in the atmosphere. All neutrons that passed a horizontally infinite detector layer between 1.75 and 2 m above ground were recorded if they had prior soil contact. Using a detector layer instead of a dedicated volume detector is equivalent to many detectors located side-by-side (cf. KÖHLI ET AL., 2015), and dramatically decreases the number of neutrons that need to be simulated.

3.2.3 **Evaluation of model results**

Neutrons exhibit different sensitivity and behavior depending on their energy level, which needs to be considered when evaluating neutron modeling results. Here, we consider neutrons ≤ 0.5 eV and define these as thermal neutrons. This cutoff energy allows for a comparison with earlier modeling results with the Monte Carlo N-Particle Extended (MCNPX) model (e.g., MCJANNET ET AL., 2014; ANDREASEN ET AL., 2016; 2020).

The kinetic energy of epithermal neutrons decreases monotonically with the number of scattering interactions. In contrast, the kinetic energy of thermal neutrons can increase due to interactions with the environment. Therefore, it is possible that the energy of a thermal neutron increases above 0.5 eV again after the initial thermalization. We do not consider the scattering interactions above 0.5 eV for the presented footprint calculations because we expected different behaviour due to their higher energies. Thus, scattering interactions of neutrons with energies above 0.5 eV that subsequently have energies below 0.5 eV are considered as if the energy threshold were never exceeded. If the kinetic energy between two interactions increased by ≥ 1 eV, we assume that it was absorbed and that a new neutron was released by the target nucleus (i.e., via evaporation).

Following earlier studies describing the epithermal neutron footprint (DESILETS AND ZREDA, 2013; KÖHLI ET AL., 2015; SCHRÖN ET AL., 2017), we define the horizontal footprint (R_{86}) as the lateral distance that 86 % of the thermal neutrons travelled from their first soil contact (as thermal neutron) until the passing of the detector layer. The vertical footprint (D_{86}) is defined as 86 % of the depth of all scattering interactions in soil that thermal neutrons experienced before passing the detector layer.

3.3 **Results**

3.3.1 **River experiment**

Figure 3.1 shows the results for the measured transect across the Rhine River. On the first measurement day, the soil along the river was significantly drier (red dots; ~0.06 m^3/m^3) than on the second day (blue dots; ~0.23 m^3/m^3). As expected, significantly lower neutron intensities were measured on the river compared to the shore areas for both moderated and bare detectors. This difference is less pronounced for moderated detectors than for bare detectors. In addition, the moderated neutrons at the shore showed a clear soil moisture content dependence, while the neutrons measured with the bare detectors were less affected by soil moisture content.

Figure 3.1 also shows URANOS simulation results for different soil moisture contents of the shores ranging from 0.10 to 0.50 m^3/m^3. For this, air humidity (8 g/m^3) and air pressure (1011 mbar) were set to the average conditions during the experiment with dry conditions. The cutoff rigidity was set to 3.15 GeV and obtained from the COSMOS Cutoff Rigidity

Calculator (http://cosmos.hwr.arizona.edu/Util/rigidity.php). Neutrons passing the detector layer were accumulated in 50 m distance intervals from the river center. Moderated neutron counts were assumed to constitute of 70 % epithermal neutrons (1 eV – 1 MeV) and 30 % thermal neutrons (McJannet et al., 2014), which is a first order estimate because the actual mixing ratio measured by a moderated detector also contains up to 40 % neutrons with energies above 1 MeV and also depends on ambient hydrogen content (Köhli et al., 2018). To consider the energy-dependent sensitivity of the neutron detector, we approximated the neutron counts of a bare detector by weighting the neutrons passing the detector layer with $\frac{1}{\sqrt{Energy}}$ (Weimar et al., 2020). We observed variable amounts of biomass along the driven transect and assumed this to amount to up to 23 kg/m^2. To account for the influence of aboveground biomass (Franz et al., 2013b; Jakobi et al., 2018), we reduced the modeled moderated neutron intensities by 0.925 % per kg/m^2 (Baatz et al., 2015).

The URANOS model was able to reproduce reasonably well the trends in both moderated and bare neutron intensity along the transect. A simulated soil moisture content of 0.2 m^3/m^3 provided the best agreement with the measured moderated neutron intensity during the dry experiment, which is higher than the measured value of 0.06 m^3/m^3 of the upper 6 cm. We attributed this to higher soil moisture content at greater depths, resulting in a higher effective soil moisture content within the penetration depth of the CRN detector. Similarly, the measured moderated neutron intensity during the wet experiment showed the best agreement with a simulated soil moisture content of 0.40 m^3/m^3 (measured soil moisture content was 0.23 m^3/m^3 in the upper 6 cm). Both the measured and modeled bare neutron intensities showed stronger gradients than the moderated neutrons near the riverbanks and no clear dependence on soil moisture content. The stronger near-shore gradients confirm that the thermal neutron footprint is substantially smaller than the epithermal neutron footprint. However, the footprint cannot be accurately identified with such experimental setups, as it is deformed and biased to drier areas and thus lacks the radial symmetry required to derive a meaningful footprint (Köhli et al., 2015; Schattan et al., 2019). The reasonable agreement between the observed and simulated neutron intensities shows that the relevant physical processes are sufficiently considered in URANOS. Therefore, it will be used to assess the footprint characteristics of thermal neutrons in the following.

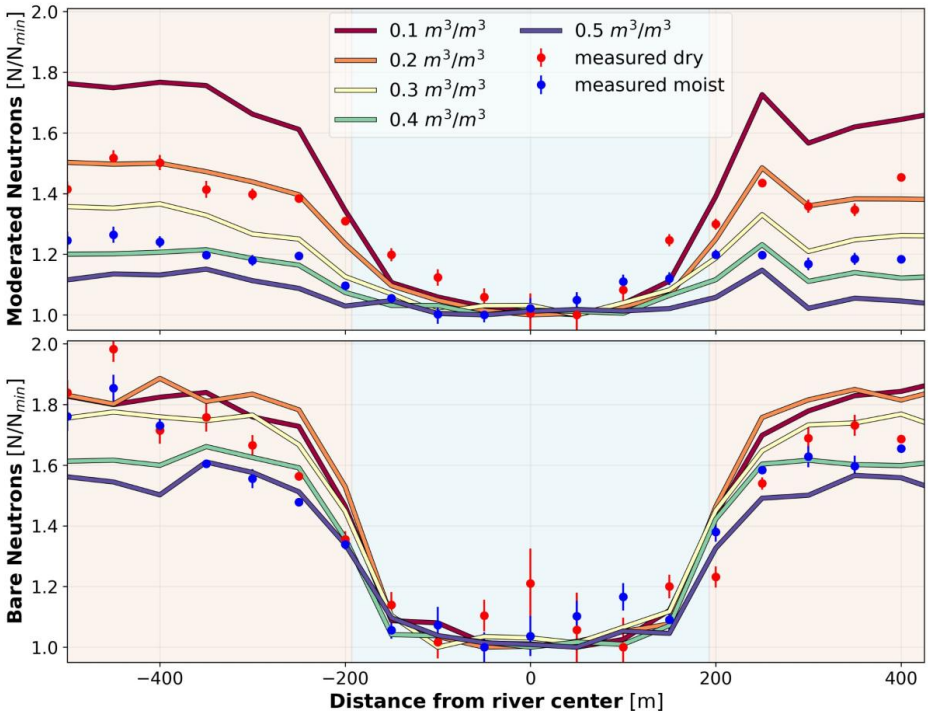

Figure 3.1: Moderated (upper subplot) and bare (lower subplot) neutron intensity measured (blue and red dots) along an approximately 1 km long transect with the Rhine river in the center (blue zone). In comparison, neutron intensity obtained from URANOS simulations for shore soil moisture contents (orange zones) ranging between 0.10 m^3/m^3 and 0.50 m^3/m^3 are shown. For this, moderated neutron intensity was obtained using 70 % epithermal neutrons and 30 % thermal neutrons. Bare neutron intensity was obtained by weighting neutrons passing the detector layer with $\frac{1}{\sqrt{Energy}}$ *(black line in Figure 3a in* WEIMAR ET AL., *2020).*

3.3.2 **Horizontal thermal neutron footprint**

Figure 3.2 shows the simulated thermal neutron intensity as a function of the radial distance from the first soil contact after thermalization until passing the detector layer for soil moisture contents ranging from 0.06 – 0.50 m^3/m^3 and for a constant air humidity of 10 g/m^3. In addition, Figure 3.2 shows R_{86} and an analytical function that was fitted to the neutron intensity and can be used to obtain the radial weights (W_r, horizontal weighting function):

$$W_r = r^{*F_1}\left(e^{-r^{*F_2}F_3 r^*} + \frac{F_4}{r^*}\right)^{r^*F_5+F_6}, \quad 0 \leq r^* < 300 \tag{3.1}$$

where F_1 - F_6 are parametric functions that all depend on soil moisture content [m^3/m^3] (see Appendix II). For obtaining r^*, the radial distance from the detector, r in m, can be rescaled for the influence of pressure (p [mbar]) using the approach from KÖHLI ET AL. (2015, Equation 5):

$$r^* = r\left(\frac{0.5}{0.86 - e^{-p/1012}}\right)^{-1} \tag{3.2}$$

However, we suggest to only apply the pressure rescaling to radii > 5 m as we found no evidence that the geometrically controlled peak within the first meters (compare Figure 3.2) is influenced by air pressure.

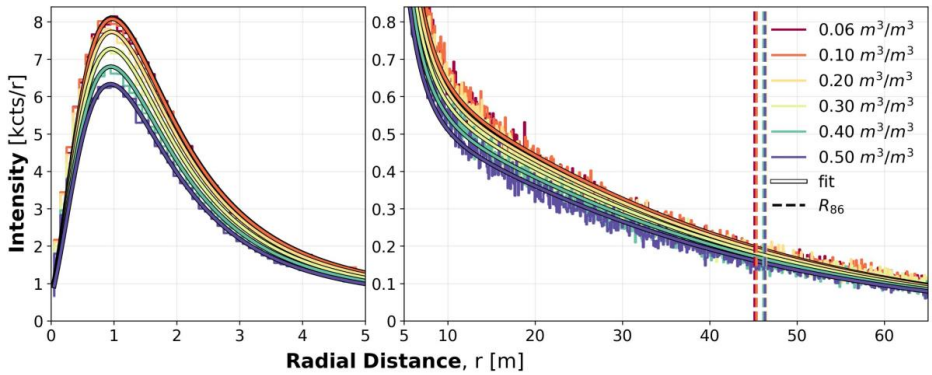

Figure 3.2: Horizontal intensity of simulated thermal neutrons as a function of distance from the first interaction in the soil to detection for different soil moisture contents ranging from 0.06 – 0.50 m^3/m^3 and constant absolute humidity of 10 g/m^3. The dotted lines indicate the 86 % cumulative contribution quantile (R_{86}) for a specific soil moisture content and the solid lines show an analytical fit to the horizontal intensity (Wr – Equation (3.1)).

We found that more than 45 % of the thermal neutrons originated from within 5 m distance from the detector. As in the case of epithermal neutrons (KÖHLI, 2019), a peak in neutron intensity occurred at these short distances, which is geometrically controlled by the height of the detector above the ground. We also found that the detector height affects R_{86} but not D_{86} (see Appendix III). The radial neutron intensity depended on soil moisture content and this dependency was more pronounced at shorter distances from the detector. In addition, R_{86} increased slightly with increasing soil moisture content. Within the considered soil moisture content and air humidity range from 0.01 – 0.50 m^3/m^3 and 1 to 21 g/m^3, R_{86} ranged between 43 and 48 m. In contrast to the strong dependence of the epithermal neutron footprint on air humidity (KÖHLI ET AL., 2015), an increase in air humidity from 1 to 21 g/m^3 for a soil moisture content of 0.20 m^3/m^3 only resulted in a decrease in R_{86} of thermal neutrons by ~2 m. This weak dependence on air humidity can be explained by the shorter

travel paths of thermal neutrons and the associated lower probability of interaction with water vapor nuclei compared to epithermal neutrons (DESILETS AND ZREDA, 2013). Because of this weak dependence, we did not consider air humidity as a parameter in Equation (3.1).

3.3.3 **Vertical thermal neutron footprint**

Figure 3.3 shows the contribution of scattering interactions of detected thermal neutrons as a function of depth in the soil for soil moisture contents ranging from 0.06 – 0.50 m^3/m^3 with a constant air humidity of 10 g/m^3 and for various distances from the detector. Furthermore, Figure 3.3 shows D_{86} (i.e. the penetration depth) and the fitted analytical function (W_d, vertical weighting function):

$$W_d = d^{F_7}\left(e^{-d^{F_8}F_9 d} + \frac{F_{10}}{d}\right)^{dF_{11}+F_{12}}, \quad 1 \leq d \leq 150 \tag{3.3}$$

where F_7 - F_{12} are parameter functions dependent on soil moisture content [m^3/m^3] (see Appendix II) and d in cm is the soil depth.

The simulations for the vertical thermal neutron footprint indicate that the penetration depth decreases from 65 to 10 cm with increasing soil moisture content from 0.01 – 0.50 m^3/m^3 (not all shown) and decreases slightly with increasing radial distance (Figure 3.3). Compared to epithermal neutrons, the radial decrease of D_{86} with distance was far less pronounced for thermal neutrons (cf. KÖHLI ET AL., 2015; SCHRÖN ET AL., 2017). Figure 3.3 also shows a strong dependence on soil moisture content for the contribution of the scattering interactions to the overall measured signal. For short distances (i.e. at ~1 m distance), the normalized contribution to the overall signal in the soil strongly varied within the first centimeters. In contrast, the vertical weights of epithermal neutrons decrease monotonous (FRANZ ET AL., 2012b; KÖHLI ET AL., 2015; SCHRÖN ET AL., 2017). There was only a small radial dependence of the vertical contribution. Therefore, this was not considered in the vertical weighting function (Equation (3.3)). The best agreement between the modeled contribution to the total signal and W_d obtained from Equation (3.3) was found at ~5 m distance from the detector (Figure 3.3). Considering that soil moisture content measurements for calibration are usually generated from mixed samples in 5 cm intervals (e.g., ZREDA ET AL., 2012; SCHEIFFELE ET AL., 2020) or from distributed sensor networks

with the first measurement in a soil depth of ~5 cm (e.g., BOGENA ET AL., 2013), the weighing function fits the simulation results well enough for practical applications.

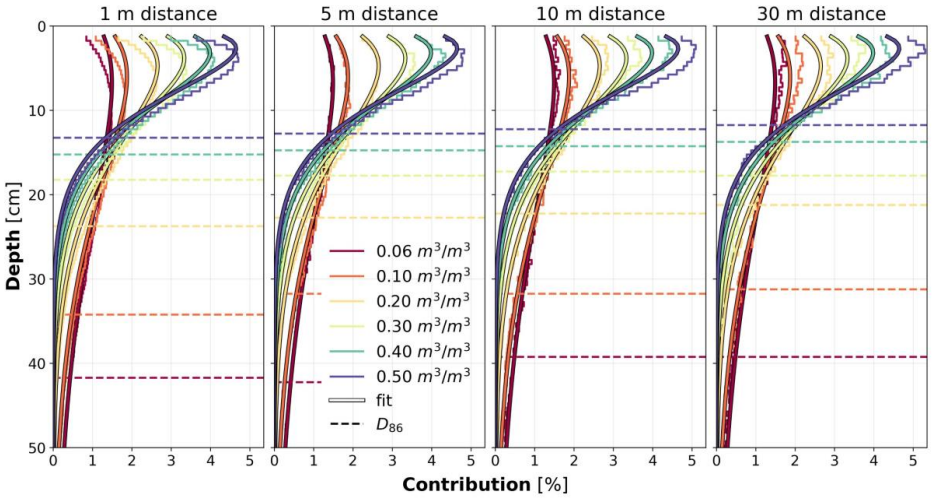

Figure 3.3: Vertical contribution of all scattering interactions of thermal neutrons to the total neutron flux at 1, 5, 10, and 30 m distance from the first interaction in the soil to detection for different soil moisture contents ranging from 0.06 – 0.50 m^3/m^3 and constant absolute humidity of 10 g/m^3. The dotted lines indicate the 86 % cumulative contribution quantile (D_{86}) for a specific soil moisture content and the solid lines show an analytical fit to the vertical contribution (W_d – Equation (3.3)).

3.4 **Discussion**

The footprint definitions used in this study have shown good results for the weighting of reference soil moisture content measurements in many experimental studies with epithermal neutrons (e.g., SCHRÖN ET AL., 2017; BOGENA ET AL., 2020; SCHEIFFELE ET AL., 2020). We therefore expect that these definitions are also appropriate for thermal neutrons. Furthermore, the use of the same definitions allows for easier comparison with previous work. Nonetheless, it is worth mentioning two issues with the used definitions for the thermal neutron footprint. First, the use of 86 % quantiles to summarize the footprint characteristics provides a favourable impression of the size of the footprint. In reality, a large fraction of both epithermal and thermal neutrons is expected to originate from a region close to the detector (KÖHLI ET AL., 2015; Figure 3.2). Second, the use of the first soil contact of a neutron to determine the horizontal intensity and all scattering interactions to determine the vertical contribution is a simplification that not necessarily represents the

neutron signal measured by the detector. In future studies, an attempt should be made to formulate the definitions for the lateral and vertical footprint more consistently.

In our opinion, defining the origin of a thermal neutron by its first soil contact with kinetic energies ≤ 0.5 eV is a meaningful choice, because this is in proximity to the kinetic energy (~0.17 eV) where the dominant physical response of neutrons changes from elastic scattering interactions to absorption (cf. KÖHLI ET AL., 2018; WEIMAR ET AL., 2020). Nevertheless, it is unclear to which extent the sensitivity of thermal neutrons to soil moisture content depends on soil interactions with higher energies before a neutron is moderated down to thermal energies. Thus, defining the first soil contact as thermal neutron as origin may provide biased results.

The density of aboveground thermal neutrons not only depends on the rate of higher energy neutrons that are thermalized, but also on the absorption by nuclei mainly in soils (ZREDA ET AL., 2008; DESILETS ET AL., 2010). For instance, ANDREASEN ET AL. (2016) found that the gadolinium concentration in soils needed to be considered to simulate realistic thermal neutron intensities. In this study, we did not explicitly consider the effect of modified soil chemistry on the footprint properties of thermal neutrons. However, we found only a reduction in R_{86} by ~2 m and a reduction in D_{86} by ~5 cm when adding 10^{-6} g/cm^3 ^{10}B to the soil in the model domain (for a soil moisture content of 0.20 m^3/m^3). This ^{10}B content approximately represents the cumulative absorption cross section (SEARS, 1992) of the European median amounts of the most important soil elements (SALMINEN ET AL., 2005). Consequently, we assume that the influence of soil chemistry on the thermal neutron footprint is small in most cases.

Standard neutron detectors that use HDPE for moderation typically show a contribution of ~20 - 30 % thermal neutrons to the moderated signal (MCJANNET ET AL., 2014; KÖHLI ET AL., 2018). Similarly, epithermal neutrons also influence the signal of a bare detector, but to a lesser degree (ANDREASEN ET AL., 2016). For future studies, it would be important to investigate the contribution of thermal and epithermal neutrons to the moderated and bare neutron detectors in more detail. This would allow a complementary use of the weighting schemes from SCHRÖN ET AL. (2017) for epithermal neutrons and the weighting scheme (Equations. (3.1) – (3.3)) proposed in this study for thermal neutrons to more accurately describe the total measured neutron signals of moderated and bare detectors.

3.5 **Conclusions and Outlook**

This study presents for the first time a detailed assessment of the thermal neutron footprint of cosmic ray neutrons using the neutron transport model URANOS. Our neutron transport simulations showed that the horizontal footprint of thermal neutrons (≤ 0.5 eV) depends only slightly on soil moisture content and ranges between 43 to 48 m for soil moisture contents between 0.01 and 0.50 m^3/m^3. In contrast, we found that the penetration depth of thermal neutrons strongly depends on soil moisture content and ranges from 10 to 65 cm for soil moisture contents between 0.01 and 0.50 m^3/m^3. Furthermore, we found a low influence of air humidity on the footprint of thermal neutrons. In addition, we measured neutron intensity along a transect that crossed a river using a highly sensitive cosmic ray rover. Since the URANOS neutron transport model was able to adequately reproduce the measured bare neutron intensities of the transect across the river, we are confident that it is suitable for the thermal neutron footprint simulations presented here. Our results should enable new applications using thermal neutrons, such as the improved correction of biomass for soil moisture content determination or the detection of biomass changes. For future studies, we suggest to investigate the dependence of the thermal neutron footprint on soil chemistry, vegetation, detector height above ground, and soil bulk density in more detail. In addition, future research should investigate the contributions of epithermal and thermal neutrons to the measured signals of different types of bare and moderated detectors. Furthermore, the applicability of the pressure, air humidity, and incoming cosmic ray neutron standard correction models for thermal neutrons should be investigated.

4 Potential of thermal neutrons to correct cosmic ray soil moisture content measurements for dynamic biomass effects

Abstract

Cosmic ray neutron sensors (CRNS) allow to determine field-scale soil moisture content non-invasively due to the dependence of aboveground measured epithermal neutrons on the amount of hydrogen. Because other pools besides soil contain hydrogen (e.g., biomass), it is necessary to consider these for accurate soil moisture content measurements, especially when they are changing dynamically (e.g., arable crops, de- and reforestation). In this study, we compare four approaches for the correction of biomass effects on soil moisture content measurements with CRNS using experiments with three crops (sugar beet, winter wheat, and maize) on similar soils: I) site-specific functions based on in-situ measured biomass, II) a generic approach, III) the thermal-to-epithermal neutron ratio (N_r), and IV) the thermal neutron intensity. Calibration of the CRNS during bare soil conditions resulted in root mean square errors (RMSE) of 0.097, 0.041, and 0.019 m^3/m^3 between estimated and reference soil moisture content of the cropped soils, respectively. Considering in-situ measured biomass for correction reduced the RMSE to 0.015, 0.018, and 0.009 m^3/m^3. When thermal neutron intensity was considered for correction, similarly accurate results were obtained. Corrections based on N_r and the generic approach were less accurate. We also explored the use of CRNS for biomass estimation. The use of N_r only provided accurate biomass estimates for sugar beet. However, significant site-specific relationships between biomass and thermal neutron intensity were obtained for all three crops. It was concluded that thermal neutron intensity can be used to correct soil moisture content estimates from CRNS and to estimate biomass.

Key Points

- Cosmic ray soil moisture content measurements were most accurate when corrected with in-situ biomass or thermal neutron intensity
- The effect of biomass on epithermal and thermal neutron intensity is plant-specific
- Biomass could be estimated from thermal neutron intensity for three crop types, but not with the thermal-to-epithermal neutron ratio

---

This chapter is based on a manuscript submitted to *Water Resour. Res.* (Preprint available):

JAKOBI, J., HUISMAN, J. A., FUCHS, H., VEREECKEN, H., AND BOGENA, H. R. (in revision), Potential of thermal neutrons to correct cosmic-ray soil moisture content measurements for dynamic biomass effects, doi: 10.1002/essoar.10510176.2.

4.1 **Introduction**

Cosmic ray neutron (CRN) sensing is a non-invasive method for soil moisture content measurement (ZREDA ET AL., 2008). By now, it has become a widely used method for soil moisture content determination and cosmic ray neutron sensors (CRNS) are operated in more than 200 locations worldwide (BOGENA ET AL., 2015; ANDREASEN ET AL., 2017b), also in regional (e.g., BAATZ ET AL., 2014; BOGENA ET AL., 2018), national (e.g., ZREDA ET AL., 2012; COOPER ET AL., 2021), and continent-wide networks (e.g., HAWDON ET AL., 2014; BOGENA ET AL., 2021). The aboveground epithermal neutron intensity (energy range from ~0.5 eV to 100 keV; ZREDA ET AL., 2008) is inversely related to the hydrogen content of the environment. Since hydrogen is mostly located in soil water in terrestrial environments, the measurement of the aboveground epithermal neutron intensity can be used to estimate soil moisture content (DESILETS ET AL., 2010). The sensing volume of CRNS is much larger compared to most other ground-based soil moisture sensing techniques and corresponds to a cylinder with 130 - 240 m radius and 15 – 83 cm soil depth depending on the soil moisture content (KÖHLI ET AL., 2015; SCHRÖN ET AL., 2017).

It is important to note that hydrogen is also stored in other environmental pools besides soil, which may cause deviations between soil moisture content determined with CRNS and reference measurements. Common additional hydrogen sources are snow (TIAN ET AL., 2016; BOGENA ET AL., 2020), biomass (FRANZ ET AL., 2013b; BAATZ ET AL., 2015; BARONI AND OSWALD, 2015; TIAN ET AL., 2016; FERSCH ET AL., 2018; JAKOBI ET AL., 2018), ponding water (SCHRÖN ET AL., 2017), and interception by vegetation (BARONI AND OSWALD, 2015; ANDREASEN ET AL., 2016; JAKOBI ET AL., 2018), as well as the litter layer (BOGENA ET AL., 2013). The timing of the observed deviations may help to identify the most probable source of additional hydrogen affecting the epithermal neutron intensity. In the absence of snow, earlier CRN sensing studies on agricultural sites typically identified biomass as the most important reason for deviations between the CRNS derived soil moisture content and in-situ measured reference soil moisture content (e.g., BARONI AND OSWALD, 2015; TIAN ET AL., 2016; JAKOBI ET AL., 2018). Thus, the removal of the effect of biomass is crucial for accurate soil moisture content estimation especially on agricultural sites. Although methods to correct soil moisture content for the presence of biomass have been developed (e.g., HAWDON ET AL., 2014; BAATZ ET AL., 2015; JAKOBI ET AL., 2018), they typically require laborious biomass measurements that are often not available.

To circumvent the need for laborious biomass measurements for correction, several studies attempted to directly determine the amount of aboveground biomass from epithermal CRNS measurements and in-situ soil moisture content measurements (FRANZ ET AL., 2013b; BARONI AND OSWALD, 2015). More recently, it was shown that the ratio of thermal (≤ 0.5 eV) to epithermal neutron intensity (N_r) can be used to determine aboveground biomass and to correct biomass effects on CRN measurements (TIAN ET AL., 2016; JAKOBI ET AL., 2018). The dependency of N_r on biomass was also confirmed by neutron transport modeling of a forest site (ANDREASEN ET AL., 2017a) and by a comparison of the measured N_r with vegetation indices derived from remote sensing (VATHER ET AL., 2020). However, it has not yet been investigated in detail why N_r depends on biomass and whether N_r-based correction methods can be applied for different vegetation types. Such investigations are particularly important given that the intensity of thermal neutrons also depends on soil moisture content and soil chemistry, since thermal neutrons are particularly strongly absorbed by certain elements in the soil (ZREDA ET AL., 2008; ANDREASEN ET AL., 2016). In addition, recent studies have shown that the sensing volume of thermal neutrons is much smaller than in the case of epithermal neutrons (BOGENA ET AL., 2020; RASCHE ET AL., 2021). Using neutron transport simulations, it was found that thermal neutrons have a radial footprint of approximately 45 m that increases slightly with increasing soil moisture content and a sensing depth that increases from 10 to 65 cm with decreasing soil moisture content from 0.50 to 0.01 m^3/m^3 (Chapter 3).

The aim of this study is to compare four approaches for the correction of crop biomass effects on CRNS soil moisture content measurements using measurements of thermal and epithermal neutron intensity, reference soil moisture content, as well as biomass development for three crops (sugar beet, maize, and winter wheat). In particular, we considered the following approaches for correction: I) local linear regression models based on epithermal neutron intensity, in-situ soil moisture content, and in-situ biomass measurements, II) the empirical generic approach developed by BAATZ ET AL. (2015), III) local linear regression models based on both epithermal neutron and N_r measurements, and IV) local linear regression models based on both epithermal neutron and thermal neutron measurements. In addition, we evaluated to what extent aboveground biomass can be determined from N_r and from thermal neutron intensity for the three crops considered in this study.

4.2 **Materials and Methods**

4.2.1 **The Selhausen experimental site**

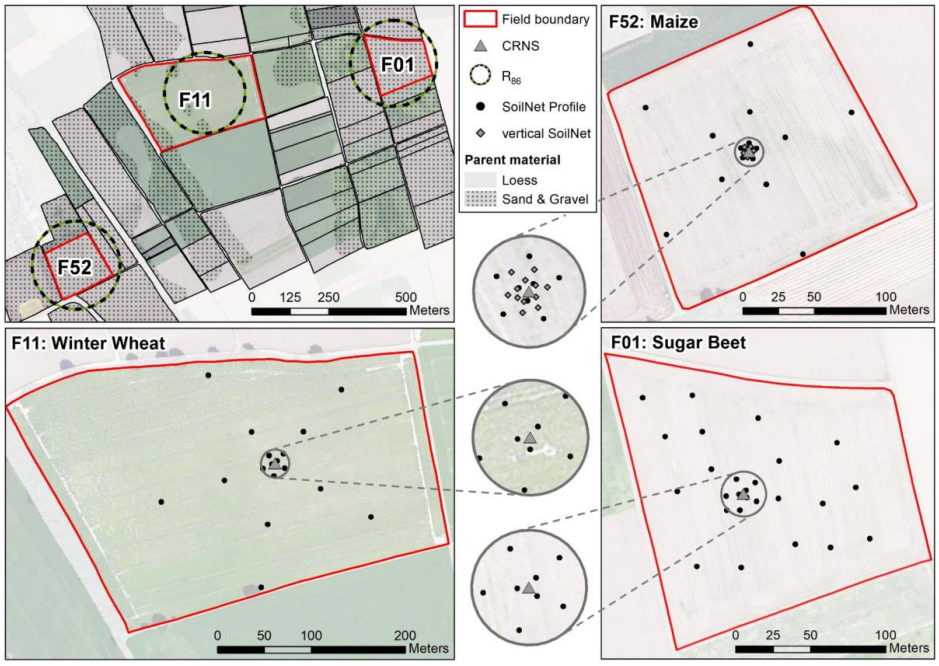

Figure 4.1: Map of the Selhausen experimental site showing an overview of the fields with dominant parent material and the footprint radii (R_{86}) of the three experiments estimated using the average soil moisture content, air humidity, pressure, and vegetation height conditions, respectively (i.e., winter wheat: 132 m; sugar beet: 157 m; maize: 146 m). Furthermore, the SoilNet locations within the three fields and magnifications with 15 m radius around the CRNS are shown for winter wheat and sugar beet. For the maize experiment, the magnification shows an area with a 10 m radius around the CRNS. Base maps: ESRI World Imagery and Contributors.

The Selhausen experimental site is located in western Germany, approximately 40 km west of Cologne (50.865°N, 6.447°E) and is part of the TERENO (TERrestrial ENvironmental Observatories) Rur hydrological observatory (BOGENA ET AL., 2018). The site is located in the temperate maritime climate zone with a mean annual temperature and precipitation of 10.2 °C and 714 mm, respectively (KORRES ET AL., 2015). The experimental site consists of 52 fields managed by local farmers. The main soil type is Cambisol with a silty loam soil texture (RUDOLPH ET AL., 2015; BROGI ET AL., 2019) on top of Pleistocene sand and gravel sediments interrupted by subsurface channels of the Rhine/Meuse river system filled with finer sediment (WEIHERMÜLLER ET AL., 2007). This subsoil heterogeneity leads to characteristic biomass patterns, especially on the sand and gravel dominated fields

(compare Figure 4.1; RUDOLPH ET AL., 2015; BROGI ET AL., 2020). The experiments presented in this study were conducted on three different fields (Figure 4.1) with three different crops, and in three years: winter wheat on field F11 in 2015 (FUCHS, 2016), sugar beet on field F01 in 2016 (JAKOBI ET AL., 2018), and maize on field F52 in 2018.

4.2.2 **Auxiliary meteorological data**

Air temperature, relative humidity, and atmospheric pressure were measured on-site during the experiments. The absolute humidity necessary for neutron count correction was calculated from relative humidity and air pressure. Data gaps in absolute humidity and atmospheric pressure were filled based on linear regression models obtained for the entire measurement period. For this, time series of the same variables were obtained from a climate station situated next to the CRNS on field site F11 (SE_EC_001, http://teodoor.icg.kfa-juelich.de/ibg3searchportal2/index.jsp, compare Figure 4.1). Hourly precipitation sums were obtained from a nearby climate station ~400 m northeast of the field site F11 (SE_BDK_002).

4.2.3 **In-situ soil moisture content measurements**

We used SoilNet wireless sensor networks (BOGENA ET AL., 2010) for obtaining reference in-situ soil moisture content at 18 – 26 locations within each field (Figure 4.1). At each location, soil moisture content was measured in three depths using two soil moisture content sensors (sugar beet and maize: SMT100, Truebner GmbH, Neustadt, Germany; winter wheat: SPADE, sceme.de GmbH, Horn-Bad Meinberg, Germany). Two sensors were installed at each depth to increase the measurement volume and to identify malfunctioning sensors. Each sensor was calibrated individually to translate the sensor response into dielectric permittivity (BOGENA ET AL., 2017). The measured permittivity was related to soil moisture content with the TOPP ET AL. (1980) equation.

The measurement designs at the three field sites differed because of the differently sized fields and to account for the high soil heterogeneity in the case of sugar beet (JAKOBI ET AL., 2018). For winter wheat, we installed sensors at five locations at distances of 11, 50, and 110 m from the CRNS (i.e. 15 locations), as suggested by SCHRÖN ET AL. (2017). Additionally, sensors were installed at three locations at 3 m distance from the CRNS to account for the higher sensitivity near the detector. At all locations, the measurement depths

were 5, 10, and 20 cm. For sugar beet, 18 locations with measurement depths of 5, 20, and 50 cm were distributed in the field. Additionally, sensors were installed at three locations at 3 m distance and at five locations at 11 m distance from the CRNS. For these locations, the measurement depths were 5, 10, and 20 cm (JAKOBI ET AL., 2018). For maize, sensors were installed at 18 locations at distances of 2, 6, 25, and 80 m from the CRNS. At 2 m distance, sensors were installed at 3 locations. At the other distances, sensors were installed at 5 locations. For all 18 locations, the measurement depths were 5, 15, and 30 cm. For this experiment, we additionally installed 12 SMT100 sensors vertically at distances of < 5 m from the CRNS to determine the integral soil moisture content from 0 to 10 cm depth (Figure 4.1) to account for the sensitivity of CRN measurements to soil moisture content changes at shallow depths (FRANZ ET AL., 2012b; KÖHLI ET AL., 2015; SCHRÖN ET AL., 2017).

4.2.4 **In-situ soil sampling**

Additional hydrogen pools in the soil (θ_{off} [g/g]) modify the dependency of epithermal neutrons on soil moisture content (ZREDA ET AL., 2012) and reduce the effective sensing depth of CRNS (e.g., FRANZ ET AL., 2012b). We determined θ_{off} alongside bulk density (ϱ_{bd} [g/cm^3]) from soil samples of 30 cm length and 5 cm diameter obtained using a HUMAX soil corer (Martin Bruch AG, Rothenburg, Switzerland). Soil samples were taken at all SoilNet locations except for the 12 vertically inserted SMT100 sensors. For obtaining ϱ_{bd}, the soil cores were divided into 5 cm segments and oven-dried at 105 °C for 24 h. Subsequently, the soil samples were sieved and depth-specifically mixed for each field. Subsamples of 20 mg were taken from these bulk samples and heated to 1000 °C to obtain θ_{off} from the weight loss using the stoichiometric ratio of oxygen to hydrogen in H_20 (i.e., ~7.94). In this case, θ_{off} contains lattice water (LW [g/g]) and soil organic carbon (SOC [g/g]), which are traditionally determined separately and summed (e.g., ZREDA ET AL., 2012; SCHEIFFELE ET AL., 2020).

4.2.5 **Weighting of reference measurements**

KÖHLI ET AL. (2015) showed that the footprint of epithermal neutrons varies depending on soil moisture content, air humidity, air pressure, soil bulk density, and vegetation height. These findings were extended for short distances (< 1 m) by SCHRÖN ET AL. (2017). In this

study, we used the most recent method for vertical and horizontal weighting of in-situ reference soil moisture content measurements of which a brief description is given in the following. For a complete description of the weighting procedure, we refer to SCHRÖN ET AL. (2017).

For all experiments, we first obtained the vertical weights (i.e., W_d; SCHRÖN ET AL., 2017) for each SoilNet location and measurement depth. Subsequently, W_d was used to derive a vertically weighted soil moisture content for each location and measurement time. For the vertical and horizontal weighting of in-situ ϱ_{bd} and θ_{off} measurements, we used the average of the HUMAX sample depth-intervals, i.e., 2.5, 7.5, 12.5, 17.5, 22.5, and 27.5 cm. For maize and winter wheat, the reference soil moisture content locations were determined following the radial sensitivity of CRNS. Thus, a horizontal weighting was already implicitly considered. To avoid a double weighting, we first averaged the measurements for each radius. Subsequently, the results for each radius were averaged to obtain the vertically and horizontally weighted reference soil moisture content ($\theta_{reference}$), ϱ_{bd}, and θ_{off}. For sugar beet, the reference measurement were weighted using the location-specific horizontal weights (i.e., W_r, SCHRÖN ET AL., 2017). At each measurement time, the procedure to determine the vertical and horizontal weighting was iterated four times, which was sufficient to reach convergence.

4.2.6 **Biomass measurements**

During the winter wheat, maize, and sugar beet experiments, we sampled above- and belowground biomass at eight, five, and nine locations, respectively. At least four measurement locations were sampled in < 20 m distance from the CRNS. At each sampling location, 1 m of row was harvested, sealed air-tight, and transported to the laboratory. Here, soil residues were removed and samples were split into above- and belowground biomass, and subsequently weighed and oven-dried at ≤ 105 °C until a constant weight was reached. Due to limited oven capacity, subsamples of ~20 % of the original sample weight were occasionally used. Areal average moist and dry above- and belowground biomass was calculated using the arithmetic mean of all samples. As suggested by FRANZ ET AL. (2013b), we assumed that the water equivalent contained in biomass (BWE [mm]) can be approximated by the sum of the weight loss from oven-drying and the stoichiometric amount of hydrogen and oxygen contained in cellulose (f_{ew}, ~55.6 %):

$$BWE = \left[\left(BM_f - BM_d\right) + f_{ew}\, BM_d\right]\frac{1}{p_d}\varrho w \tag{4.1}$$

where ϱ_w is the density of water (1 g/cm^3), p_d is the distance between rows (m; sugar beet: 0.465 m, winter wheat: 0.12 m, maize: 0.45 m), and BM_f and BM_d are the fresh and dry biomass weights per 1 m of row [kg], respectively. We used Equation (4.1) to determine aboveground *BWE* (BWE_a), belowground *BWE* (BWE_b), while total *BWE* (BWE_{tot}) was obtained as $BWE_a + BWE_b$.

For sugar beet and winter wheat, biomass was sampled on 11 days, respectively. However, for winter wheat two of the belowground biomass samples were calculated from aboveground biomass information according to BARET ET AL. (1992). For maize, the observation period was only 3 months due to a drought-related emergency harvest and biomass was only measured at five days. Therefore, additional *BWE* estimates were obtained from bi-weekly leaf area index (*LAI*) measurements with a SS1 SunScan Canopy Analysis System (Delta-T Devices, Cambridge, United Kingdom). For this, we used an exponential model to relate *BWE* and *LAI* of maize:

$$BWE_{LAI} = a_1 LAI^{b1} \tag{4.2}$$

where a_1 and b_1 are fitting parameters and BWE_{LAI} [mm] is the *BWE* predicted from *LAI*. We fitted Equation (4.2) for the prediction of aboveground *BWE* ($BWE_{a,LAI}$) and belowground *BWE* ($BWE_{b,LAI}$), while total *BWE* ($BWE_{tot,LAI}$) was obtained as $BWE_{a,LAI} + BWE_{b,LAI}$. Linear interpolation was used to obtain *BWE* estimates at non-sampled times.

4.2.7 **Cosmic Ray Neutron Measurements**

We used different types of CRNS (i.e. CRS-1000, CRS-2000/B, mobile CRNS, Hydroinnova LLC, Albuquerque, NM, USA) with moderated and bare detector tubes for measuring epithermal and thermal neutron intensity, respectively. For more information on the measurement principle, we refer to ZREDA ET AL. (2012). FERSCH ET AL. (2020) provide an overview of the different detector types. We collocated several CRNS in all three fields and summed up the measured neutron counts to achieve lower measurement uncertainty compared to a single sensor (cf. Chapter 2). In particular, we operated 7 moderated and 3 bare neutron detectors in the sugar beet field, 8 moderated and 4 bare detectors in the winter wheat field, and 4 moderated and 3 bare detectors in the maize field.

Before aggregation, outliers were removed from the raw neutron count time series (N_{raw}) of the individual detectors, irrespective of detector type, using two filtering steps. First, extreme outliers were removed using two threshold values:

$$N_{c1} = \begin{cases} N_{raw} > 50 \dfrac{cts}{h} \\ N_{raw} < 10 \dfrac{kcts}{h} \end{cases} \tag{4.3}$$

Second, outliers relative to the 24 hours moving average (N_{c24m}) ± the Poissonian uncertainty (e.g., KNOLL, 2010) associated to the 24 hours moving sum ($\sqrt{N_{c24s}}$) were removed:

$$N_c = \begin{cases} N_{c1} > N_{24m} - \sqrt{N_{c24s}} \\ N_{c1} < N_{24m} + \sqrt{N_{c24s}} \end{cases} \tag{4.4}$$

Subsequently, the filtered hourly thermal (T_c) and epithermal (E_c) neutron count rates were summed up.

The measurements of some of the thermal and epithermal detectors contained larger data gaps. We obtained scaling factors (s_f) for each experiment and each detector relative to the cumulative average count rate during times when all detectors of the same type (i.e. T_c or E_c) were working. The s_f were used to account for missing data during summation as follows:

$$\begin{aligned} E_s &= E_c \frac{1}{\sum s_f} \\ T_s &= T_c \frac{1}{\sum s_f} \end{aligned} \tag{4.5}$$

where E_s and T_s are the summed epithermal and thermal neutron count series adjusted for data gaps.

Corrected epithermal neutron intensities (E) were obtained from E_s by applying established correction procedures for variations in air pressure (DESILETS AND ZREDA, 2003), incoming cosmic ray neutron intensity (DESILETS AND ZREDA, 2001), and air humidity (ROSOLEM ET AL., 2013) (see Appendix I). For these corrections, we used the average pressure, absolute humidity and incoming cosmic ray neutron intensity measured during each of the three experiments. The reference incoming cosmic ray neutron intensity was obtained from the

neutron monitor at Jungfraujoch (JUNG; via the NMDB neutron monitor database at www.nmdb.eu). Following the experimental findings from JAKOBI ET AL. (2018), we obtained the corrected thermal neutron intensity (T) from T_s by applying corrections for pressure and absolute humidity only.

4.2.8 The thermal-to-epithermal neutron ratio

TIAN ET AL. (2016) found a positive correlation between BWE_a of maize and soy bean and the ratio of thermal-to-epithermal neutrons (N_r). Such a correlation was also found for the sugar beet dataset used in this study (JAKOBI ET AL., 2018). In this study, we obtained N_r according to JAKOBI ET AL. (2018):

$$N_r = \frac{T}{E}\frac{\bar{E}}{\bar{T}} \tag{4.6}$$

where $\bar{E}$ and $\bar{T}$ are the arithmetic means of the epithermal and thermal neutron intensity measured during each experiment, and E and T are the 12-hourly moving averages of the epithermal and thermal neutron intensity. We used linear models for relating N_r and BWE_a (JAKOBI ET AL., 2018):

$$BWE_{a,Nr} = a_2 Nr + b_2 \tag{4.7}$$

where $BWE_{a,Nr}$ is the BWE_a estimated from N_r and a_2 and b_2 are calibration parameters. We also used a linear model for relating T and BWE_{tot}:

$$BWE_{tot,T} = a_3 T + b_3 \tag{4.8}$$

where $BWE_{tot,T}$ is the BWE_{tot} estimated from T and a_3 and b_3 are calibration parameters.

4.2.9 Conversion of neutrons to soil moisture content

We obtained volumetric soil moisture content (θ) from E with a modified approach following DESILETS ET AL. (2010), which showed good performance in several previous studies (e.g., RIVERA VILLARREYES ET AL., 2011; BAATZ ET AL., 2014; DONG ET AL., 2014; DIMITROVA-PETROVA ET AL., 2020):

$$\theta = \varrho_{bd}\left(\frac{p_0}{\frac{fE}{N_0} - p_1} - p_2 - \theta_{off}\right) \tag{4.9}$$

where p_i (= 0.0808, 0.372 and 0.115) are fitting parameters obtained from neutron transport modeling, f is a temporally variable correction factor (derived from biomass measurements, N_r, or T), and N_0 is the epithermal neutron intensity above dry soil. In this study, we obtained N_0 from the 12-hourly moving average of the epithermal neutron intensity using three different strategies:

- In calibration strategy A, a single value for N_0 (i.e., $N_{0,opt}$) was obtained using the whole reference soil moisture content time series and assuming f = 1 (i.e. no additional correction).
- In calibration strategy B, a single value for N_0 (i.e., $N_{0,bare}$) was obtained for the first two days of the reference soil moisture content observations and assuming f = 1. This strategy represents the typical calibration approach using campaign-style soil sampling (e.g., ZREDA ET AL., 2012).
- In calibration strategy C, we obtained 12-hourly N_0-values using Equation (4.9) and assuming f = 1. We used the resulting N_0 time series for predicting biomass, N_r, or T related effects on epithermal CRN measurements.

For calibration strategies A and B, N_0 is obtained by minimization of the root mean square error (RMSE) between the reference and the estimated soil moisture content.

4.2.10 **Biomass, N_r and thermal neutron corrections**

We tested four regression models for obtaining the correction factor f in Equation (4.9) using either BWE_a (e.g., BAATZ ET AL., 2015), BWE_{tot}, N_r (e.g., JAKOBI ET AL., 2018), or T:

$$N_{0,BWEa} = a_4\, BWE_a + N_{0,BWEa=0} \tag{4.10}$$

$$N_{0,BWEtot} = a_5\, BWE_{tot} + N_{0,BWEtot=0} \tag{4.11}$$

$$N_{0,Nr} = a_6\, N_r + N_{0,Nr=0} \tag{4.12}$$

$$N_{0,T} = a_7\, T + N_{0,T=0} \tag{4.13}$$

where a_4, a_5, a_6, and a_7 [cph] are empirical factors representing the change in N_0 per mm BWE_a, mm BWE_{tot}, N_r, or T, respectively and $N_{0,BWEa=0}$, $N_{0,BWEtot=0}$, $N_{0,Nr=0}$, and $N_{0,T=0}$ represent N_0 when BWE_a, BWE_{tot}, N_r, or T, respectively equal 0. Subsequently, we derived f by assuming that the changes in estimated N_0 and epithermal neutron intensity are proportional:

$$f_{BWEa} = \left(1 + \frac{a_4}{N_{0,BWEa=0}} BWE_a\right)^{-1} \tag{4.14}$$

$$f_{BWEtot} = \left(1 + \frac{a_5}{N_{0,BWEtot=0}} BWE_{tot}\right)^{-1} \tag{4.15}$$

$$f_{Nr} = \left(1 + \frac{a_6}{N_{0,Nr=0}} N_r\right)^{-1} \tag{4.16}$$

$$f_T = \left(1 + \frac{a_7}{N_{0,T=0}} T\right)^{-1} \tag{4.17}$$

where f_{BWEa}, f_{BWEtot}, f_{Nr}, and f_T are correction factors to be used with $N_{0,BWEa=0}$, $N_{0,BWEtot=0}$, $N_{0,Nr=0}$, and $N_{0,T=0}$, respectively in Equation (4.9). We also obtained correction factors for BWE_a and BWE_{tot} based on the empirical generic biomass correction model of BAATZ ET AL. (2015), who found a reduction in epithermal neutron intensity of ~0.5 % per mm BWE_a:

$$f_{BWEa,Baatz} = 1 + BWE_a \frac{6.4}{1215} \tag{4.18}$$

$$f_{BWEtot,Baatz} = 1 + BWE_{tot} \frac{6.4}{1215} \tag{4.19}$$

where $f_{BWEa,Baatz}$ and $f_{BWEtot,Baatz}$ again are correction factors to be used in Equation (4.9) and the constants 6.4 and 1215 [cph] are the reduction per mm BWE_a and N_0 when BWE_a equals 0, respectively.

4.3 **Results**

4.3.1 **Data Overview**

Table 4.1 provides a summary of the basic soil properties for the three cropped fields. The bulk density generally increased with depth for all three fields, while the additional hydrogen pools θ_{off} were relatively constant with depth. It was found that the weighted bulk densities were lower than the arithmetic mean due to the decreasing sensitivity of CRNS with increasing depth.

Table 4.1: Soil bulk density (ϱ_{bd}), gravimetric soil moisture content (θ_g), and additional hydrogen pools in the soil (θ_{off}) from the HUMAX samples taken on 6 Mai 2015 for winter wheat, 6 June 2016 and 4 November 2016 for sugar beet, and 29 Mai 2018 for maize. Please note that the sugar beet soil sampling results differ in comparison to JAKOBI ET AL. (2018) and SCHEIFFELE ET AL. (2020), because the average of two sampling campaigns was used here whereas the two previous studies only used the results from the campaign on 6 June.

Depth [cm]	Winter Wheat			Sugar Beet			Maize		
	ϱ_{bd} [g/cm^3]	θ_g [g/g]	θ_{off} [g/g]	ϱ_{bd} [g/cm^3]	θ_g [g/g]	θ_{off} [g/g]	ϱ_{bd} [g/cm^3]	θ_g [g/g]	θ_{off} [g/g]
0 – 5	1.188	0.200	0.033	1.34	0.194	0.027	1.242	0.176	0.048
5 – 10	1.262	0.197	0.032	1.396	0.189	0.027	1.256	0.192	0.049
10 – 15	1.280	0.193	0.032	1.397	0.189	0.027	1.331	0.191	0.049
15 – 20	1.274	0.190	0.032	1.375	0.187	0.028	1.344	0.196	0.049
20 – 25	1.280	0.190	0.032	1.429	0.178	0.026	1.358	0.202	0.05
25 – 30	1.284	0.122	0.032	1.464	0.170	0.026	1.288	0.198	0.048
Average	1.261	0.182	0.032	1.400	0.185	0.027	1.303	0.192	0.049
Weighted	1.247	0.192	0.023	1.379	0.189	0.016	1.277	0.186	0.034

Table 4.2: Minimum, average, and maximum corrected epithermal and thermal neutron count rates measured during the experiments in sugar beet, winter wheat, and maize fields.

Experiment	Corrected Epithermal Neutrons [cts/h]			Corrected Thermal Neutrons [cts/h]		
	Minimum	***Average***	***Maximum***	***Minimum***	***Average***	***Maximum***
Sugar Beet	8952	10425	11856	2076	2458	2786
Winter Wheat	6063	7350	8542	1296	1562	1849
Maize	4248	5273	5868	1877	2148	2499

An overview of the precipitation, normalized neutron count rates, BWE, and reference soil moisture content for the three cropped fields is given in Figure 4.2. The minimum, average, and maximum epithermal and thermal neutron intensity after correction are provided in Table 4.2. Figure 4.2e shows that the maximum BWE_b for the three crops differed strongly. Both winter wheat and maize showed relatively low maximum BWE_b values (0.89 and 0.85 mm, respectively), whereas the maximum BWE_b for sugar beet was tenfold higher (8.23

mm). For maize, BWE_a and BWE_b were derived from *LAI* using Equation (2.2) (Figure 4.3). The high R^2 ($\geq$ 0.95) indicates that *LAI* was a good predictor for BWE_a and BWE_b. Therefore, we used the *LAI*-derived BWE of maize in the remainder of the manuscript.

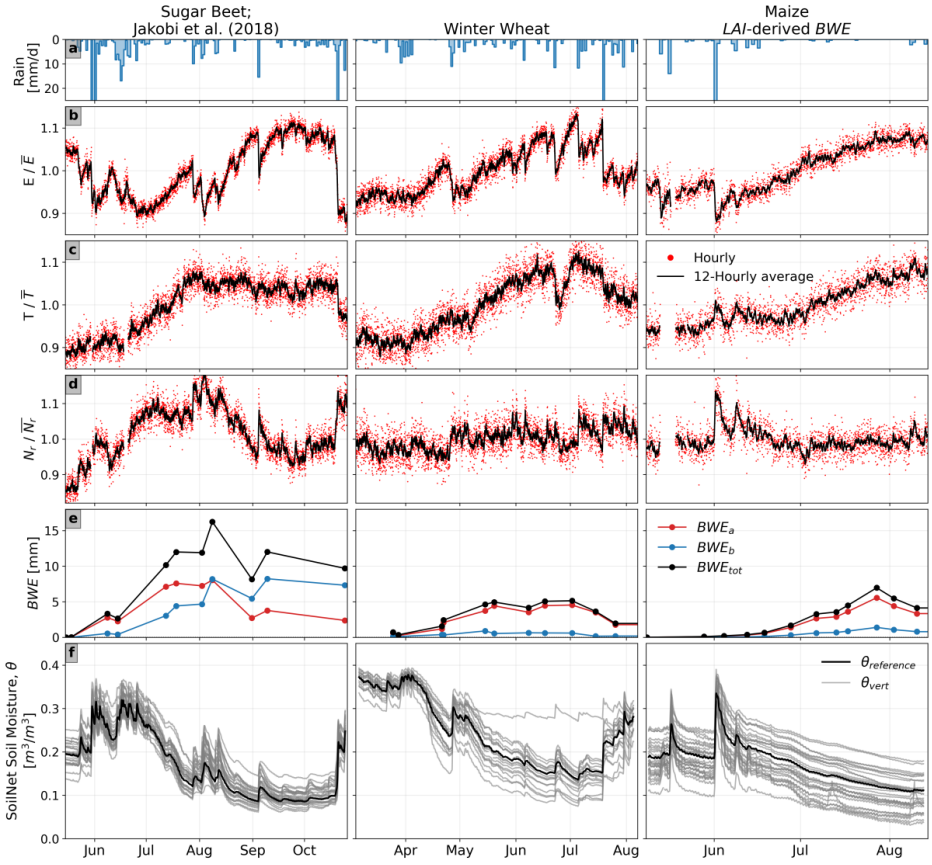

Figure 4.2: Time series of a) precipitation, b) epithermal neutron intensity (E) normalized by the average E, c) thermal neutron intensity (T) normalized by the average T, d) neutron ratio (N_r), e) aboveground, belowground, and total biomass water equivalent (BWE_a, BWE_b, and BWE_{tot}, respectively), and f) soil moisture content obtained from the vertically and horizontally weighted SoilNet measurements (black, $\theta_{reference}$) and the vertically weighted SoilNet measurements (grey, θ_{vert}).

Figure 4.2f shows the vertically weighted soil moisture content measured at all SoilNet locations as well as the horizontally and vertically weighted reference soil moisture content for the three crops. The average reference soil moisture content for sugar beet and maize was notably lower (~0.17 m^3/m^3) compared to winter wheat (0.24 m^3/m^3) due to the drought conditions in 2016 and 2018.

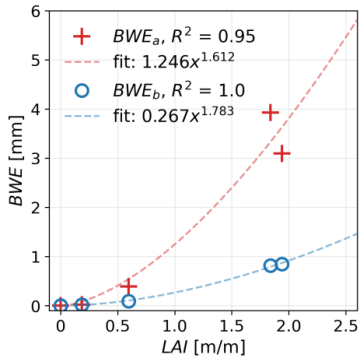

Figure 4.3: Relationship between leaf area index (LAI) and above- and belowground biomass water equivalent (BWE_a and BWE_b, respectively) for maize. The coefficients of determination (R^2) and the exponential models for predicting BWE from LAI are also provided.

4.3.2 The effect of time-variable biomass on CRNS derived soil moisture content

To investigate the influence of vegetation biomass on soil moisture content estimates with CRNS, we first calibrated N_0 during bare soil condition (calibration strategy B, Figure 4.4c, red). For all three crops, the soil moisture content estimated from the CRN measurements in this way deviated from the reference soil moisture content. This was attributed to increasing biomass associated with crop growth (Figure 4.4c, red areas) and resulted in a high RMSE of 0.097 m^3/m^3 for sugar beet, 0.041 m^3/m^3 for winter wheat, and 0.019 m^3/m^3 for maize. For sugar beet and winter wheat, the CRNS mostly overestimated soil moisture content, indicating that the additional hydrogen in the biomass decreased the local epithermal neutron intensity. This effect was particularly strong in case of sugar beet due to its higher above- and belowground biomass. Interestingly, CRNS mostly underestimated soil moisture content for maize, even though the progressing growth of maize should have resulted in more neutron moderation (i.e. soil moisture content overestimation). This counterintuitive result can be explained by the fact that the atomic nuclei of the high-growing maize surrounding the CRNS acted as scattering centers that effectively increased the neutron travel paths and thus the local epithermal neutron intensity (LI ET AL., 2019). In contrast to maize, winter wheat and sugar beet did not grow high enough in the near field of the detector, so this effect was not observed.

Figure 4.4c also shows the results of calibration strategy A, which considers all reference soil moisture content data but no time-variable changes in biomass. For maize and winter wheat, the reference and CRNS derived soil moisture content showed good agreement and

the RMSE was relatively low (i.e., 0.031 m^3/m^3 for winter wheat and 0.011 m^3/m^3 for maize). For sugar beet, the visual agreement was not as good, and this was supported by the higher RMSE (0.042 m^3/m^3).

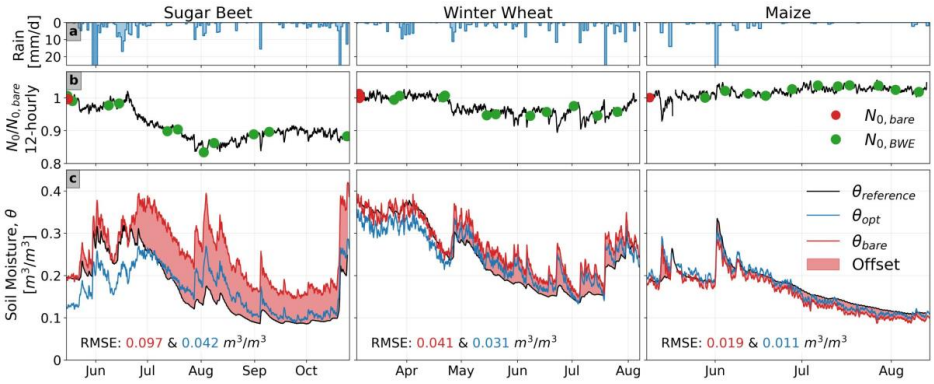

Figure 4.4: Time series of a) precipitation, b) N_0 at biomass sampling dates, and c) offset between reference soil moisture content and CRNS derived soil moisture content using strategy B (i.e. bare soil calibration). CRNS derived soil moisture content using strategy A (in blue), i.e., by optimizing the entire time series of reference soil moisture content, is also shown.

4.3.3 **Soil moisture content correction with local biomass measurements**

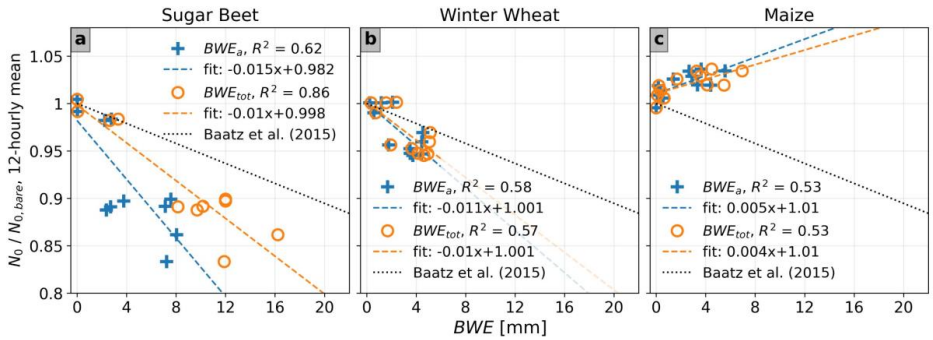

Figure 4.5: Scatterplots and corresponding linear regressions for predicting the change in N_0 from BWE_a (blue) and BWE_{tot} (orange), respectively. The slopes of all linear fits were significantly different from 0 (i.e., the two-sided p-value was < 0.05 for a test with the null hypothesis that the slope is equal to zero). Additionally, the empirical model from BAATZ ET AL. (2015) for predicting the change in N_0 from BWE_a is shown.

To quantify the effect of biomass on soil moisture content obtained with CRNS, we established linear regression models between the in-situ measured BWE_a and BWE_{tot} and the calibration parameter N_0 (Figure 4.5). We found distinct differences in the N_0 – BWE relationships for the three crops. For sugar beet and winter wheat, N_0 showed a negative

relationship with *BWE*, whereas for maize this relationship was positive for reasons already provided. For sugar beet, the slopes of the $N_0 - BWE_a$ and $N_0 - BWE_{tot}$ relationships differed more strongly compared to the other crops (Figure 4.5a), which can be explained by the higher amount of belowground biomass compared to maize and winter wheat (see also Figure 4.2e). In addition, the $N_0 - BWE_{tot}$ relationship for sugar beet resulted in a higher R^2-value compared to the $N_0 - BWE_a$ relationship, indicating that the total biomass should be preferably used for correction in case of sugar beet. Figure 4.5 also shows that the relationship suggested by BAATZ ET AL., 2015 (i.e. a reduction of ~0.5 % of N_0 per mm BWE_a) was not able to represent the influence of biomass on N_0, except to some extent for winter wheat.

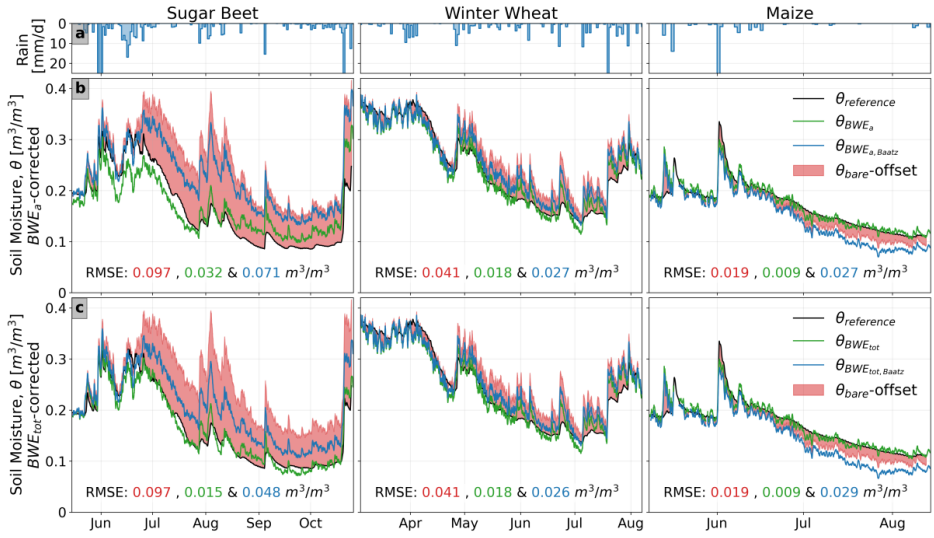

Figure 4.6: Times series of a) precipitation, b) CRNS derived soil moisture content corrected for aboveground biomass, and c) CRNS derived soil moisture content corrected for total biomass. For the biomass correction, local linear regression models (green) and the empirical approach from BAATZ ET AL. (2015) (blue) were considered. For comparison, the vertically and horizontally weighted reference soil moisture content (black) and the offset due to the bare soil calibration (red) are shown.

In a next step, the BWE_a and BWE_{tot} regression models were used for the correction of CRNS soil moisture content using Equations (4.14) and (4.15). Figure 4.6 shows that these corrections were able to effectively reduce the biomass effects for all three crops. In case of winter wheat and maize, a correction based on BWE_a was sufficient to obtain a low RMSE (0.018 and 0.009 m^3/m^3, respectively). In the case of sugar beet, a correction based on BWE_{tot} led to a substantially lower RMSE of 0.015 m^3/m^3 compared to 0.032 m^3/m^3 when only BWE_a was considered.

For winter wheat, the relationship of BAATZ ET AL. (2015) showed an acceptable performance in terms of RMSE in comparison to the linear regression models (Figure 4.6). For sugar beet, the RMSE considering biomass correction with the relationship of BAATZ ET AL. (2015) increased CRNS accuracy compared to the worst-case calibration (i.e. strategy B), but was much higher in comparison to the linear regression models (Figure 4.6), even when BWE_{tot} (Equation (4.19), RMSE of 0.048 m^3/m^3) was used instead of BWE_a (Equation (4.18), RMSE of 0.071 m^3/m^3). As the empirical correction proposed by BAATZ ET AL. (2015) greatly relies on forest biomass data, it implicitly considers a root-shoot ratio valid for trees (i.e., in the order of ~0.2 – 0.6; MOKANY ET AL., 2006). In contrast, the root-shoot ratio of crops changes with time. Sugar beet, for example, showed an increase from ~0.2 to ~6 for the root-shoot ratio. Therefore, the root biomass is not adequately represented by the relationship of BAATZ ET AL. (2015). For maize, the relationship of BAATZ ET AL. (2015) resulted in a decreased accuracy due to the additional neutron scattering processes discussed earlier.

4.3.4 **Soil moisture content correction with the neutron ratio**

We also investigated the possibility of using N_r for the correction of CRNS derived soil moisture content (TIAN ET AL., 2016; JAKOBI ET AL., 2018; VATHER ET AL., 2020). For this, we established linear regression models between N_0 and N_r (Figure 4.7) using all measurements from the observation period (Figure 4.7, black) and measurements on biomass measurement dates only (Figure 4.7, orange). For sugar beet (JAKOBI ET AL., 2018) and winter wheat, linear relationships between N_r and N_0 were found when considering the whole measurement period (Figure 4.7a and Figure 4.7b). For maize, a much flatter regression slope was found (Figure 4.7c) and the R^2 was also lower (0.06) compared to sugar beet (0.44) and winter wheat (0.52). If only days with in-situ BWE samples were considered, the R^2 for sugar beet (0.77) and winter wheat (0.70) increased, while the R^2 for maize decreased to 0.03. Except for maize with in-situ biomass sample times only, all slopes were significantly different from 0 ($p < 0.05$).

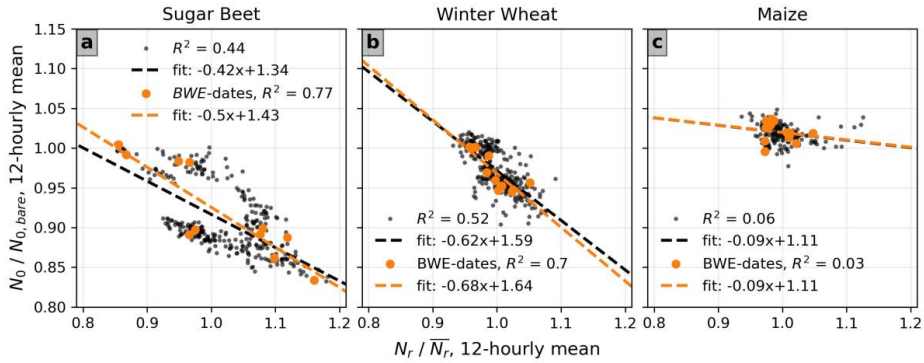

Figure 4.7: Relationships between normalized N_r and normalized N_0. Additionally, the relationships when using the biomass sampling dates (orange) only are shown. Except for the relationship for maize considering only the times of BWE measurements, all linear regressions have slopes that are significantly different from 0 (i.e., the two sided p-value was < 0.05 for tests with the null hypothesis that the slopes are equal to zero).

The linear regression models for predicting N_0 from N_r were also used for the correction of soil moisture content estimates using Equation (4.16) (Figure 4.8). For all three crop types, the soil moisture content estimates obtained using a correction based on N_r were more accurate than the estimates obtained using calibration strategy B as indicated by the lower RMSE of 0.032, 0.022 and 0.011 m^3/m^3 for sugar beet, winter wheat and maize, respectively. If only N_r values at times of biomass measurements were used to derive the correction models (Figure 4.7, orange), similar results were obtained except for maize due to the insignificant regression model (Figure 4.7c).

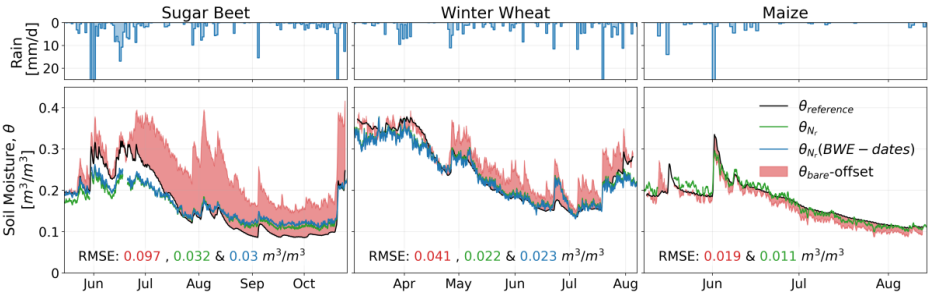

Figure 4.8: Times series of the CRNS derived soil moisture content corrected with N_r (green) and N_r obtained during times of biomass sampling (blue). For comparison, the vertically and horizontally weighted reference soil moisture content (black) and the offset resulting from bare soil calibration of the CRNS (red) are also shown.

4.3.5 **Soil moisture content correction with thermal neutrons**

In a next step, we investigated the possibility of using thermal neutron intensity for the correction of biomass effects on soil moisture content estimation with CRNS. For this, we established linear regression models for predicting the change in the calibration parameter N_0 from thermal neutron intensity using all measurements from the observation periods (Figure 4.9, black) and measurements from the biomass measurement dates only (Figure 4.9, orange). All three crop types showed linear $T - N_0$ relationships like the relationships between BWE_{tot} and N_0 (Figure 4.5), with sugar beet showing the steepest regression slope and maize showing a positive relationship between T and N_0. When only the biomass measurement dates were used, higher correlations were obtained (Figure 4.9a-c). However, the regression results were similar to the case where all data were considered.

Subsequently, the linear regression models for predicting the change in N_0 from thermal neutron intensity were used for correcting CRNS soil moisture content estimates using Equation (4.17) (Figure 4.10). For all three crop types, the correction using thermal neutrons produced better results than the calibration strategy B as indicated by the decrease in RMSE to 0.017, 0.019, and 0.009 m^3/m^3 for sugar beet, winter wheat, and maize, respectively. The results were similar when the linear regression models based only on days with biomass measurements were considered (Figure 4.9, orange).

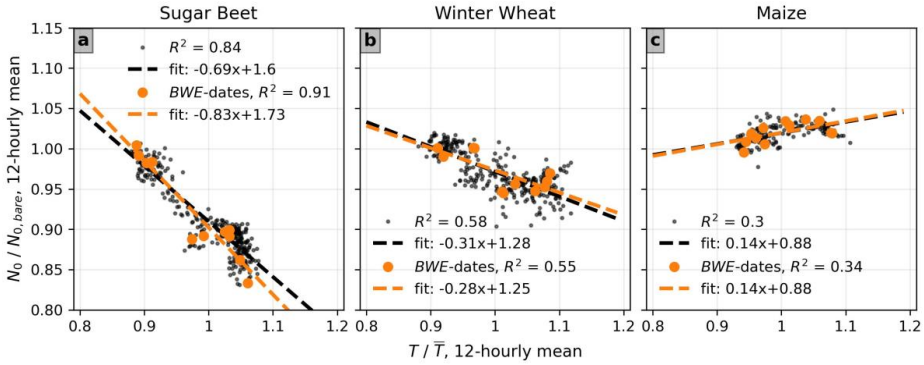

Figure 4.9: Relationship between normalized thermal neutron intensity and normalized N_0 for (a) sugar beet, (b) winter wheat, and (c) maize (black). Additionally, the relationships if only observations at dates of biomass water equivalent (BWE) sampling (orange) were considered are shown. The slopes of all regression models were significantly different from 0 (i.e., the two sided p-value was < 0.05 for tests with the null hypothesis that the slopes are equal to zero).

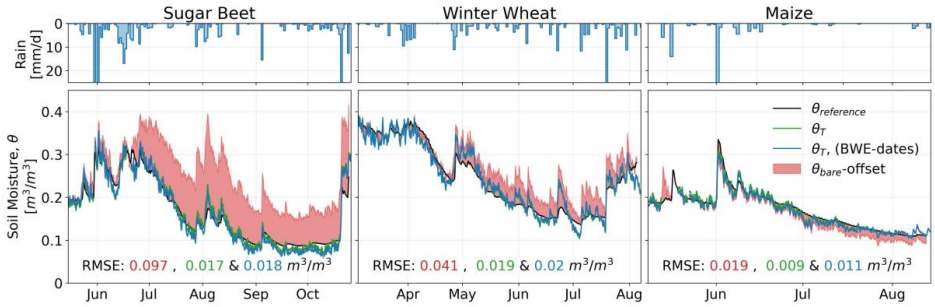

Figure 4.10: Times series of the CRNS derived soil moisture content corrected with thermal neutrons (green) and with thermal neutrons obtained during dates of biomass sampling (blue). For comparison, the vertically and horizontally weighted reference soil moisture content (black) and the offset obtained from bare soil calibration (red) are shown.

4.3.6 **Biomass estimation from the neutron ratio**

After evaluating different approaches for correcting soil moisture content estimates, we now evaluate the potential of N_r for estimating crop biomass development (TIAN ET AL., 2016; ANDREASEN ET AL., 2017a; JAKOBI ET AL., 2018). The N_r for sugar beet was linearly correlated with in-situ measured BWE_a (Figure 4.11a; JAKOBI ET AL., 2018). In contrast, the linear regressions for winter wheat and maize did not indicate significant slopes (i.e., the two-sided p values for a test with the null hypothesis that the slopes are equal to zero were > 0.05, Figure 4.11b and Figure 4.11c). This means that the prediction of aboveground biomass from N_r was not possible for winter wheat and maize in our study. TIAN ET AL. (2016) and VATHER ET AL. (2020) suggested to use uncorrected thermal and epithermal neutron intensities for the derivation of N_r. However, this reduced the R^2 of the N_r - BWE_a relationship from 0.12 to 0.00 for winter wheat and from 0.92 to 0.73 for sugar beet, while it increased R^2 only slightly for maize (from 0.02 to 0.04). It has to be noted that an outlier was removed for sugar beet (Figure 4.11a, circle with dot; also see Jakobi et al., 2018). If this measurement was included in the analysis, the R^2 was reduced to 0.68.

Because N_r could also be influenced by changes in soil moisture content, we also investigated the N_r – soil moisture content relationship. However, we found only weak relationships for all three crops that could not be well described with linear or exponential models (Figure 4.11d – Figure 4.11f). For winter wheat and maize, the slopes of the linear regressions were significantly different from 0 (i.e., two-sided $p < 0.05$, Figure 4.11e and Figure 4.11f). However, the low R^2-values (≤ 0.34) indicated only weak dependencies. For

sugar beet, the R^2 was 0.00. These results confirm previous findings by TIAN ET AL. (2016) and ANDREASEN ET AL. (2017a) that N_r is only weakly related to soil moisture content.

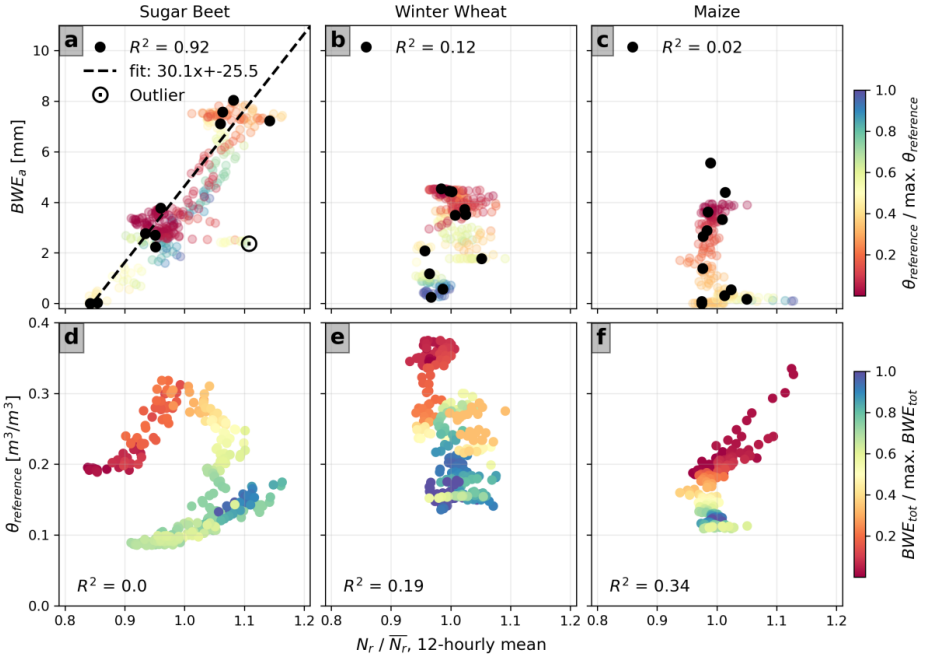

Figure 4.11: Relationships of neutron ratio (N_r) normalized with the average N_r of the whole time series and measured aboveground biomass water equivalent (BWE_a) of (a) sugar beet, (b) winter wheat, and (c) maize and relationships of N_r with horizontally and vertically weighted reference soil moisture content ($\theta_{reference}$) for (d) sugar beet, (e) winter wheat, and (f) maize, respectively. The colouring sequences in subplots a) – c) indicate changes in $\theta_{reference}$. The colouring sequences in subplots c) – f) indicate changes in BWE_{tot} (linearly interpolated). Additionally, the linear regression model for deriving BWE_a from N_r for the Sugar Beet experiment is shown. The slopes of the linear regressions were significantly different from 0 for the relationships presented in subplots a), e), and f) (i.e., the two-sided p-value was < 0.05 for a test with the null hypothesis that the slope is equal to zero).

We observed hysteretic behavior in the soil moisture content - N_r relationship for sugar beet (Figure 4.11d). Similarly, the $N_r - N_0$ relationship also showed hysteresis (Figure 4.7a). The color sequence showing the development of BWE_{tot} (Figure 4.11d) indicates that the hysteresis could be related to sugar beet growth, which is also characterized by changes in plant structure (e.g., development of leaves and tap roots; see also Appendix IV). However, the hysteresis could also be an effect of the soil (and plant) heterogeneity in field F01 (shown in Figure 1 in JAKOBI ET AL., 2018), which may affect thermal and epithermal neutron intensities differently due to the different radial footprints. We also tested if BWE_b or BWE_{tot} for sugar beet could be predicted from N_r, but found lower R^2 values (0.35 and

0.73, respectively) in comparison to the R^2 calculated between N_r and BWE_a (0.92, Figure 4.11a).

4.3.7 **Biomass estimation from thermal neutrons**

Finally, we investigated the potential of T for estimating biomass of the considered crops (Figure 4.12a - Figure 4.12c). For all three crop types, T was linearly related with in-situ measured BWE_{tot}. R^2 was lowest for winter wheat (0.69), while it was 0.87 for sugar beet and maize. The steepest regression slope was obtained for sugar beet, while the slopes for maize and especially for winter wheat were much lower. For sugar beet, the R^2 was slightly lower compared to the R^2 that was found for predicting BWE_a from N_r. For winter wheat, the relatively low R^2 may be related to the large equipment island, where only a thin grass cover was present and no crops were growing. Thus, soil moisture content may have been of greater importance for the thermal neutron intensity in the case of winter wheat as compared to sugar beet and maize.

The scatter plots (Figure 4.12d–f) suggest that the thermal neutron intensity is influenced by soil moisture content, which seems to contradict our findings above. However, this apparent dependence of thermal neutron intensity on soil moisture content can be explained by the fact that for our experiments the increase of biomass usually coincides with decreasing soil water content due to increasing water demand of the crops (see Figure 4.2e and Figure 4.2f). In addition, there are also periods where the thermal neutron intensity stayed almost constant during bare field conditions, while the reference soil moisture content increased considerably (Figure 4.12d and Figure 4.12f) indicating that thermal neutron intensity was independent of soil moisture content.

Since all relationships were significant, the linear regression models from Figure 4.12a–c were used for estimating temporally variable BWE_{tot} for all three crop types (Figure 4.13). The RMSE indicated an estimation accuracy of 1.92, 0.97, and 0.98 mm for sugar beet, winter wheat and maize, respectively, which corresponded to 22, 33, and 42 % of the average interpolated BWE_{tot}. Larger deviations were mostly associated with precipitation events, which sometimes resulted in a decrease of the thermal neutron intensity and thus underestimated BWE_{tot} (e.g., at the end of the measurement period of sugar beet). In other periods, the thermal neutron intensity and thus BWE_{tot} increased with precipitation (e.g., beginning of June for maize). For winter wheat, BWE_{tot} was systematically underestimated

from the end of April until the beginning of June and overestimated from the beginning of July until the end of the observation period (Figure 4.13). These deviations can also be identified in Figure 4.12b (with T ~1 and BWE ~2 – 4 mm) and can possibly be explained with a change in plant structure in the growing season.

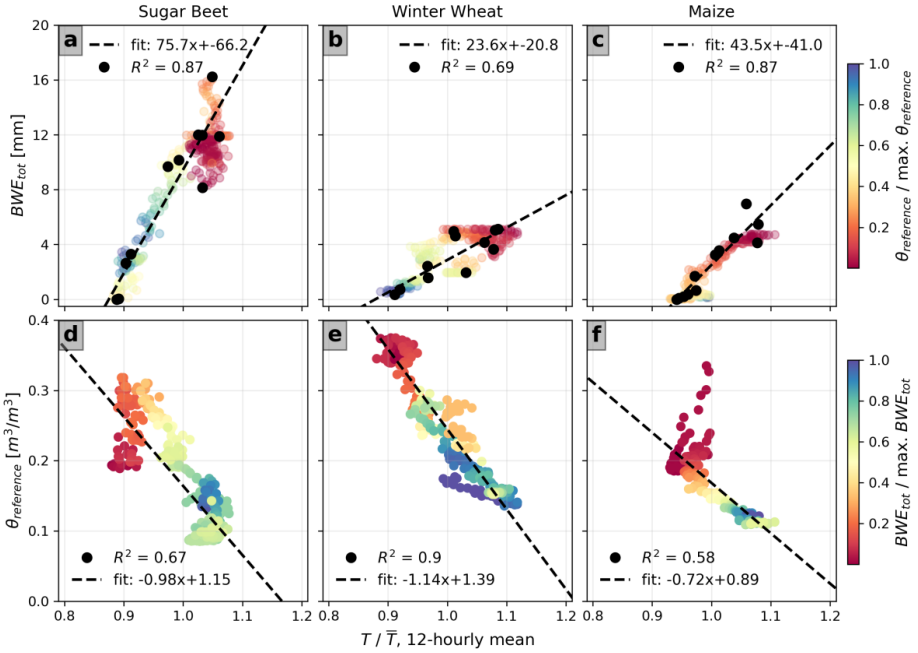

Figure 4.12: Scatter plots of normalized thermal neutron intensity (T) and BWE_{tot} as well as T and the reference soil moisture content ($\theta_{reference}$) for (a, d) sugar beet, (b, e) winter wheat, and (c, f) maize. The colouring sequence in subplots a) – c) indicate changes in $\theta_{reference}$. The colouring sequence in subplots d) – f) indicate changes in BWE_{tot} (linearly interpolated). All linear regressions have slopes that are significantly different from 0 (i.e., the two sided p-value was < 0.05 for tests with the null hypothesis that the slopes are equal to zero).

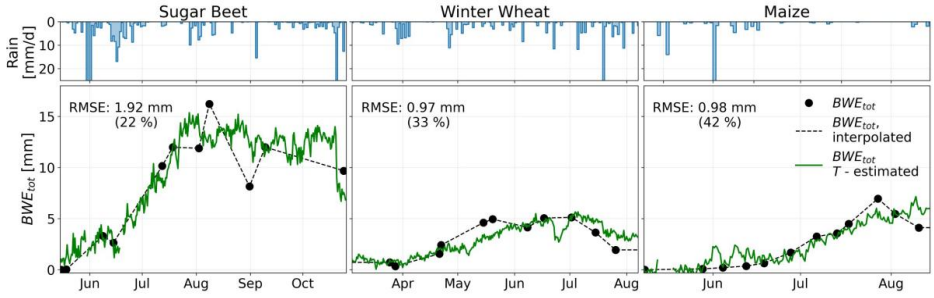

Figure 4.13: Time series of precipitation and the measured (black dots), interpolated (striped lines), and thermal neutron (T) estimated (green lines) sum of the above- and belowground biomass water equivalent (BWE_{tot}) for sugar beet, winter wheat, and maize. Furthermore, the root mean square error (RMSE) and the RMSE relative to the average interpolated BWE_{tot} are provided.

4.4 Discussion

4.4.1 Correction of biomass effects on soil moisture content estimates with CRNS

Table 4.3: Calibration/correction strategies, measurement requirements, and associated root mean square error (RMSE) of the CRNS derived soil moisture content estimations for the three crops. Green and orange highlight the best and second-best performance, respectively, and red highlights the worst performance in RMSE.

Calibration/Correction strategy	Measurement Requirements (in addition to epithermal CRN measurements)	Sugar Beet	Winter Wheat	Maize
		RMSE [m^3/m^3]		
Optimized (no correction, strategy A)	Multiple in-situ soil moisture contents (here continuous measurements)	**0.042**	**0.031**	**0.011**
Bare soil (no correction, strategy B)	One in-situ soil moisture content in the beginning of the measurement	**0.097**	**0.041**	**0.019**
BWE_a	Multiple aboveground biomasses and in-situ soil moisture contents measured at the same time	**0.032**	**0.018**	**0.009**
BWE_{tot}	Multiple total biomasses and in-situ soil moisture contents measured at the same time	**0.015**	**0.018**	**0.009**
$BWE_{a,\ Baatz}$	One in-situ soil moisture content with low aboveground biomass and multiple aboveground biomasses	**0.071**	**0.027**	**0.027**
$BWE_{tot,\ Baatz}$	One in-situ soil moisture content with low total biomass and multiple total biomasses	**0.048**	**0.026**	**0.029**
N_r (N_r at *BWE*-dates)	Multiple in-situ soil moisture contents and thermal neutron detectors	**0.032 (0.03)**	**0.022 (0.023)**	**0.011 (-)**
T (T at *BWE*-dates)	Multiple in-situ soil moisture contents and thermal neutron detectors	**0.017 (0.018)**	**0.019 (0.02)**	**0.009 (0.011)**

The strategies for correcting soil moisture content estimates with CRNS for biomass effects, the associated measurement requirements, and the resulting RMSE are summarized in Table 4.3. We found that correcting the epithermal neutron intensities based on local linear regression models between N_0 and *BWE*, N_r or the thermal neutron intensity led to improved performance compared to the widely used bare soil calibration (e.g., ZREDA ET AL., 2012; BAATZ ET AL., 2014; HAWDON ET AL., 2014; BOGENA ET AL., 2018; COOPER ET

AL., 2021). Considering in-situ measured BWE_{tot} always resulted in the most accurate CRNS based soil moisture content estimates, but this requires several reference soil moisture content and biomass measurements during the growing season. The second highest accuracy was achieved when thermal neutron intensity was used for correction (see Table 4.3). This correction approach only requires thermal neutron and soil moisture content measurements. Even though N_r was insensitive to biomass changes of winter wheat and maize in this study, the accuracy achieved using a correction based on N_r was similar to the accuracy achieved with in-situ measured aboveground biomass with the added advantage that no in-situ biomass information is required (see Table 4.3; TIAN ET AL., 2016; JAKOBI ET AL., 2018; VATHER ET AL., 2020). The empirical relation of BAATZ ET AL. (2015) also resulted in a considerable improvement in accuracy for sugar beet and winter wheat, and the performance could possibly be improved if an exponential instead of a linear model would be considered (e.g., HAWDON ET AL., 2014). However, the relation of BAATZ ET AL. (2015) failed to represent the effect of maize biomass on the epithermal neutron intensity, because of the observed increase in N_0 with increasing biomass (see Figure 4.5c). Nevertheless, considering the biomass effect on CRNS based soil moisture content estimates through this type of generic empirical model is still appealing because it only requires biomass estimates and no soil moisture content measurements are required (Table 4.3; HAWDON ET AL., 2014; BAATZ ET AL., 2015).

The improved accuracy of the soil moisture content estimates after correction using thermal neutron intensity or N_r may potentially also be explained by the shallower penetration depth of thermal neutrons (Chapter 3) compared to epithermal neutrons (FRANZ ET AL., 2012b; KÖHLI ET AL., 2015; SCHRÖN ET AL., 2017). It is possible that the corrections considering thermal neutrons (i.e., also N_r) compensate for the vertical soil moisture content heterogeneity. To this end, reference soil moisture content information in depths < 5 cm was not available in our experiments and thus not considered in the vertical weighting function for epithermal neutrons of SCHRÖN ET AL. (2017). This would be consistent with earlier studies that reported the strong influence of vertical soil moisture content heterogeneity on the accuracy of soil moisture content estimation from epithermal neutrons (FRANZ ET AL., 2013a; BARONI ET AL., 2018; SCHEIFFELE ET AL., 2020) and suggested to additionally install point sensors for estimating a field-representative shape of the soil moisture content profile (SIGOUIN ET AL., 2016; BARONI ET AL., 2018; SCHEIFFELE ET AL., 2020).

4.4.2 **Biomass estimation with CRNS**

The experiments with three crop types showed that N_r cannot generally be used for the prediction of aboveground biomass, as suggested in earlier studies (TIAN ET AL., 2016; ANDREASEN ET AL., 2017a; JAKOBI ET AL., 2018; VATHER ET AL., 2020). The estimation of aboveground biomass from N_r was possible for sugar beet, but not for winter wheat and maize in this study (Figure 4.11). In contrast, the estimation of total biomass (above- and belowground biomass) from thermal neutron intensity alone was possible for all investigated crops. However, the empirical relationships between thermal neutron intensity and biomass varied considerably between the three crops (Figure 4.12a-c). A possible explanation for this could be a variation in soil chemistry that affected the intensity of the thermal neutrons differently for the three investigated fields (ZREDA ET AL., 2008). However, this is unlikely as the three fields are very close to each other and with the same geology, so that the differences in soil chemistry are only marginal. Therefore, we assume that the relationship between the thermal neutron intensity and biomass is mainly plant-specific, i.e. influenced by plant structure.

Furthermore, we found that the observed correlation between thermal neutron intensity and soil moisture content (Figure 4.12d-f) is only apparent due to the simultaneous development of biomass. This finding is supported by the study of TIAN ET AL. (2016) in which thermal neutron intensity also increased mainly with increasing biomass (see Figure 4 in TIAN ET AL., 2016). Since snow is expected to affect thermal neutron intensity in a similar way as vegetation cover, our interpretations are also supported by findings from DESILETS ET AL. (2010). They showed that the thermal neutron intensity increased strongly with the onset of snow precipitation, while the epithermal neutron intensity decreased. This finding was verified using neutron transport simulations, where a ~2.5 fold increase in thermal neutron intensity for increasing snow thickness up to ~3 g/cm^2 was found as compared to snow free conditions (see Figure 4 in ZWECK ET AL., 2013). In contrast, the reduction in thermal neutron intensity due to increasing soil moisture content from ~0.10 – 0.45 m^3/m^3 can be approximated from neutron transport simulations presented in Figure 2 of ZREDA ET AL. (2008) and is expected to amount up to ~20 % only, depending on soil chemistry. Consequently, thermal neutron intensity should be affected more strongly by crop biomass than soil moisture content, thus opening the possibility of biomass estimation from thermal neutron intensity as shown in our study.

4.4.3 **Vegetation influence on neutron intensities**

Figure 4.14 summarizes important vegetation-related processes controlling epithermal and thermal neutron intensity. In case of bare soil conditions (Figure 4.14a), thermal neutrons are mainly produced in the ground. In case vegetation is present, epithermal neutron intensity is decreased by moderation of biomass, resulting in additional production of thermal neutrons (Figure 4.14c). Moreover, in case large amounts of belowground biomass are present (e.g., as for sugar beet), thermal neutron production in the ground is additionally enhanced (Figure 4.14b). When the detector is surrounded by tall vegetation (e.g., as for maize), the greater density of scattering centers (i.e., atomic nuclei of the biomass) increases the local neutron density, resulting in a higher neutron detection probability (LI ET AL., 2019). This phenomenon was observed for maize in this study (Figure 4.5c), but not for the other crops. This indicates that neutron intensity also depends on vegetation structure and the detector position relative to the vegetation.

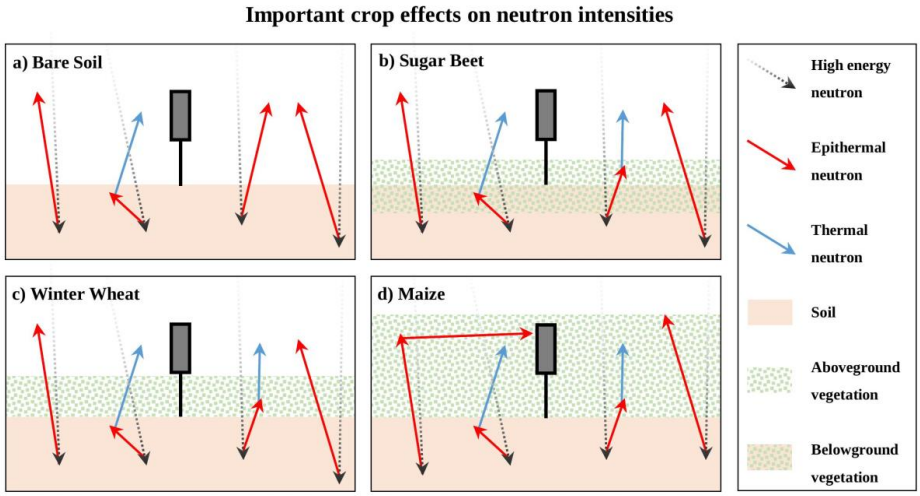

Figure 4.14: Summary of important vegetation related processes for thermal and epithermal neutrons for (a) bare soil, (b) sugar beet, (c) winter wheat, and (d) maize.

4.5 **Conclusions and Outlook**

In our study we used sugar beet, winter wheat, and maize, to analyze the effect of crop biomass on estimating soil moisture content with CRNS. We found that correcting the influence of vegetation using local linear regression models based on the calibration parameter N_0 consistently improved the accuracy of soil moisture measurements with

CRNS. The best performance in terms of RMSE was obtained when both above- and belowground biomass were considered for correction. When only aboveground biomass was considered, the performance decreased when high amounts of belowground biomass were present (i.e., in the case sugar beet). The empirical linear relationship of BAATZ ET AL. (2015) also improved measurement accuracy, except for maize where the accuracy was considerably lower after correction. In contrast, a vegetation correction based on the thermal-to-epithermal neutron ratio (N_r) or thermal neutron intensity always improved the accuracy of soil moisture content measurement with CRNS. Different from results presented in earlier studies (TIAN ET AL., 2016; JAKOBI ET AL., 2018), N_r was not consistently related to changes in aboveground biomass. However, we found that thermal neutron intensity could also be used to predict changes in total biomass (i.e., the sum of above- and belowground biomass water equivalent - BWE_{tot}).

For future studies, we suggest to investigate the dependency of thermal neutrons on different biomass and vegetation structures in more detail. To this end, irrigation experiments or neutron transport simulations could allow for the investigation of neutron intensities with constant soil moisture content and changing biomass/vegetation structures (and vice versa). The influence of the vegetation structure (i.e., the density of stalks, fruit bodies and the plant height) should also be investigated using neutron transport modelling. Similarly, forest sites are interesting to consider as we anticipate a different behavior of thermal neutrons in comparison to sites were all hydrogen sources are at the same height or below the detectors (Chapter 3; ANDREASEN ET AL., 2017a; ANDREASEN ET AL., 2020).

5 Synopsis

In this chapter the results of this work are summarized and final conclusions are drawn. Based on this, knowledge gaps are identified and some of these are adressed with two examples, allowing for preleminary conclusions.

5.1 **Final summary and conclusions**

Cosmic ray neutron sensors (CRNS) are widely used for soil moisture content measurements because they allow for the non-invasive derivation of an integrated signal that is representative for scarcely monitored scales (compare Figure 1.1). However, the accuracy of soil moisture content measurements with CRNS depends on statistical measurement uncertainty, which hampered interpretation in earlier studies (i.e., distinction of statistical effects from effects of environmental water), especially when CRNS were used in mobile mode. Moreover, the presence of other pools of hydrogen than soil moisture content in the surroundings of the instrument (e.g., biomass) reduce the accuracy of soil moisture content measurements with CRNS. This can be overcome by considering the thermal-to-epithermal neutron ratio (N_r) for correction of such influences. However, in earlier studies, N_r could not be evaluated in detail because certain basic concepts, such as the footprint of the measured thermal neutron signal, were yet unknown. Additionally, N_r was not yet compared exhaustively with other existing methods that consider the effect of biomass on soil moisture content measurements with CRNS. These were the starting points for the work presented in this thesis.

In Chapter 2 the influence of statistical measurement uncertainty on soil moisture content estimates with CRNS was investigated. The measurement uncertainty of the raw neutron counts is determined using Poisson statistics. This means that an increase in neutron intensity corresponds to both a decrease in measurement uncertainty and a decrease in soil moisture content. For stationary applications, the uncertainty from raw neutron counts in soil moisture content measurements with CRNS is routinely considered with aggregation ≥ 12 h. Mobile measurements with CRNS target the spatial mapping of soil moisture content, and therefore such long aggregation is undesirable. Consequently, mobile CRNS (e.g., CRNS mounted on cars - “CRN rover”) have to be more efficient, either by using multiple or larger detectors. However, accurate estimation of soil moisture content with mobile CRNS is still not possible without aggregation of neutron counts. To facilitate the estimation of the uncertainty from raw epithermal neutron counts, an easy to apply approach based on a 3rd order Taylor expansion was introduced. The Taylor expansion approach showed excellent agreement in comparison to the uncertainty assessed with Monte Carlo simulations and in comparison to the statistical measurement uncertainty determined in an experiment. Therefore, the new method was used to assess how the aggregation of raw epithermal neutron counts affects the soil moisture content

measurement uncertainty with two CRN rover experiments. Results showed that the proposed method is well suited for estimating the aggregation time (or the spatial aggregation) until a desired threshold in statistical uncertainty is reached. This was done exemplary using the dataset from DONG AND OCHSNER (2018), and during the evaluation a mistake was found in the conversion from gravimetric [g/g] to volumetric [m^3/m^3] soil moisture units in their publication, which resulted in a commentary (Appendix V). Furthermore, it was shown that the Taylor expansion approach can help in evaluating the extent of the effects of additional errors. For instance, with large soil moisture heterogeneities, small deviations in detector position affected the soil moisture content measurement accuracy. In contrast, with relatively homogeneous soil moisture conditions, the spatial variations in soil bulk density, and the effects of vegetation and roads were expected to be of greater importance than the uncertainty from raw epithermal neutron counts. In Chapter 2.3.1 the combined measurement uncertainties from raw epithermal neutron counts and soil bulk density were investigated with a theoretic example. On this basis, it was shown that the proposed method allows the comparison of the uncertainty from raw epithermal neutron counts with other errors. Finally, the consideration of the statistical measurement uncertainty was found to be crucial, especially for mobile soil moisture content measurements with CRNS. In this case, the measurement uncertainty translates to speed, which determines the spatial resolution and must be balanced against the accuracy requirements of the soil moisture product.

In Chapter 3 the footprint of thermal neutrons was investigated. This was done because N_t was considered promising for the estimation of biomass and for the consideration of biomass-related effects on soil moisture content measurements with CRNS. However, the footprint size of thermal neutrons and other basic properties were unknown, which hampered the interpretation of N_t. First, the horizontal footprint of thermal and epithermal neutrons was assessed experimentally to gain a coarse understanding of its characteristics. For this, the river Rhine was crossed with the Jülich CRN rover (also see Chapter 2.2.1 and Figure 2.1) with dry and wet soil moisture conditions, respectively. From the experiments, it was found that the horizontal thermal neutron footprint is smaller than that of epithermal neutrons. In a next step, the river-crossing experiments were reproduced with the neutron transport model URANOS (Ultra Rapid Adaptable Neutron-Only Simulations, KÖHLI ET AL., 2015). The measured signals did not fully match the simulation results, which was attributed to a mismatch of the measurement depths of in-situ reference measurements and

CRN measurements. Also, the effect of biomass on thermal neutron intensity (discussed in Chapter 4) was not considered in the simulations. Additional simplifications were necessary, because the composition of the energy dependent contribution to the measured signals of moderated (for measuring epithermal neutrons) and bare detectors (for measuring thermal neutrons), respectively, are not yet fully known. Despite such simplifications, the trends in the measured neutron intensities could be well reproduced with URANOS and therefore it was used to assess the footprint properties of thermal neutrons. The radial footprint (i.e, R_{86} – the distance up to which 86 % of the detected neutrons originate) of thermal neutrons ranges between 43 and 48 m and slightly increases with increasing soil moisture content. The vertical footprint (i.e., D_{86} – 86 % of the depth of all scattering interaction in the soil before detection) ranges between 10 and 65 cm soil depth for soil moisture contents from 0.50 to 0.01 m^3/m^3. Additionally, weighting functions were derived from the distance and depth dependent thermal neutron intensities and it was shown that the approach for assessing the dependency of pressure on epithermal neutrons from KÖHLI ET AL. (2015) can also be applied for thermal neutrons. The dependency of the thermal neutron footprint on detector height was also investigated and it was shown, that R_{86} increases approximately 5 m with 5 m increase in detector height, while D_{86} remains relatively unchanged (see Appendix III). Moreover, it was demonstrated that the footprint of thermals neutrons depends on soil chemistry. For this purpose, a ^{10}B component was added to the model domain, representing the cumulative absorption cross section of the most important soil elements in Europe. This reduced R_{86} and D_{86} by ~2 m and ~5 cm, respectively.

In Chapter 4, experiments with three crops (i.e., sugar beet, winter wheat, and maize) were used to first show and then and remove the effect of the hydrogen stored in dynamically growing biomass on soil moisture content measurements with CRNS. Four approaches for the consideration of biomass effects were compared: I) site-specific correction functions with in-situ measured biomass, II) the generic approach of BAATZ ET AL. (2015), III) site-specific correction functions with N_r, and IV) site-specific correction functions with thermal neutron intensity. When calibrated during bare soil conditions, the root mean square error (RMSE) between reference soil moisture content and soil moisture content estimated with CRNS was 0.097, 0.041, and 0.017 m^3/m^3 for the three crops, respectively. The consideration of in-situ measured biomass (i.e., the sum of above- and belowground biomass) was the most effective in removing the biomass effect on soil moisture content

measured with CRNS and reduced the RMSE by 84, 56, and 47 %, respectively. Considering thermal neutron intensity for correction was similarly accurate (reduction in RMSE by 82, 54, and 47 %). Also using in-situ measured aboveground biomass (reduction in RMSE by 67, 56, and 47 %) or N_r (reduction in RMSE by 67, 46, and 35 %) for the correction improved the measurement accuracy considerably. The generic approach from BAATZ ET AL. (2015) was not as effective and did not generally improve the measurement accuracy in comparison to calibration during bare soil conditions (reduction in RMSE by 26 and 36 % for sugar beet and winter wheat, respectively, but an increase in RMSE by 60 % for maize). This was due to an increase in epithermal neutron intensity, as the plant parts of the maize acted as additional scattering centres, effectively increasing the measured epithermal neutron intensity. This increase even overcompensated for the neutron attenuating effect of the biomass due to elastic collisions with hydrogen. In addition, it was found that biomass estimation from N_r was possible for sugar beet, but not for winter wheat and maize. Nonetheless, site and plant specific linear regression models of thermal neutron intensity and biomass were found for all crops. It was thus concluded that thermal neutron intensity has potential for the measurement of biomass and for the consideration of biomass related effects on soil moisture content measurements with CRNS.

Overall, stationary and mobile CRN measurements provide accurate estimates of soil moisture content when appropriate measures are taken to consider and remove measurement uncertainties or factors not considered during calibration. Such information has practical relevance in several contexts. For agriculture in arid regions, for example, information on field scale soil moisture content can be useful for irrigation scheduling and optimal use of limited water resources. In this context, vegetation monitoring with thermal neutron intensity provides additional information for the agricultural management. Furthermore, pre-storm soil moisture content is crticial for the prediction of flood events and landslides and thus important information for warning the public of such events. Finally, CRNS derived soil moisture content can be used to validate and improve global data products from remote sensing and landsurface models that provide soil moisture content information in regions were in-situ obervations are scarce.

5.2 **Outlook and preliminary work**

The findings and methods developed in this thesis allow for an improved characterization of soil moisture content measurements with CRNS and provide a new approach for the

measurement of biomass with CRNS. However, there are a range of limitations to the presented findings which are summarized in the following. In addition, preliminary ideas for future developments are identified and two examples are presented.

The uncertainty assessment presented in Chapter 2 is limited to the effects of neutron count statistics and uncertainty in soil bulk density measurements on the accuracy of soil moisture content measurement with CRNS. However, numerous additional uncertainties exist, that were not considered in Chapter 2. Examples are I) the uncertainty in the calibration parameter of the standard approach for the conversion of epithermal neutron intensities to soil moisture content "N_0" (DESILETS ET AL., 2010), II) the measurement uncertainties in the variables used for correction of epithermal neutron intensities (i.e., pressure, temperature, relative humidity, and incoming CRN measurements), III) the uncertainty in soil moisture content measurements used for calibration, and IV) the uncertainties from additional hydrogen pools (e.g., lattice water, soil organic carbon, biomass, roads, interception, and litter layer). Most of these uncertainties were already accounted for in previous studies (e.g., BARONI ET AL., 2018; GUGERLI ET AL., 2019) but a unified approach is not yet available and would be highly beneficial. To this end, the described Taylor expansion approach for considering the uncertainty from raw neutron counts could be integrated into a more exhaustive uncertainty assessment.

The thermal neutron footprint simulations presented in Chapter 3 did not include the influences of vegetation and soil bulk density. Furthermore, the influences of soil chemistry and detector height above ground were not considered in the analytical weighting functions. Future work could investigate this in more detail for a deeper understanding of the representativeness of the measured thermal neutron signal. Moreover, the used definitions have great impact on the estimated footprints (e.g., RASCHE ET AL., 2021) and not all of these were discussed exhaustively in the original manuscript (i.e., Chapter 3). For instance, the origin of a thermal neutron was defined by its first soil contact below 0.5 eV, which may not be representative for the thermal neutrons measured by the CRNS for at least two reasons. First, it was demonstrated that thermal neutrons are more dependent on vegetation than on soil moisture content (Chapter 4), and consequently it might be more appropriate to consider neutron scatterings in vegetation rather than in the soil to define the footprint. Second, it is unclear to which extent interactions of neutrons above the cutoff of 0.5 eV are of importance. This cutoff is artificially defined by cadmium (i.e. neutrons $\leq$ 0.5 eV are effectively blocked by cadmium), which was used in earlier studies for the shielding of

CRN detectors (e.g., ANDREASEN ET AL., 2016; the "cadmium-difference method"). However, cadmium is highly toxic, and its use in natural environments is questionable. As a replacement, gadolinium can be used for the shielding of CRN detectors (WEIMAR ET AL., 2020), which strongly reduces neutrons ≤ 0.2 eV and was considered in the study by RASCHE ET AL. (2021). In addition, the horizontal and vertical footprint definitions differed (i.e., the first soil contact and the number of all scattering interactions in the soil, respectively). Future works should attempt to formulate the footprint definitions more consistently (i.e., also for epithermal neutrons). For example, the focal point of all neutron interaction (i.e., the average distance of all interactions until a neutron is measured) in the soil could be used. Alternatively, the first soil contact and the maximum depth of a neutron could be considered (RASCHE ET AL., 2021). It would also be possible to consider ensembles of footprint definitions, which would furthermore allow for uncertainty analysis. However, as for the definitions used in Chapter 3, these options would be arbitrary choices. An option that circumvents the drawbacks of the discussed footprint definitions would be to consider a measurable concept. SCHRÖN (2017) proposed to define the footprint based on the distance in which a change in soil moisture content is still observable in the measured neutron signal. Unfortunately, this would come with the drawback that the footprint definition depends on the sensitivity of the neutron detector (SCHRÖN, 2017). Furthermore, this definition may be problematic for defining the thermal neutron footprint because the dependency of thermal neutron intensity on soil moisture content is not well understood yet.

The dependency of thermal neutron intensity on pressure, air humidity, incoming CRN, biomass, vegetation structure (i.e., the density of plants, stalks, fruit bodies and plant height), and soil chemistry are also not well understood. Neutron transport simulations could enable the discrimination of the influences from these variables on thermal neutron intensity. Similarly, additional experimental evidence could be helpful. For instance, irrigation experiments could allow to distinguish effects from biomass/vegetation structure and soil moisture content. Also dedicated field experiments with crops not yet investigated in detail (e.g., winter barley, rape seed, potato) and time series (or time lapse observations) covering multiple cropping periods on the same location could be considered. To this end, it would be helpful to reduce the measurement uncertainty, e.g., by collocation of multiple detectors (see Chapter 4) or by using high sensitivity devices (e.g., CRN rovers). In addition, vegetation proxies should be considered to characterize vegetation (and reduce

labor-intensive biomass sampling), as thermal neutron intensity is expected to be sensitive to plant structure. For this, possible options are plant height, stem diameter, leaf area index (see maize experiment in Chapter 4), and canopy geometry measurements. For more continuous observations of vegetation proxies, ground-based 3D LiDAR (Light Detection And Ranging; allows to derive e.g., plant height, aboveground biomass (HOFFMEISTER ET AL., 2016)) measurements could be considered.

5.2.1 Example 1: Long-term vegetation monitoring with thermal neutrons

From field F11 of the TERENO (TERrestrial ENvironmental Observatories) test site Selhausen (see Figure 4.1), there are longer time series of neutron counts compared to the dataset used in Chapter 4 (winter wheat experiment) and accompanying plant height data is available. These were used in the following to evaluate if thermal neutron intensity could potentially be used to monitor biomass development over multiple cropping periods. Additionally, the dependency of thermal neutrons on soil moisture content and incoming CRN was investigated. For this, a dataset containing neutron counts, variables necessary for correction (i.e., air pressure, air humidity, and temperature), and soil moisture content time series was retrieved (BOGENA AND NEY, 2021). A description of the soil moisture content data product derivation from epithermal neutron counts measured by Selhausen CRNS station can be found in BOGENA ET AL. (2021). Daily precipitation sums were obtained from a climate station ~400 m northeast (SE_BDK_002, http://teodoor.icg.kfa-juelich.de/ibg3searchportal2/index.jsp). Thermal neutron intensity was corrected as described in Chapter 4.2.7 (also see Appendix I). Additionally, the correction of thermal neutron intensity for incoming CRN was tested (ZREDA ET AL., 2012; Equation (A.2)) using the neutron monitor at Jungfraujoch (JUNG; via www.nmdb.eu; as reference value thermal neutron intensity of the first day of the observation period was used). As the study period was covered by only one detector rather than multiple detectors (in comparison to the experiments presented in Chapter 4), daily rather than 12-hourly aggregation was used to reduce the inherent uncertainy in CRN measurements (see Chapter 2).

An overview of precipitation, thermal neutron intensity, and soil moisture content measurements with CRNS is given in Figure 5.1. An increasing trend was observed for the pressure- and humidity-corrected thermal neutron intensity (Figure 5.1b, red), which was

removed when additionally incoming CRN were used for correction (Figure 5.1b, black). After correction, a relatively stable minimum range of ~310 - 330 cts/h was found with plant heights ≤ ~20 cm (compare Figure 5.1b and Figure 5.1d). However, there are slight differences between the minimum values for the different cropping periods, possibly due to different managements such as tillage and soil preparation for the next crop.

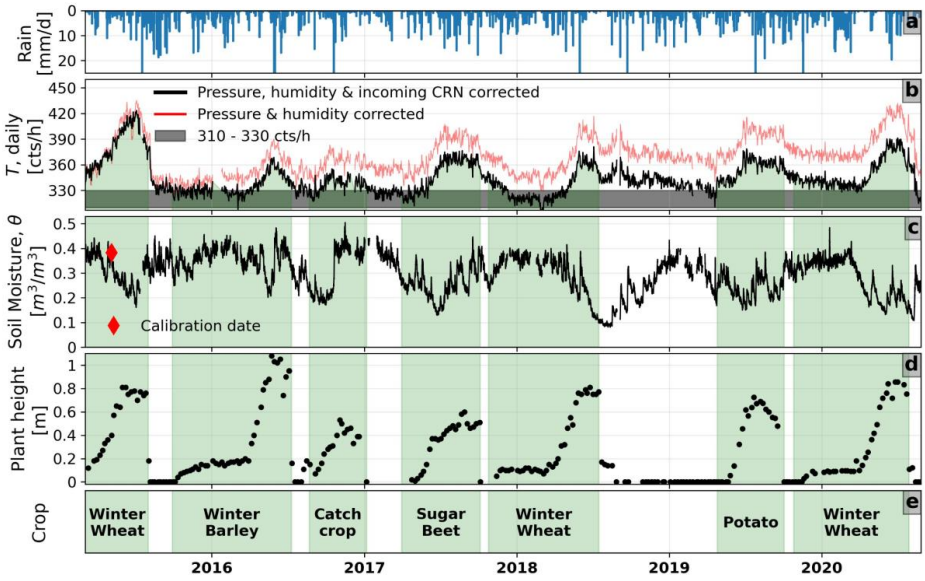

Figure 5.1: Time series from the field site F11 (see Figure 4.1) showing a) precipitation, b) thermal neutron intensity (T) before (red) and after (black) correction with incoming cosmic ray neutrons, c) soil moisture content estimated from epithermal neutrons (retrieved from BOGENA AND NEY (2021)), d) plant height, and e) crop rotation. Subplots b) - e) also show cropped periods (i.e., from sowing until harvest; green). Plant height measurements presented in subplot d) included stems of harvested plants, which is why there is sometimes a discrepancy between cropping period and plant height (e.g., end of winter wheat period in 2018).

Thermal neutron intensity clearly followed typical crop development patterns until the summer 2018, when a heatwave across northern and central Europe resulted in yield losses (e.g., BEILLOUIN ET AL., 2020). Succeeding this event, thermal neutron intensity did not return to the formerly identified minimum range until potatoes were planted in May 2019, even though the field was uncultivated. Unlike in the experiments presented in Chapter 4, the plant height and soil moisture content time series shown in Figure 5.1 were not always co-developing. For example, towards the end of the winter barley cropping period in 2016, there was a sharp decrease in soil moisture content (i.e., a sharp increase in epithermal neutron intensity), while thermal neutron intensity remained relatively unchanged. In

contrast, soil moisture content increased towards the end of the sugar beets period in 2017, and thermal neutron intensity remained nearly constant.

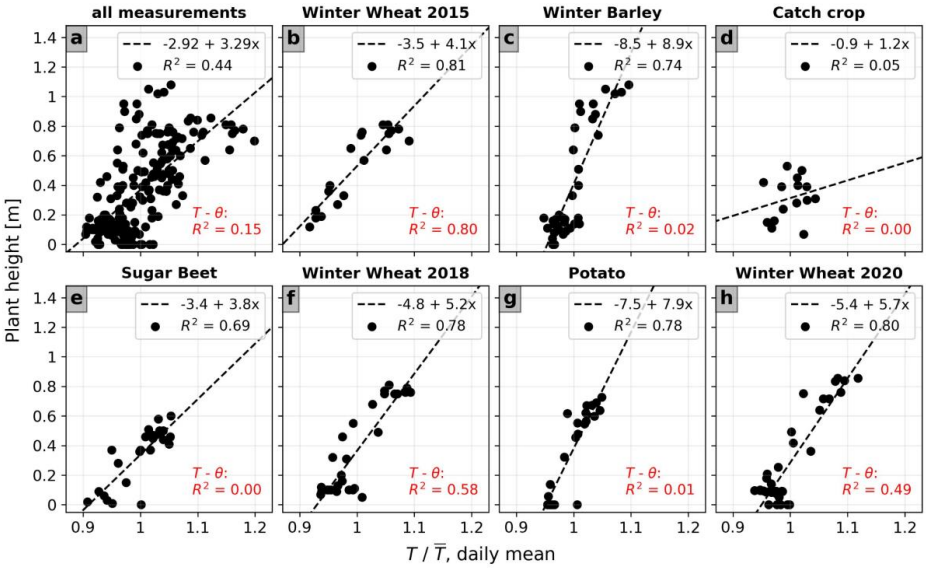

Figure 5.2: Scatter plots showing plant height as a function of thermal neutron intensity (T) relative to the mean of T of the entire study period from the field site F11 of a) all measurements during the study period and b) - h) the individual cropping periods (green areas in Figure 5.1). Additionally, corresponding linear regression models and R^2 are shown. Except for the linear regression model shown in d) all slopes were significantly different from 0 (i.e., the two sided p-value was < 0.05 for tests with the null hypothesis that the slopes are equal to zero). In the lower right corner of all subplots the R^2 of the thermal neutron intensity – soil moisture content (θ) relationships are shown (red).

Scatter plots, linear regression models, and R^2-values of the thermal neutron intensity – plant height relationships for the entire study period and for the individual cropping periods (corresponding to the green colored periods in Figure 5.1) are shown in Figure 5.2. All linear regression models were positively correlated, but the slopes differed considerably, especially between the different crop types. The weakest regression slope was found for catch crop, followed by the scatter plot with all measurements during the study period and sugar beet. In contrast, the regression slopes for winter barley and potato were the steepest and all the three regression slopes of the winter wheat periods were in the middle range. Except for the catch crop model, all linear regression models had slopes that were significantly different from 0. For all measurements during the study period R^2 was 0.44, while R^2 was 0.05 for the catch crop period, and ≥ 0.69 for the other individual cropping periods. It has to be noted, that R^2 increased considerably when thermal neutron intensity

was aggregated over longer time intervals, e.g., weekly aggregation increased R^2 to values > 0.83, except for all measurements during the study period (0.47) and the catch crop period (0.41). The R^2 of the thermal neutron intensity - soil moisture content relationships were consistently lower (Figure 5.2, red) than the R^2 of the thermal neutron intensity – plant height relationships. In addition, only for four of the thermal neutron intensity - soil moisture content relationships (i.e., the relationships considering all measurements during the study period, winter wheat 2015, 2018, and 2020) the slopes were significantly different from 0 (not shown).

In conclusion, these findings indicate that I) thermal neutron intensity depends on the incoming CRN intensity, II) thermal neutron intensity is more related to changes in vegetation than changes in soil moisture content, III) plant height is of importance for understanding the effect of vegetation on thermal neutron intensity, and IV) when calibrated locally and for individual cropping periods, thermal neutron intensity has potential for the measurement of plant height on agricultural sites. However, the relatively poor correspondence in case of the catch crop period indicates that the relationships between thermal neutron intensity, plant height, and other plant parameters (e.g., biomass, leaf area index) are not clear and should be further investigated, i.e., with neutron transport simulations or additional experiments.

5.2.2 **Example 2: Value and limits of CRN rover observations**

For this thesis, epithermal and thermal neutron intensities in the Rur catchment, were regularly monitored with the Jülich CRN rover (see Chapter 2.2.1) between 2018 and 2020 with over 40 measurement days. During these surveys, many of the stationary CRNS in the TERENO Rur hydrological observatory (BOGENA ET AL., 2018) were visited for the calibration of the CRN rover (e.g., CHRISMAN AND ZREDA, 2013; DONG ET AL., 2014; FRANZ ET AL., 2015; DONG AND OCHSNER, 2018). However, due to synergies with other projects, lack of time or for other practical reasons, the same path could not always be chosen. Nonetheless, the observations open a multitude of possible applications. For instance, the dataset is useful for the characterization of the influence of soil chemistry on thermal neutron intensity. Also, an attempt could be made to validate the assumption that the calibration parameter of the standard approach for the conversion of epithermal neutrons to soil moisture content (i.e., "N_0"; DESILETS ET AL., 2010) is stable in space (e.g., BAATZ ET AL., 2015; HEISTERMANN ET AL., 2021b). Roads typically produce more

epithermal neutrons than the surrounding soils and therefore CRN measurement on roads (i.e., with rovers) usually result in an underestimation of the surrounding soil moisture content (SCHRÖN ET AL., 2018a). As the directional sensing of epithermal neutrons seems feasible (FRANCKE ET AL., 2021) the simultaneous measurement with vertically and horizontally oriented detectors may allow for the discrimination of road and soil moisture content effects on epithermal neutron intensities. The measurements for this dataset were obtained with different detector orientations and therefore could allow the development of such an approach. Furthermore, the vegetation along the CRN rover transects was very diverse (i.e., forest, agriculture, grassland, meadow). Therefore, this dataset is also useful for further studies on the dependence of neutron intensities and neutron footprints on vegetation.

In the following, the 9.5 hours survey from 27 November 2018 is presented as an example. The measured neutron intensities were corrected for atmospheric pressure, air humidity, and incoming CRN as described in Chapter 4.2.7 (i.e., thermal neutron intensity was not corrected for incoming CRN). To reduce uncertainty in the raw neutron counts (see Chapter 2), 21 consecutive measurements were averaged (moving average; record period was 10 sec). Only measurements with a moving average speed of ≤ 50 km/h were considered, resulting in a spatial support of at least ~3 km. θ_{off} (the sum of lattice water and soil organic carbon) along the CRN rover transect was estimated from a linear regression model with latitude (values at the stationary CRNS are given in BAATZ ET AL. (2015) and BOGENA ET AL. (2018); $R^2 = 0.63$). The local soil bulk densities at the stationary CRNS were assigned to CRN rover measurement locations with distances ≤ 1km, while the average soil bulk density of all stationary CRNS was used for the remaining CRN rover measurement locations. The approach from DESILETS ET AL. 2010 was used for calibration with soil moisture content measurements from stationary CRNS (retrieved from BOGENA AND NEY, 2021) and epithermal neutron measurements with the CRN rover at distances ≤ 30 m. From this, N_0 (a free calibration parameter, see e.g., Chapter 2.2.4) was obtained by minimization of the RMSE between the reference soil moisture content and the soil moisture content estimated with the CRN rover.

Figure 5.3a shows the locations of the stationary CRNS used for calibration as well as a map of the soil moisture content estimated with the CRN rover along the transect. The northern part of the Rur catchment was much drier than the southern part at the time of measurement. Overestimation of soil moisture content can be expected in regions were the

measurements were obtained on wide roads (SCHRÖN ET AL., 2018a), such as in the northwest area of Figure 5.3a (i.e., > 10 m wide). In principal, the influence of roads on epithermal neutron intensities could be corrected (SCHRÖN ET AL., 2018a), but additional information on road width and material would be required, which was not available. In addition, the road correction from SCHRÖN ET AL. (2018a) was developed for road widths ≤ 7 m, which were generally exceeded along the investigated paths.

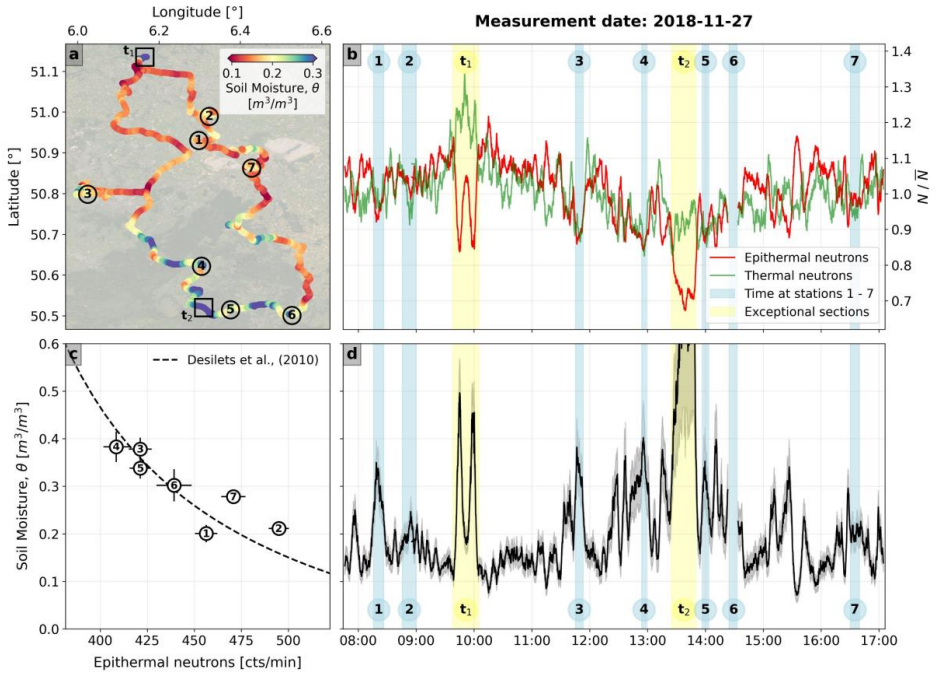

Figure 5.3: Cosmic ray neutron (CRN) rover transect of the Rur catchment from 27 November 2018. a) Map of soil moisture content measured with the CRN rover, locations of the stationary cosmic ray neutron sensors (CRNS) (circles), and locations with exceptional epithermal neutron intensities (squares). Base map: ESRI world imagery and contributors. b) 21 measurements rolling mean of epithermal and thermal neutron intensities relative to the mean intensity, respectively. c) Scatter plot of epithermal neutron intensities measured with the CRN rover and reference soil moisture content. Error bars indicate the uncertainty from raw epithermal neutron counts of the CRN rover, also propagated to soil moisture content with equations (2.10) and (2.11). The calibration curve for the CRN rover according DESILETS ET AL. (2010) is also shown (N_0 = 773 cts/min). d) Soil moisture content measured with the CRN rover. Gray shaded areas indicate the uncertainty in soil moisture content from raw neutron counts. Subplots b) and d) also show CRN rover locations with distances ≤ 30 m to stationary CRNS (lightblue) and sections with exceptionally low epithermal neutron intensities (light yellow). The peak in soil moisture at 13.30 is not shown as such values were considered unrealistic.

The relative epithermal and thermal neutron intensities and the times when the CRN rover was standing at the stationary CRNS are shown in Figure 5.3b (red, green and light blue,

respectively). From this, two sections with outstanding reduction in epithermal neutron intensities can be identified (light yellow in Figure 5.3b). This is also reflected in the soil moisture content estimates shown on the map in Figure 5.3a (black squares) and in Figure 5.3d (light yellow). For these sections, an overestimation of soil moisture content can be expected because they correspond to forested areas (the TERENO sites Wildenrath and Wüstebach; e.g., BAATZ ET AL., 2015; VATHER ET AL., 2020). Moreover, the epithermal neutron intensity within these sections decreased and, consequently, the uncertainty from raw epithermal neutron counts in the soil moisture content estimates increased considerably (see gray shaded areas in Figure 5.3d; obtained with equations (2.10) and (2.11)). Interestingly, thermal neutron intensity increased only in section t_1, even though a positive relation with biomass was expected in both sections (see Chapter 4). This can be explained with the strong dependency of the thermal neutron intensity on features close to the detector (almost 50 % of the detected neutrons originate from distances ≤ 5 m; see Figure 3.2), as the tree trunks were denser and closer to the CRN rover in section t_1, while they were less dense and further away in section t_2.

Figure 5.3c shows the calibration curve and a scatter plot of reference soil moisture content at stationary CRNS as a function of epithermal neutron intensities measured with the CRN rover. Additionally, the uncertainty in raw epithermal neutron counts and the uncertainty in soil moisture content estimates from raw epithermal neutron counts (obtained with equations (2.10) and (2.11)) for the CRN rover are shown as error bars. It is possible that for the stationary CRNS at the agricultural sites 1, 2 and 7, undetermined features were not considered in the calibration. This could be explained with a difference in biomass and/or vegetation structures between the time of calibration of the stationary CRNS and the calibration shown in Figure 5.3c.

In conclusion these findings indicate, that I) the influence of roads on soil moisture content measurements with CRN rover surveys cannot be easily addressed, II) the use of thermal neutron intensity for the correction of biomass effects on soil moisture content measurements with CRN rovers is particularly challenging because of the difference in footprint size of epithermal and thermal neutrons, and III) the uncertainty estimation tool introduced in Chapter 2 is useful to distinguish the statistical measurement uncertainty from raw neutron counts in soil moisture content measurements with CRNS from other errors. In future, the mobile application of CRNS could rely on regularly scheduled transport vehicles (e.g., trains or busses). In this way, measurements could be made more reliably

along the same path, which would allow diurnal changes to be recorded and drastically reduce the workload (SCHRÖN ET AL., 2021). Another interesting possibility for mobile CRNS application is the airborne measurement (e.g., with blimps), which would allow coverage of larger areas and would be independent of road infrastructure (HEISTERMANN ET AL., 2021a).

Appendix

Appendix I: Standard processing

The measured epithermal neutron intensities presented in Chapters 2 - 5 were processed with three standard procedures described in the following. With respect to thermal neutron intensity, the appropriate processing is still under debate and therefore the procedure that was applied is separately described for each chapter.

With an increase in atmospheric pressure, the number of collisions of high-energy neutrons increases and the epithermal neutron intensity measured at the ground surface consequently decreases. To account for this, the approach from DESILETS AND ZREDA (2003) can be used:

$$f_p = \exp\left(\frac{P_0 - P}{L}\right) \tag{A.1}$$

where P and P_0 are the locally measured air pressure [mbar] and an arbitrarily chosen reference value, respectively (e.g., in this work either 1013.25 mbar - the normal pressure at sea level – or the average over the respective investigation period was chosen), L [g/cm^3] is the local mass attenuation length that decreases with latitude (i.e., in this work 131.6 g/cm^3 was chosen; DESILETS AND ZREDA, 2003) and f_p is a temporal variable correction factor to account for the influence of pressure on the epithermal neutron intensity.

With an increase in the incoming cosmic ray neutron intensity also the epithermal neutron intensity at the ground surfaces increases (DESILETS AND ZREDA, 2001). A well established method to correct the measured epithermal neutron intensities with the temporal variation observed at one (or the mean of several) of the worldwide distributed neutron monitors is the approach from ZREDA ET AL. (2012):

$$f_i = \frac{I_{ref}}{I} \tag{A.2}$$

where I [cts/h] is the countrate of the neutron monitor obtained via the neutron monitor database (www.nmdb.eu; in this work the neutron monitor at Jungfraujoch (JUNG) was used), I_{ref} [cts/h] is an arbitrary reference value (in this work either a fixed value of 150 cts/h, the average over the respective investigation period, or a value from the beginning of the investigation period was chosen), and f_i is a temporal variable correction factor for the influence of the incoming cosmic ray neutron intensity on the epithermal neutron intensity.

With increasing water vapor, the loss of kinetic energy of neutrons in the atmosphere increases. ROSOLEM ET AL. (2013) found that this can be accounted for with:

$$f_h = 1 + 0.0054(h - h_0) \tag{A.3}$$

where h is the locally measured absolute air humidity [g/cm^3], h_0 is an arbitrarily chosen reference air humidity (i.e., in this work it was set to 0 g/cm^3), and f_h is a temporal variable correction factor to account for the influence of air humidity on the epithermal neutron intensity.

To apply the corrections given in Equations ((A.1) - (A.3)), the measured raw epithermal neutron intensity (E_{raw} [cts/time]) is multiplied with the respective correction factor:

$$E = E_{raw} * f_p * f_i * f_h \tag{A.4}$$

where E [cts/time] is the corrected epithermal neutron intensity.

Appendix II: Thermal neutron footprint - weighting functions and parameters

The article "JAKOBI, J., HUISMAN, J. A., RASCHE, D., VEREECKEN, H., AND BOGENA, H. R. (2021), The footprint characteristics of cosmic ray thermal neutrons." presented in chapter 3 inlcudes an appendix, which is presented below.

The parameter functions F_i all depend on soil moisture content (θ_v [m^3/m^3]) and can be subdivided into a set of linear functions (Equations (A.5)) and a set of power functions (Equations (A.6)):

$$F_1, F_2, F_3, F_6, F_8, F_9 = p_3\theta_v + p_4 \quad \text{(A.5)}$$

$$F_4, F_5, F_7, F_{10}, F_{11}, F_{12} = p_3{\theta_v}^{p_4} \quad \text{(A.6)}$$

The parameters that apply to the functions F_i are provided in Table A.1.

Table A.1: Parameters for the functions F_i.

Parameter-function	p_3	p_4
F_1	-1.90331	18.33714
F_2	0.03771	-0.34645
F_3	-0.04252	1.55665
F_4	1.44161	0.00355
F_5	0.00767	-0.01029
F_6	-1.86707	18.32828
F_7	-164.3489	0.12357
F_8	-0.107	-0.79174
F_9	0.49036	5.19522
F_{10}	1.01168	-0.00738
F_{11}	0.10415	0.79743
F_{12}	-164.80664	0.12448

Appendix III: Dependency of the thermal neutron footprint on detector height

The article "JAKOBI, J., HUISMAN, J. A., RASCHE, D., VEREECKEN, H., AND BOGENA, H. R. (2021), The footprint characteristics of cosmic ray thermal neutrons." presented in chapter 3 inlcudes supporting information, which is presented below.

We investigated the effect of detector height above ground on the thermal footprint characteristics using URANOS simulation by taking a model domain with 0.20 m^3/m^3 soil moisture content and 10 g/m^3 air humidity as an example. We found a strong dependency of the radial intensity and footprint (R_{86}) on detector height (see Figure A.1). As shown in the left plot in Figure A.1, the peak of radial intensity in the close range of the detector becomes much flatter with increasing detector height. Furthermore, it can be seen in the right plot of Figure A.1 that with increasing height of the detector, R_{86} increases (by approx. 5 m increase in R_{86} per 5 m increase in detector height). On the other hand, the vertical contribution to the total measured signal and D_{86} is almost independent of detector height (Figure A.2). However, with increasing detector height the uncertainty in the obtained results increased (i.e., the number of scattering interactions in the ground decreased), which is indicated by the increasing fluctuations in Figure A.2.

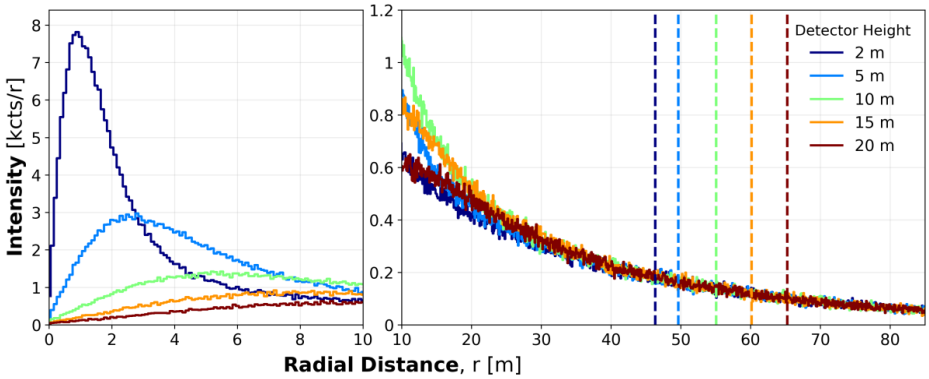

Figure A.1: Horizontal intensity of simulated thermal neutrons as a function of distance from the first interaction in the soil to detection for different detector heights ranging from 2 – 20 m above ground with constant soil moisture content of 0.20 m^3/m^3 and constant absolute humidity of 10 g/m^3. The dotted lines indicate the 86 % cumulative contribution quantile (R_{86}) for a specific detector height above ground.

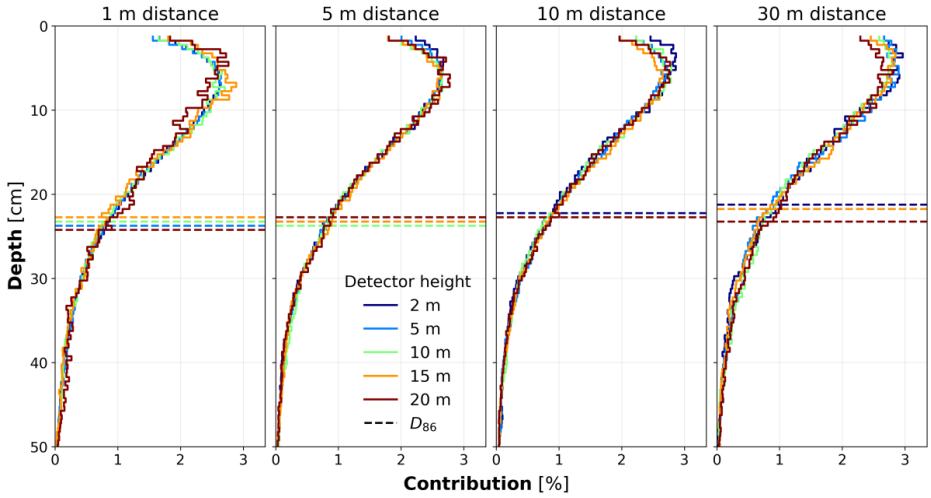

Figure A.2: Vertical contribution of all scattering interactions of thermal neutrons to the total neutron flux at 1, 5, 10, and 30 m distance from the first interaction in the soil to detection for different detector heights ranging from 2 – 20 m with constant soil moisture content of 0.20 m^3/m^3 and constant absolute humidity of 10 g/m^3. The dotted lines indicate the 86 % cumulative contribution quantile (D_{86}) for a specific detector height above ground.

Appendix IV: Hysteresis in the sugar beet experiment

The manuscript "JAKOBI, J., HUISMAN, J. A., FUCHS, H., VEREECKEN, H., AND BOGENA, H. R. (in revision), Potential of thermal neutrons to correct cosmic-ray soil moisture content measurements for dynamic biomass effects." presented in chapter 4 inlcudes an appendix, which is presented below.

For sugar beet, we found hysteretic behavior in the $N_r - N_0$ (Figure 4.7a), N_r – soil moisture content (Figure 4.11d), and the thermal neutron intensity – soil moisture content (Figure 4.12d) relationships. Here, we investigate this hysteresis in more detail. From Figure A.3a-c it can be seen that the hysteresis also occurred in the epithermal neutron - soil moisture content relationship. In this case, three stages with different slopes can be identified. The coloring indicates that the different responses were related to the growth of biomass with the largest effect from belowground biomass (e.g., Figure A.3b at E = 0.9 and $\theta_{reference}$ = 0.3). Similarly, the thermal neutron intensity was strongly influenced by belowground biomass (Figure A.3e).

Figure A.4 shows that the hysteresis in the epithermal neutron intensity can be effectively removed with corrections considering in-situ measured BWE_{tot}, N_r or thermal neutron intensity, which is also indicated by the improvement in soil moisture content estimation in comparison to the bare soil calibration (i.e., calibration strategy B; see Table 4.3). However, the relation to soil moisture content was changed when N_r was used for correction. This may be related to the different footprints of thermal and epithermal neutrons and could possibly be accounted for by refitting the parameters p_i (Equation (4.9); DESILETS ET AL., 2010), as shown in earlier studies. For instance, RASCHE ET AL. (2021) found that the sum of thermal and epithermal neutrons could be used for soil moisture content estimation if p_i were refitted. In this context, it has to be noted that KÖHLI ET AL. (2021) showed that Equation (4.9) is over-parameterized and suggested that their reformulated equation should be much better suited for parameter fitting. However, this was beyond the scope of our study.

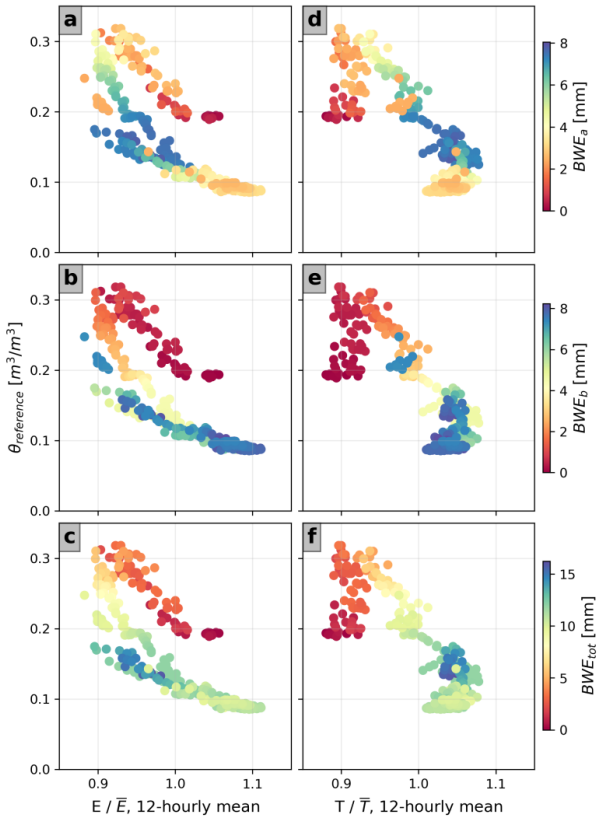

Figure A.3: Relationships of epithermal (a) – c)) and thermal neutron (d) - f)) intensities relative to their respective mean of the whole time series and reference soil moisture content for the Sugar Beet experiment. The colouring sequences indicate changes in biomass water equivalent (BWE, linearly interpolated), differentiated in aboveground BWE (BWE_a; a) and d)), belowground BWE (BWE_b; b) and e)), and the sum of above- and belowground BWE (BWE_{tot}: c) and f)).

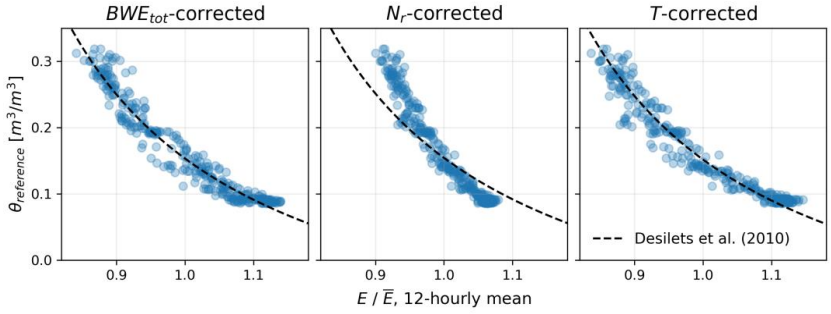

Figure A.4: Relationships of epithermal neutron intensity corrected for the influences of the sum of above- and belowground biomass water equivalent (BWE_{tot}), thermal-to-epithermal neutron ratio (N_r), and thermal neutron intensity (T) relative to their respective mean of the whole time series for sugar beet and reference soil moisture content ($\theta_{reference}$). For comparison also Equation (4.9) is shown (using $f = 1$ and $N_{0,BWetot=0}$, $N_{0,Nr=0}$, and $N_{0,T=0}$, respectively).

Appendix V: Comment on Dong and Ochsner (2018): "Soil Texture often Exerts stronger Influence Than Precipitaion on Mesoscale Soil Moisture Patterns"

Abstract

In their study, DONG AND OCHSNER (2018) used an extensive dataset of 18 cosmic ray neutron rover surveys along a 150 km long transect on unpaved roads to assess the influence of precipitation and soil texture on mesoscale soil moisture patterns. Based on their analysis, they concluded that soil texture, represented by sand content, exerted a stronger influence on mesoscale soil moisture variability than precipitation, represented by the antecedent precipitation index, on 17 of the 18 survey days. However, we found that DONG AND OCHSNER (2018) made a mistake in their calculation of volumetric soil moisture content. After correction, the validity of the original conclusions of DONG AND OCHSNER (2018) was considerably weakened, as soil texture exerted a stronger influence on soil moisture content than precipitation on 12 of the 18 survey days only.

Key points

- DONG AND OCHSNER (2018) concluded that soil texture exerted a stronger influence on mesoscale soil moisture variability than precipitation
- DONG AND OCHSNER (2018) made a mistake in their calculation of volumetric soil moisture content
- We found that correlations between soil moisture content and soil texture and precipitation were significantly different in only 8 of 18 surveys

---

This chapter is based on a comment published as:

JAKOBI, J., HUISMAN, J. A., AND BOGENA, H. R. (2020), Comment on Dong and Ochsner (2018): "Soil Texture often Exerts Stronger Influence Than Precipitation on Mesoscale Soil Moisture Patterns", *Water Resour. Res.*, 57, e2020WR027790, doi: 10.1029/2020WR027790.

The cosmic ray neutron (CRN) rover is a mobile application of the CRN sensing method to measure field-scale soil moisture content noninvasively by surveying large regions (SCHRÖN ET AL., 2018a). DONG AND OCHSNER (2018) used an extensive dataset of 18 CRN rover surveys along an approx. 150 km long transect to assess the influence of precipitation and soil texture on mesoscale soil moisture patterns. To this end, they used sand content to represent soil texture and the antecedent precipitation index (API) to represent the influence of precipitation. Based on autocorrelation and Pearson correlation analysis, DONG AND OCHSNER (2018) concluded that soil texture exerted a stronger influence on mesoscale soil moisture variability than precipitation on 17 out of 18 survey days.

We attempted to reproduce the results of DONG AND OCHSNER (2018) and found an error in the calculation of volumetric soil moisture content from neutron count rates in their analysis (data was retrieved from https://osf.io/59j6c/). DONG AND OCHSNER (2018) wrongly derived volumetric soil moisture content from gravimetric soil moisture content (θ_g [g/g]) by dividing with the soil bulk density (ϱ_{bd} [g/cm^3]). Obviously, the correct approach to obtain the volumetric soil moisture content (θ_v [m^3/m^3]) would be the multiplication of θ_v with ϱ_{bd}:

$$\theta_v = \frac{\theta_g \varrho_{bd}}{\varrho_w} \tag{A.7}$$

where ϱ_w (= 1 g/cm^3) is the density of liquid water (e.g., MARSHALL ET AL., 2012). Figure A.5 exemplary shows the wrong volumetric soil moisture content as published by DONG AND OCHSNER (2018) in comparison to our own calculation of volumetric soil moisture content with Equation (A.7) for one measurement day. We found a considerably higher soil moisture content for all survey days after correction, which is not surprising because bulk density was always higher than 1.36 g/cm^3.

After correction of the originally published soil moisture content values of DONG AND OCHSNER (2018), some differences with the soil moisture content values we obtained from the neutron count rates were still present (Figure A.6). These differences are most pronounced between ~35 and ~75 km, where a distinct drop in soil bulk density that was used by DONG AND OCHSNER (2018, lower panel of Figure 3) is visible. The soil data we extracted from the same database as used by DONG AND OCHSNER (2018) (SSURGO, https://websoilsurvey.sc.egov.usda.gov/, retrieved on 13 April 2020) did not feature this decrease in soil bulk density (not shown), which explains most of the remaining differences in water content estimates shown in Figure A.6.

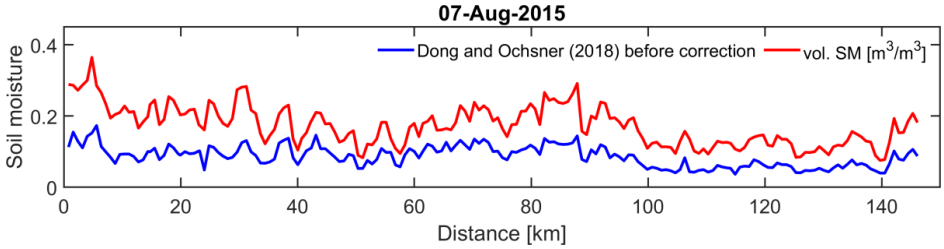

Figure A.5: Soil moisture content along one of the measurement transects from DONG AND OCHSNER (2018). Originally published soil moisture content (blue) and correctly derived volumetric soil moisture content using Equation (A.7) (red).

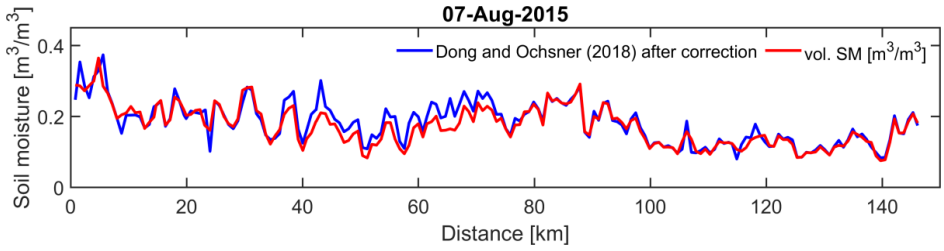

Figure A.6: Soil moisture content along one of the measurement transects from DONG AND OCHSNER (2018). Corrected volumetric soil moisture content obtained from the published soil moisture content (blue), and the volumetric soil moisture content obtained in this study (red).

In a next step, we evaluated how the corrected soil moisture content estimates affected the results and conclusions from DONG AND OCHSNER (2018). For this, the Pearson correlation coefficients presented in Figure 9 of DONG AND OCHSNER (2018) were extracted using plot digitizer software (http://apps.automeris.io/wpd/). We found that the correlation between sand content and volumetric soil moisture content was systematically lower compared to the original findings when using the corrected soil water content estimates (Figure A.7). The average absolute Pearson correlation coefficient was reduced from 0.65 to 0.51 for sand content. In the case of API, the average absolute Pearson correlation coefficient slightly increased from 0.42 to 0.44. Because of these changes, the correlation with API was no longer systematically lower than the correlation with sand content. We found a higher correlation between sand content and soil moisture content in only 12 of 18 surveys, which is substantially lower than the 17 out of 18 surveys reported in DONG AND OCHSNER (2018). In addition, the difference between the correlation with API and sand content was lower than 0.03 for 4 out of these 12 survey days (12-May-15, 29-June-15, 27-Jan-16 and 27-April-16, see Figure A.7). We also used a Fisher z test to determine whether the Pearson correlation coefficients of soil moisture content with API and soil moisture content with sand content were significantly different (e.g., RAMSEYER, 1979; see Figure A.7, black

circles). After correction of the falsely derived soil moisture content, we found significant differences on 8 out of the 18 survey days, whereas significant differences were found on 12 out of the 18 survey days before correction. In addition, the Pearson correlation coefficients for API were negative on four survey days with significantly higher Pearson correlation coefficients for sand content. As already stated by DONG AND OCHSNER (2018), such negative correlation coefficients with API are physically implausible. Consequently, the conclusion that soil texture exerted a stronger influence on soil moisture content than precipitation is considerably weakened based on our analysis.

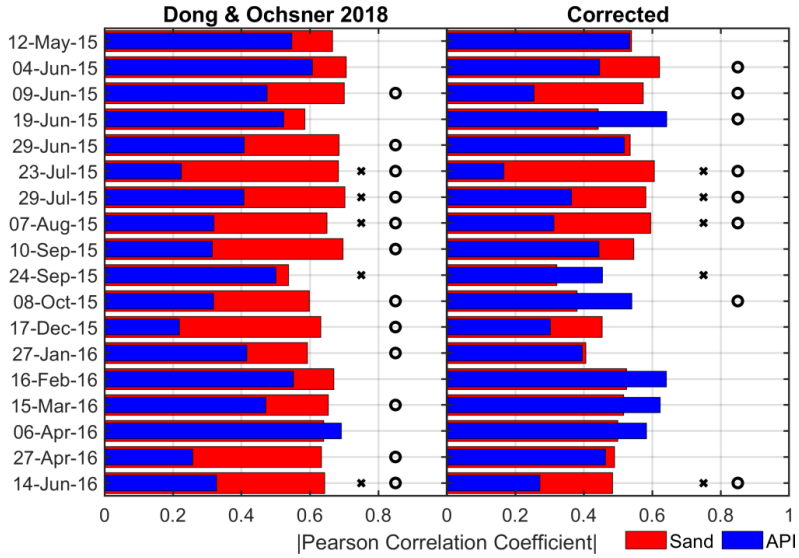

Figure A.7: Pearson correlation coefficients between soil moisture content and API and soil moisture content and sand content with the published, falsely derived volumetric soil moisture content (subplot titled "Dong & Ochsner 2018") and with the corrected volumetric soil moisture content (subplot titled "Corrected"). The correlation coefficients with sand content were all negative. The correlation coefficients with API were mostly positive, but some were negative and those are marked with crosses. The black circles indicate dates with significant difference between the correlation coefficients with API and sand content, respectively, obtained using a Fisher z test (e.g., RAMSEYER, 1979).

We found that the correlation coefficients were also influenced by the extraction of soil properties from the SSURGO database and the rover location assignment to some extent. Both steps involve some degree of subjectivity, as there are many complex processing steps involved. With the help of the authors, we have been able to reproduce the processing steps of DONG AND OCHSNER (2018) as well as possible. The remaining minor differences are most likely due to a recent update of the database after the original publication.

DONG AND OCHSNER (2018) used volumetric soil moisture content for their analysis, which is perhaps more uncertain than gravimetric water content due to the need for uncertain bulk density values for conversion. Therefore, we also repeated the analysis for gravimetric soil moisture content and found higher correlation with sand content while correlations with API were relatively similar. In addition to the uncertainties in soil bulk density, lattice water, and organic matter content, the cosmic ray neutron method is also susceptible to other uncertainties that are not considered here and in the study by DONG AND OCHSNER (2018), e.g., the uncertainty in raw neutron counts (Chapter 2), the influence of vegetation (e.g., AVERY ET AL., 2016; FERSCH ET AL., 2018; JAKOBI ET AL., 2018), and the influence of roads (SCHRÖN ET AL., 2018a). We hope that this exchange will generate further interest in the use of the CRN rover method to improve our understanding of the controls on mesoscale soil moisture patterns.

Bibliography

ANDREASEN, M., JENSEN, K. H., ZREDA, M., DESILETS, D., BOGENA, H., AND LOOMS, M. C. (2016), Modeling cosmic ray neutron field measurements, *Water Resour. Res.*, *52*(8), 6451–6471, doi:10.1002/2015WR018236.

ANDREASEN, M., JENSEN, K. H., DESILETS, D., ZREDA, M., BOGENA, H. R., AND LOOMS, M. C. (2017a), Cosmic-ray neutron transport at a forest field site: the sensitivity to various environmental conditions with focus on biomass and canopy interception, *Hydrol. Earth Syst. Sci.*, *21*(4), 1875–1894, doi:10.5194/hess-21-1875-2017.

ANDREASEN, M., JENSEN, K. H., DESILETS, D., FRANZ, T. E., ZREDA, M., BOGENA, H. R., AND LOOMS, M. C. (2017b), Status and Perspectives on the Cosmic-Ray Neutron Method for Soil Moisture Estimation and Other Environmental Science Applications, *Vadose Zone Journal*, *16*(8), vzj2017.04.0086, doi:10.2136/vzj2017.04.0086.

ANDREASEN, M., JENSEN, K. H., BOGENA, H., DESILETS, D., ZREDA, M., AND LOOMS, M. C. (2020), Cosmic Ray Neutron Soil Moisture Estimation Using Physically Based Site-Specific Conversion Functions, *Water Resour. Res.*, *56*(11), doi:10.1029/2019WR026588.

AVERY, W. A., FINKENBINER, C., FRANZ, T. E., WANG, T., NGUY-ROBERTSON, A. L., SUYKER, A., ARKEBAUER, T., AND MUÑOZ-ARRIOLA, F. (2016), Incorporation of globally available datasets into the roving cosmic-ray neutron probe method for estimating field-scale soil water content, *Hydrol. Earth Syst. Sci.*, *20*(9), 3859–3872, doi:10.5194/hess-20-3859-2016.

BAATZ, R., BOGENA, H. R., HENDRICKS FRANSSEN, H.-J., HUISMAN, J. A., QU, W., MONTZKA, C., AND VEREECKEN, H. (2014), Calibration of a catchment scale cosmic-ray probe network: A comparison of three parameterization methods, *Journal of Hydrology*, *516*, 231–244, doi:10.1016/j.jhydrol.2014.02.026.

BAATZ, R., BOGENA, H. R., HENDRICKS FRANSSEN, H.-J., HUISMAN, J. A., MONTZKA, C., AND VEREECKEN, H. (2015), An empirical vegetation correction for soil water content quantification using cosmic ray probes, *Water Resour. Res.*, *51*(4), 2030–2046, doi:10.1002/2014WR016443.

BABAEIAN, E., SADEGHI, M., JONES, S. B., MONTZKA, C., VEREECKEN, H., AND TULLER, M. (2019), Ground, Proximal, and Satellite Remote Sensing of Soil Moisture, *Rev. Geophys.*, *57*(2), 530–616, doi:10.1029/2018RG000618.

BALDONCINI, M., ALBÉRI, M., BOTTARDI, C., CHIARELLI, E., RAPTIS, K. G. C., STRATI, V., AND MANTOVANI, F. (2018), Investigating the potentialities of Monte Carlo simulation for assessing soil water content via proximal gamma-ray spectroscopy, *Journal of environmental radioactivity*, *192*, 105–116, doi:10.1016/j.jenvrad.2018.06.001.

BARET, F., OLIOSO, A., AND LUCIANI, J. L. (1992), Root biomass fraction as a function of growth degree days in wheat, *Plant Soil*, *140*(1), 137–144, doi:10.1007/BF00012815.

BARONI, G., AND OSWALD, S. E. (2015), A scaling approach for the assessment of biomass changes and rainfall interception using cosmic-ray neutron sensing, *Journal of Hydrology*, *525*, 264–276, doi:10.1016/j.jhydrol.2015.03.053.

BARONI, G., SCHEIFFELE, L. M., SCHRÖN, M., INGWERSEN, J., AND OSWALD, S. E. (2018), Uncertainty, sensitivity and improvements in soil moisture estimation with cosmic-ray neutron sensing, *Journal of Hydrology*, *564*, 873–887, doi:10.1016/j.jhydrol.2018.07.053.

BEILLOUIN, D., SCHAUBERGER, B., BASTOS, A., CIAIS, P., AND MAKOWSKI, D. (2020), Impact of extreme weather conditions on European crop production in 2018, *Philosophical transactions of the Royal Society of London. Series B, Biological sciences*, *375*(1810), 20190510, doi:10.1098/rstb.2019.0510.

BISSELL, V. C., AND BURSON, Z. G. (1974), Deep snow measurements suggested using cosmic radiation, *Water Res*, *10*(6), 1243–1244, doi:10.1029/WR010i006p01243.

BLÖSCHL, G., AND SIVAPALAN, M. (1995), Scale issues in hydrological modelling: A review, *Hydrol. Process.*, *9*(3-4), 251–290, doi:10.1002/hyp.3360090305.

BOGENA, H. R., HERBST, M., HUISMAN, J. A., ROSENBAUM, U., WEUTHEN, A., AND VEREECKEN, H. (2010), Potential of Wireless Sensor Networks for Measuring Soil Water Content Variability, *Vadose Zone Journal*, *9*(4), 1002–1013, doi:10.2136/vzj2009.0173.

BOGENA, H. R., KUNKEL, R., PÜTZ, T., VEREECKEN, H., KRÜGER, E., ZACHARIAS, S., DIETRICH, P., WOLLSCHLÄGER, U., KUNSTMANN, H., PAPEN, H., SCHMID, H. P., MUNCH, J. C., PRIESACK, E., SCHWANK, M., BENS, O., BRAUER, A., BORG, E., AND HAJNSEK, I. (2012), TERENO - Long-term monitoring network for terrestrial environmental research, *Hydrologie und Wasserbewirtschaftung*, *56*(3), 138–143.

BOGENA, H. R., HUISMAN, J. A., BAATZ, R., HENDRICKS FRANSSEN, H.-J., AND VEREECKEN, H. (2013), Accuracy of the cosmic-ray soil water content probe in humid forest ecosystems: The worst case scenario, *Water Resour. Res.*, *49*(9), 5778–5791, doi:10.1002/wrcr.20463.

BOGENA, H. R., HUISMAN, J. A., GÜNTNER, A., HÜBNER, C., KUSCHE, J., JONARD, F., VEY, S., AND VEREECKEN, H. (2015), Emerging methods for noninvasive sensing of soil moisture dynamics from field to catchment scale: a review, *WIREs Water*, *2*(6), 635–647, doi:10.1002/wat2.1097.

BOGENA, H. R., HUISMAN, J. A., SCHILLING, B., WEUTHEN, A., AND VEREECKEN, H. (2017), Effective Calibration of Low-Cost Soil Water Content Sensors, *Sensors (Basel, Switzerland)*, *17*(1), doi:10.3390/s17010208.

BOGENA, H. R., MONTZKA, C., HUISMAN, J. A., GRAF, A., SCHMIDT, M., STOCKINGER, M., HEBEL, C. VON, HENDRICKS-FRANSSEN, H. J., VAN DER KRUK, J., TAPPE, W., LÜCKE, A., BAATZ, R., BOL, R., GROH, J., PÜTZ, T., JAKOBI, J., KUNKEL, R., SORG, J., AND VEREECKEN, H. (2018), The TERENO-Rur Hydrological Observatory: A Multiscale Multi-Compartment Research Platform for the Advancement of Hydrological Science, *Vadose Zone Journal*, *17*(1), 180055, doi:10.2136/vzj2018.03.0055.

BOGENA, H. R., HERRMANN, F., JAKOBI, J., BROGI, C., ILIAS, A., HUISMAN, J. A., PANAGOPOULOS, A., AND PISINARAS, V. (2020), Monitoring of Snowpack Dynamics With Cosmic-Ray Neutron Probes: A Comparison of Four Conversion Methods, *Front. Water*, *2*, doi:10.3389/frwa.2020.00019.

BOGENA, H. R., SCHRÖN, M., JAKOBI, J., NEY, P., ZACHARIAS, S., ANDREASEN, M., BAATZ, R., BOORMAN, D., DUYGU, B. M., EGUIBAR-GALÁN, M. A., FERSCH, B., FRANKE, T., GERIS, J., GONZÁLEZ SANCHIS, M., KERR, Y., KORF, T., MENGISTU, Z., MIALON, A., NASTA, P., NITYCHORUK, J., PISINARAS, V., RASCHE, D., ROSOLEM, R., SAID, H., SCHATTAN, P., ZREDA, M., ACHLEITNER, S., ALBENTOSA-HERNÁNDEZ, E., AKYÜREK, Z., BLUME, T., DEL CAMPO, A., DIMITROVA-PETROVA, K., EVANS, J. G., FRANCES, F., GÜNTNER, A., HERRMANN, F., IWEMA, J., JENSEN, K. H., KUNSTMANN, H., LIDÓN, A., LOOMS, M. C., OSWALD, S., PANAGOPOULOS, A., PATIL, A., POWER, D., REBMANN, C., ROMANO, N., SCHEIFFELE, L. M., SENEVIRATNE, S., WELTIN, G., AND VEREECKEN, H. (2021), COSMOS-Europe: A European Network of Cosmic-Ray Neutron Soil Moisture Sensors, doi:10.5194/essd-2021-325.

BOGENA, H. R., AND NEY, P. (2021), Dataset of "COSMOS-Europe: A European network of Cosmic-Ray Neutron Soil Moisture Sensors", doi:10.34731/X9S3-KR48.

BRAKENSIEK, D. L., AND RAWLS, W. J. (1994), Soil containing rock fragments: effects on infiltration, *CATENA*, *23*(1-2), 99–110, doi:10.1016/0341-8162(94)90056-6.

BRINDT, N., RAHAV, M., AND WALLACH, R. (2019), ERT and salinity – A method to determine whether ERT-detected preferential pathways in brackish water-irrigated soils

are water-induced or an artifact of salinity, *Journal of Hydrology*, *574*, 35–45, doi:10.1016/j.jhydrol.2019.04.029.

BROGI, C., HUISMAN, J. A., PÄTZOLD, S., HEBEL, C. VON, WEIHERMÜLLER, L., KAUFMANN, M. S., VAN DER KRUK, J., AND VEREECKEN, H. (2019), Large-scale soil mapping using multi-configuration EMI and supervised image classification, *Geoderma*, *335*, 133–148, doi:10.1016/j.geoderma.2018.08.001.

BROGI, C., HUISMAN, J. A., HERBST, M., WEIHERMÜLLER, L., KLOSTERHALFEN, A., MONTZKA, C., REICHENAU, T. G., AND VEREECKEN, H. (2020), Simulation of spatial variability in crop leaf area index and yield using agroecosystem modeling and geophysics-based quantitative soil information, *Vadose zone j.*, *19*(1), doi:10.1002/vzj2.20009.

BROGI, C., BOGENA, H. R., PISINARAS, V., PANAGOPOULOS, A., DOMBROWSKI, O., JAKOBI, J., CHATZI, A., AND NEY, P. (2021), *Monitoring soil water content and water potential dynamics in irrigated apple orchards using cosmic-ray neutron probes*, 1st OZCAR-TERENO International Conference, Straßburg, France.

BRUNET, P., CLÉMENT, R., AND BOUVIER, C. (2010), Monitoring soil water content and deficit using Electrical Resistivity Tomography (ERT) – A case study in the Cevennes area, France, *Journal of Hydrology*, *380*(1-2), 146–153, doi:10.1016/j.jhydrol.2009.10.032.

CALLEGARY, J. B., FERRÉ, T. P. A., AND GROOM, R. W. (2007), Vertical Spatial Sensitivity and Exploration Depth of Low-Induction-Number Electromagnetic-Induction Instruments, *Vadose Zone Journal*, *6*(1), 158–167, doi:10.2136/vzj2006.0120.

CHAMBERS, J. E., GUNN, D. A., WILKINSON, P. B., MELDRUM, P. I., HASLAM, E., HOLYOAKE, S., KIRKHAM, M., KURAS, O., MERRITT, A., AND WRAGG, J. (2014), 4D electrical resistivity tomography monitoring of soil moisture dynamics in an operational railway embankment, *Near Surface Geophysics*, *12*(1), 61–72, doi:10.3997/1873-0604.2013002.

CHAN, S., NJOKU, E. G., AND COLLIANDER, A. (2014), *Soil Moisture Active Passive (SMAP), Algorithm Theoretical Basis Document, Level 1C Radiometer Data Product, Revision A*, 20 pp.

CHRISMAN, B., AND ZREDA, M. (2013), Quantifying mesoscale soil moisture with the cosmic-ray rover, *Hydrol. Earth Syst. Sci.*, *17*(12), 5097–5108, doi:10.5194/hess-17-5097-2013.

COOPER, H. M., BENNETT, E., BLAKE, J., BLYTH, E., BOORMAN, D., COOPER, E., EVANS, J., FRY, M., JENKINS, A., MORRISON, R., RYLETT, D., STANLEY, S., SZCZYKULSKA, M., TRILL, E., ANTONIOU, V., ASKQUITH-ELLIS, A., BALL, L., BROOKS, M., CLARKE, M. A., COWAN, N., CUMMING, A., FARRAND, P., HITT, O., LORD, W., SCARLETT, P., SWAIN, O., THORNTON, J., WARWICK, A., AND WINTERBOURN, B. (2021), COSMOS-UK: national soil moisture and hydrometeorology data for environmental science research, *Earth Syst. Sci. Data*, *13*(4), 1737–1757, doi:10.5194/essd-13-1737-2021.

DE JONG, S. M. DE, HEIJENK, R. A., NIJLAND, W., AND VAN DER MEIJDE, M. (2020), Monitoring Soil Moisture Dynamics Using Electrical Resistivity Tomography under Homogeneous Field Conditions, *Sensors (Basel, Switzerland)*, *20*(18), doi:10.3390/s20185313.

DESILETS, D., AND ZREDA, M. (2001), On scaling cosmogenic nuclide production rates for altitude and latitude using cosmic-ray measurements, *Earth and Planetary Science Letters*, *193*(1-2), 213–225, doi:10.1016/S0012-821X(01)00477-0.

DESILETS, D., AND ZREDA, M. (2003), Spatial and temporal distribution of secondary cosmic-ray nucleon intensities and applications to in situ cosmogenic dating, *Earth and Planetary Science Letters*, *206*(1-2), 21–42, doi:10.1016/S0012-821X(02)01088-9.

DESILETS, D., ZREDA, M., AND FERRÉ, T. P. A. (2010), Nature's neutron probe: Land surface hydrology at an elusive scale with cosmic rays, *Water Resour. Res.*, *46*(11), doi:10.1029/2009WR008726.

DESILETS, D., AND ZREDA, M. (2013), Footprint diameter for a cosmic-ray soil moisture probe: Theory and Monte Carlo simulations, *Water Resour. Res.*, *49*(6), 3566–3575, doi:10.1002/wrcr.20187.

DIMITROVA-PETROVA, K., GERIS, J., WILKINSON, M. E., ROSOLEM, R., VERROT, L., LILLY, A., AND SOULSBY, C. (2020), Opportunities and challenges in using catchment-scale storage estimates from cosmic ray neutron sensors for rainfall-runoff modelling, *Journal of Hydrology*, *586*, 124878, doi:10.1016/j.jhydrol.2020.124878.

DINGMAN, S. L. (1994), *Physical Hydrology*, 575 pp., Macmillan, New York.

DONG, J., OCHSNER, T. E., ZREDA, M., COSH, M. H., AND ZOU, C. B. (2014), Calibration and Validation of the COSMOS Rover for Surface Soil Moisture Measurement, *Vadose zone j.*, *13*(4), 1–8, doi:10.2136/vzj2013.08.0148.

DONG, J., AND OCHSNER, T. E. (2018), Soil Texture Often Exerts a Stronger Influence Than Precipitation on Mesoscale Soil Moisture Patterns, *Water Resour. Res.*, *54*(3), 2199–2211, doi:10.1002/2017WR021692.

DUNNE, T., MOORE, T. R., AND TAYLOR, C. H. (1975), Recognition and prediction of runoff-producing zones in humid regions: Hydrologic Sciences Bulletin, v. 20.

EHLERS, W., KOPKE, U., HESSE, F., AND BOHM, W. (1983), Penetration resistance and root growth of oats in tilled and untilled loess soil, *Soil and Tillage Research*, *3*(3), 261–275, doi:10.1016/0167-1987(83)90027-2.

ENTEKHABI, D., RODRIGUEZ-ITURBE, I., AND CASTELLI, F. (1996), Mutual interaction of soil moisture state and atmospheric processes, *Journal of Hydrology*, *184*(1-2), 3–17, doi:10.1016/0022-1694(95)02965-6.

EVETT, S. R., TOLK, J. A., AND HOWELL, T. A. (2003), A Depth Control Stand for Improved Accuracy with the Neutron Probe, *Vadose Zone Journal*, *2*(4), 642, doi:10.2136/vzj2003.0642.

FENTANES, J. P., BADIEE, A., DUCKETT, T., EVANS, J., PEARSON, S., AND CIELNIAK, G. (2020), Kriging-based robotic exploration for soil moisture mapping using a cosmic-ray sensor, *J. Field Robotics*, *37*(1), 122–136, doi:10.1002/rob.21914.

FERSCH, B., JAGDHUBER, T., SCHRÖN, M., VÖLKSCH, I., AND JÄGER, M. (2018), Synergies for Soil Moisture Retrieval Across Scales From Airborne Polarimetric SAR, Cosmic Ray Neutron Roving, and an In Situ Sensor Network, *Water Resour. Res.*, *54*(11), 9364–9383, doi:10.1029/2018WR023337.

FERSCH, B., FRANCKE, T., HEISTERMANN, M., SCHRÖN, M., DÖPPER, V., JAKOBI, J., BARONI, G., BLUME, T., BOGENA, H., BUDACH, C., GRÄNZIG, T., FÖRSTER, M., GÜNTNER, A., HENDRICKS FRANSSEN, H.-J., KASNER, M., KÖHLI, M., KLEINSCHMIT, B., KUNSTMANN, H., PATIL, A., RASCHE, D., SCHEIFFELE, L., SCHMIDT, U., SZULC-SEYFRIED, S., WEIMAR, J., ZACHARIAS, S., ZREDA, M., HEBER, B., KIESE, R., MARES, V., MOLLENHAUER, H., VÖLKSCH, I., AND OSWALD, S. (2020), A dense network of cosmic-ray neutron sensors for soil moisture observation in a highly instrumented pre-Alpine headwater catchment in Germany, *Earth Syst. Sci. Data*, *12*(3), 2289–2309, doi:10.5194/essd-12-2289-2020.

FINKENBINER, C. E., FRANZ, T. E., GIBSON, J., HEEREN, D. M., AND LUCK, J. (2019), Integration of hydrogeophysical datasets and empirical orthogonal functions for improved irrigation water management, *Precision Agric*, *20*(1), 78–100, doi:10.1007/s11119-018-9582-5.

FLINT, A. L., AND CHILDS, S. (1984), Physical Properties of Rock Fragments and Their Effect on Available Water in Skeletal Soils, in *Erosion and Productivity of Soils Containing Rock Fragments*, *SSSA Special Publications*, edited by J. D. Nichols et al., pp. 91–103, Soil Science Society of America, Madison, WI, USA.

FRANCKE, T., HEISTERMANN, M., KÖHLI, M., BUDACH, C., SCHRÖN, M., AND OSWALD, S. E. (2021), Assessing the feasibility of a directional CRNS-sensor for estimating soil moisture, doi:10.5194/gi-2021-18.

FRANZ, T. E., ZREDA, M., ROSOLEM, R., AND FERRE, T. (2012a), Field Validation of a Cosmic-Ray Neutron Sensor Using a Distributed Sensor Network, *Vadose zone j.*, *11*(4), doi:10.2136/vzj2012.0046.

FRANZ, T. E., ZREDA, M., FERRE, T. P. A., ROSOLEM, R., ZWECK, C., STILLMAN, S., ZENG, X., AND SHUTTLEWORTH, W. J. (2012b), Measurement depth of the cosmic ray soil moisture probe affected by hydrogen from various sources, *Water Resour. Res.*, *48*(8), doi:10.1029/2012WR011871.

FRANZ, T. E., ZREDA, M., FERRE, T. P. A., AND ROSOLEM, R. (2013a), An assessment of the effect of horizontal soil moisture heterogeneity on the area-average measurement of cosmic-ray neutrons, *Water Resour. Res.*, *49*(10), 6450–6458, doi:10.1002/wrcr.20530.

FRANZ, T. E., ZREDA, M., ROSOLEM, R., HORNBUCKLE, B. K., IRVIN, S. L., ADAMS, H., KOLB, T. E., ZWECK, C., AND SHUTTLEWORTH, W. J. (2013b), Ecosystem-scale measurements of biomass water using cosmic ray neutrons, *Geophys. Res. Lett.*, *40*(15), 3929–3933, doi:10.1002/grl.50791.

FRANZ, T. E., WANG, T., AVERY, W., FINKENBINER, C., AND BROCCA, L. (2015), Combined analysis of soil moisture measurements from roving and fixed cosmic ray neutron probes for multiscale real-time monitoring, *Geophys. Res. Lett.*, *42*(9), 3389–3396, doi:10.1002/2015GL063963.

FUCHS, H. (2016), Effects of biomass on soil moisture measurements using cosmic-ray neutron probes: Master Thesis. Radboud University, the Netherlands and University of Duisburg-Essen, Germany.

FU, J., GASCHE, R., WANG, N., LU, H., BUTTERBACH-BAHL, K., AND KIESE, R. (2017), Impacts of climate and management on water balance and nitrogen leaching from montane grassland soils of S-Germany, *Environmental pollution (Barking, Essex : 1987)*, *229*, 119–131, doi:10.1016/j.envpol.2017.05.071.

GIBSON, J., AND FRANZ, T. E. (2018), Spatial prediction of near surface soil water retention functions using hydrogeophysics and empirical orthogonal functions, *Journal of Hydrology*, *561*, 372–383, doi:10.1016/j.jhydrol.2018.03.046.

GRAY, D. M., AND NORUM, D. I. (1967), The effect of soil moisture on infiltration as related to runoff and recharge, *Proceedings of hydrology symposium No. 6*.

GRUBER, A., LANNOY, G. DE, ALBERGEL, C., AL-YAARI, A., BROCCA, L., CALVET, J.-C., COLLIANDER, A., COSH, M., CROW, W., DORIGO, W., DRAPER, C., HIRSCHI, M., KERR, Y., KONINGS, A., LAHOZ, W., MCCOLL, K., MONTZKA, C., MUÑOZ-SABATER, J., PENG, J., REICHLE, R., RICHAUME, P., RÜDIGER, C., SCANLON, T., VAN DER SCHALIE, R., WIGNERON, J.-P., AND WAGNER, W. (2020), Validation practices for satellite soil moisture retrievals: What are (the) errors?, *Remote Sensing of Environment*, *244*, 111806, doi:10.1016/j.rse.2020.111806.

GUGERLI, R., SALZMANN, N., HUSS, M., AND DESILETS, D. (2019), Continuous and autonomous snow water equivalent measurements by a cosmic ray sensor on an alpine glacier, *The Cryosphere*, *13*(12), 3413–3434, doi:10.5194/tc-13-3413-2019.

HAWDON, A., MCJANNET, D., AND WALLACE, J. (2014), Calibration and correction procedures for cosmic-ray neutron soil moisture probes located across Australia, *Water Resour. Res.*, *50*(6), 5029–5043, doi:10.1002/2013WR015138.

HEISTERMANN, M., BOGENA, H., FRANCKE, T., GÜNTNER, A., JAKOBI, J., RASCHE, D., SCHRÖN, M., DÖPPER, V., FERSCH, B., GROH, J., PATIL, A., PÜTZ, T., REICH, M., ZACHARIAS, S., ZENGERLE, C., AND OSWALD, S. (2021a), Soil moisture observation in a forested headwater catchment: combining a dense cosmic-ray neutron sensor network with roving and hydrogravimetry at the TERENO site Wüstebach, doi:10.5194/essd-2021-445.

HEISTERMANN, M., FRANCKE, T., SCHRÖN, M., AND OSWALD, S. E. (2021b), Spatio-temporal soil moisture retrieval at the catchment scale using a dense network of cosmic-ray neutron sensors, *Hydrol. Earth Syst. Sci.*, *25*(9), 4807–4824, doi:10.5194/hess-25-4807-2021.

HESS, V. F. (1912), Observations of the penetrating radiation on seven balloon flights, *Physik. Zeitschr*, *13*, 1084–1091.

HIGNETT AND EVETT (2002), *Methods of soil analysis: Part 4. Physical Methods. Neutron thermalization*, 24 pp.

HOFFMEISTER, D., WALDHOFF, G., KORRES, W., CURDT, C., AND BARETH, G. (2016), Crop height variability detection in a single field by multi-temporal terrestrial laser scanning, *Precision Agric*, *17*(3), 296–312, doi:10.1007/s11119-015-9420-y.

HUBERT, G., PAZIANOTTO, M. T., AND FEDERICO, C. A. (2016), Modeling of ground albedo neutrons to investigate seasonal cosmic ray-induced neutron variations measured at high-altitude stations, *J. Geophys. Res. Space Physics*, *121*(12), 12,186-12,201, doi:10.1002/2016JA023055.

HUISMAN, J. A., SPERL, C., BOUTEN, W., AND VERSTRATEN, J. M. (2001), Soil water content measurements at different scales: accuracy of time domain reflectometry and ground-penetrating radar, *Journal of Hydrology*, *245*(1-4), 48–58, doi:10.1016/S0022-1694(01)00336-5.

HUISMAN, J. A., HUBBARD, S. S., REDMAN, J. D., AND ANNAN, A. P. (2003), Measuring Soil Water Content with Ground Penetrating Radar: A Review, *Vadose zone j.*, *2*(4), 476–491, doi:10.2136/vzj2003.4760.

IAEA (2018), *Soil Moisture Mapping with a Portable Cosmic Ray Neutron Sensor*, INTERNATIONAL ATOMIC ENERGY AGENCY, Vienna.

JACKSON, T. J., BINDLISH, R., COSH, M. H., ZHAO, T., STARKS, P. J., BOSCH, D. D., SEYFRIED, M., MORAN, M. S., GOODRICH, D. C., KERR, Y. H., AND LEROUX, D. (2012), Validation of Soil Moisture and Ocean Salinity (SMOS) Soil Moisture Over Watershed Networks in the U.S, *IEEE Trans. Geosci. Remote Sensing*, *50*(5), 1530–1543, doi:10.1109/TGRS.2011.2168533.

JAKOBI, J., HUISMAN, J. A., VEREECKEN, H., DIEKKRÜGER, B., AND BOGENA, H. R. (2018), Cosmic Ray Neutron Sensing for Simultaneous Soil Water Content and Biomass Quantification in Drought Conditions, *Water Resour. Res.*, *54*(10), 7383–7402, doi:10.1029/2018WR022692.

JONES, W. K., AND CARROLL, T. R. (1983), Error analysis of airborne gamma radiation soil moisture measurements, *Agricultural Meteorology*, *28*(1), 19–30, doi:10.1016/0002-1571(83)90020-1.

KIESE, R., FERSCH, B., BAESSLER, C., BROSY, C., BUTTERBACH-BAHL, K., CHWALA, C., DANNENMANN, M., FU, J., GASCHE, R., GROTE, R., JAHN, C., KLATT, J., KUNSTMANN, H., MAUDER, M., RÖDIGER, T., SMIATEK, G., SOLTANI, M., STEINBRECHER, R., VÖLKSCH, I., WERHAHN, J., WOLF, B., ZEEMAN, M., AND SCHMID, H. P. (2018), The TERENO Pre-Alpine Observatory: Integrating Meteorological, Hydrological, and Biogeochemical Measurements and Modeling, *Vadose Zone Journal*, *17*(1), 180060, doi:10.2136/vzj2018.03.0060.

KLOTZSCHE, A., JONARD, F., LOOMS, M. C., VAN DER KRUK, J., AND HUISMAN, J. A. (2018), Measuring Soil Water Content with Ground Penetrating Radar: A Decade of Progress, *Vadose zone j.*, *17*(1), 180052, doi:10.2136/vzj2018.03.0052.

KNOLL, G. F. (2010), *Radiation detection and measurement*, 4th ed., xxvi, 830, John Wiley, Hoboken N.J.

KODAMA, M., NAKAI, K., KAWASAKI, S., AND WADA, M. (1979), An application of cosmic-ray neutron measurements to the determination of the snow-water equivalent, *Journal of Hydrology*, *41*(1-2), 85–92, doi:10.1016/0022-1694(79)90107-0.

KODAMA, M. (1980), Continuous monitoring of snow water equivalent using cosmic ray neutrons, *Cold Regions Science and Technology*, *3*(4), 295–303, doi:10.1016/0165-232X(80)90036-1.

KODAMA, M., KUDO, S., AND KOSUGE, T. (1985), Application of atmospheric neutrons to soil moisture measurement, *Soil science*, *140*(4), 237–242.

KÖHLI, M., SCHRÖN, M., ZREDA, M., SCHMIDT, U., DIETRICH, P., AND ZACHARIAS, S. (2015), Footprint characteristics revised for field-scale soil moisture monitoring with cosmic-ray neutrons, *Water Resour. Res.*, *51*(7), 5772–5790, doi:10.1002/2015WR017169.

KÖHLI, M., SCHRÖN, M., AND SCHMIDT, U. (2018), Response Functions for Detectors in Cosmic Ray Neutron Sensing, *Nuclear Instruments and Methods in Physics Research Section A: Accelerators, Spectrometers, Detectors and Associated Equipment*, *902*(1), 184–189, doi:10.1016/j.nima.2018.06.052.

KÖHLI, M. (2019), *The CASCADE 10B thermal neutron detector and soil moisture sensing by cosmic-ray neutrons (Doctoral thesis), Physikalisches Institut, Heidelberg University, Heidelberg, Germany.*

KÖHLI, M., WEIMAR, J., SCHRÖN, M., BAATZ, R., AND SCHMIDT, U. (2021), Soil Moisture and Air Humidity Dependence of the Above-Ground Cosmic-Ray Neutron Intensity, *Front. Water*, *2*, doi:10.3389/frwa.2020.544847.

KORRES, W., REICHENAU, T. G., FIENER, P., KOYAMA, C. N., BOGENA, H. R., CORNELISSEN, T., BAATZ, R., HERBST, M., DIEKKRÜGER, B., VEREECKEN, H., AND SCHNEIDER, K. (2015), Spatio-temporal soil moisture patterns – A meta-analysis using plot to catchment scale data, *Journal of Hydrology*, *520*, 326–341, doi:10.1016/j.jhydrol.2014.11.042.

KOSTER, R. D., DIRMEYER, P. A., GUO, Z., BONAN, G., CHAN, E., COX, P., GORDON, C. T., KANAE, S., KOWALCZYK, E., LAWRENCE, D., LIU, P., LU, C.-H., MALYSHEV, S., MCAVANEY, B., MITCHELL, K., MOCKO, D., OKI, T., OLESON, K., PITMAN, A., SUD, Y. C., TAYLOR, C. M., VERSEGHY, D., VASIC, R., XUE, Y., AND YAMADA, T. (2004), Regions of strong coupling between soil moisture and precipitation, *Science (New York, N.Y.)*, *305*(5687), 1138–1140, doi:10.1126/science.1100217.

LARSON, K. M., SMALL, E. E., GUTMANN, E. D., BILICH, A. L., BRAUN, J. J., AND ZAVOROTNY, V. U. (2008), Use of GPS receivers as a soil moisture network for water cycle studies, *Geophys. Res. Lett.*, *35*(24), doi:10.1029/2008GL036013.

LARSON, K. M., BRAUN, J. J., SMALL, E. E., ZAVOROTNY, V. U., GUTMANN, E. D., AND BILICH, A. L. (2010), GPS Multipath and Its Relation to Near-Surface Soil Moisture Content, *IEEE J. Sel. Top. Appl. Earth Observations Remote Sensing*, *3*(1), 91–99, doi:10.1109/JSTARS.2009.2033612.

LI, D., SCHRÖN, M., KÖHLI, M., BOGENA, H., WEIMAR, J., JIMÉNEZ BELLO, M. A., HAN, X., MARTÍNEZ GIMENO, M. A., ZACHARIAS, S., VEREECKEN, H., AND HENDRICKS FRANSSEN, H.-J. (2019), Can Drip Irrigation be Scheduled with Cosmic-Ray Neutron Sensing?, *Vadose zone j.*, *18*(1), 190053, doi:10.2136/vzj2019.05.0053.

LUNT, I. A., HUBBARD, S. S., AND RUBIN, Y. (2005), Soil moisture content estimation using ground-penetrating radar reflection data, *Journal of Hydrology*, *307*(1-4), 254–269, doi:10.1016/j.jhydrol.2004.10.014.

MARSHALL, T. J., HOLMES, J. W., AND ROSE, C. W. (2012), *Soil Physics*, Cambridge University Press, doi:10.1017/CBO9781139170673.

MARTÍNEZ-FERNÁNDEZ, J., GONZÁLEZ-ZAMORA, A., SÁNCHEZ, N., GUMUZZIO, A., AND HERRERO-JIMÉNEZ, C. M. (2016), Satellite soil moisture for agricultural drought monitoring: Assessment of the SMOS derived Soil Water Deficit Index, *Remote Sensing of Environment*, *177*, 277–286, doi:10.1016/j.rse.2016.02.064.

MCJANNET, D., FRANZ, T., HAWDON, A., BOADLE, D., BAKER, B., ALMEIDA, A., SILBERSTEIN, R., LAMBERT, T., AND DESILETS, D. (2014), Field testing of the universal calibration function for determination of soil moisture with cosmic-ray neutrons, *Water Resour. Res.*, *50*(6), 5235–5248, doi:10.1002/2014WR015513.

MCJANNET, D., HAWDON, A., BAKER, B., RENZULLO, L., AND SEARLE, R. (2017), Multiscale soil moisture estimates using static and roving cosmic-ray soil moisture sensors, *Hydrol. Earth Syst. Sci.*, *21*(12), 6049–6067, doi:10.5194/hess-21-6049-2017.

MEKID, S., AND VAJA, D. (2008), Propagation of uncertainty: Expressions of second and third order uncertainty with third and fourth moments, *Measurement*, *41*(6), 600–609, doi:10.1016/j.measurement.2007.07.004.

MENGEN, D., MONTZKA, C., JAGDHUBER, T., FLUHRER, A., BROGI, C., BAUM, S., SCHÜTTEMEYER, D., BAYAT, B., BOGENA, H., COCCIA, A., MASALIAS, G., TRINKEL, V., JAKOBI, J., JONARD, F., MA, Y., MATTIA, F., PALMISANO, D., RASCHER, U., SATALINO, G., SCHUMACHER, M., KOYAMA, C., SCHMIDT, M., AND VEREECKEN, H. (2021), The

SARSense Campaign: Air- and Space-Borne C- and L-Band SAR for the Analysis of Soil and Plant Parameters in Agriculture, *Remote Sensing*, *13*(4), 825, doi:10.3390/rs13040825.

MOKANY, K., RAISON, R. J., AND PROKUSHKIN, A. S. (2006), Critical analysis of root : shoot ratios in terrestrial biomes, *Global Change Biology*, *12*(1), 84–96, doi:10.1111/j.1365-2486.2005.001043.x.

MONTZKA, C., BOGENA, H., ZREDA, M., MONERRIS, A., MORRISON, R., MUDDU, S., AND VEREECKEN, H. (2017), Validation of Spaceborne and Modelled Surface Soil Moisture Products with Cosmic-Ray Neutron Probes, *Remote Sensing*, *9*(2), 103, doi:10.3390/rs9020103.

NIJLAND, W., VAN DER MEIJDE, M., ADDINK, E. A., AND JONG, S. M. DE (2010), Detection of soil moisture and vegetation water abstraction in a Mediterranean natural area using electrical resistivity tomography, *CATENA*, *81*(3), 209–216, doi:10.1016/j.catena.2010.03.005.

OHMURA, A., AND RASCHKE, E. (2005), 10 Energy budget at the earth's surface (Part 1/2), in *Observed Global Climate*, *Landolt-Börnstein - Group V Geophysics*, edited by M. Hantel, pp. 1–30, Springer-Verlag, Berlin/Heidelberg.

PARKINSON, B. W., AND SPILKER, J. J. (1996), *Global positioning system: theory and applications*, Aiaa.

PATHE, C., WAGNER, W., SABEL, D., DOUBKOVA, M., AND BASARA, J. B. (2009), Using ENVISAT ASAR Global Mode Data for Surface Soil Moisture Retrieval Over Oklahoma, USA, *IEEE Trans. Geosci. Remote Sensing*, *47*(2), 468–480, doi:10.1109/TGRS.2008.2004711.

RAMSEYER, G. C. (1979), Testing the Difference between Dependent Correlations Using the Fisher Z, *The Journal of Experimental Education*, *47*(4), 307–310, doi:10.1080/00220973.1979.11011698.

RASCHE, D., KÖHLI, M., SCHRÖN, M., BLUME, T., AND GÜNTNER, A. (2021), Towards disentangling heterogeneous soil moisture patterns in cosmic-ray neutron sensor footprints, *Hydrol. Earth Syst. Sci.*, *25*(12), 6547–6566, doi:10.5194/hess-25-6547-2021.

RAY, R. L., JACOBS, J. M., AND COSH, M. H. (2010), Landslide susceptibility mapping using downscaled AMSR-E soil moisture: A case study from Cleveland Corral, California, US, *Remote Sensing of Environment*, *114*(11), 2624–2636, doi:10.1016/j.rse.2010.05.033.

REICHENAU, T. G., KORRES, W., MONTZKA, C., FIENER, P., WILKEN, F., STADLER, A., WALDHOFF, G., AND SCHNEIDER, K. (2016), Spatial Heterogeneity of Leaf Area Index (LAI) and Its Temporal Course on Arable Land: Combining Field Measurements, Remote Sensing and Simulation in a Comprehensive Data Analysis Approach (CDAA), *PloS one*, *11*(7), e0158451, doi:10.1371/journal.pone.0158451.

RIVERA VILLARREYES, C. A., BARONI, G., AND OSWALD, S. E. (2011), Integral quantification of seasonal soil moisture changes in farmland by cosmic-ray neutrons, *Hydrol. Earth Syst. Sci.*, *15*(12), 3843–3859, doi:10.5194/hess-15-3843-2011.

ROBINSON, D. A., CAMPBELL, C. S., HOPMANS, J. W., HORNBUCKLE, B. K., JONES, S. B., KNIGHT, R., OGDEN, F., SELKER, J., AND WENDROTH, O. (2008), Soil Moisture Measurement for Ecological and Hydrological Watershed-Scale Observatories: A Review, *Vadose zone j.*, *7*(1), 358–389, doi:10.2136/vzj2007.0143.

ROBINSON, D. A., LEBRON, I., KOCAR, B., PHAN, K., SAMPSON, M., CROOK, N., AND FENDORF, S. (2009), Time-lapse geophysical imaging of soil moisture dynamics in tropical deltaic soils: An aid to interpreting hydrological and geochemical processes, *Water Resour. Res.*, *45*(4), doi:10.1029/2008WR006984.

RODRIGUEZ-ALVAREZ, N., BOSCH-LLUIS, X., CAMPS, A., VALL-LLOSSERA, M., VALENCIA, E., MARCHAN-HERNANDEZ, J. F., AND RAMOS-PEREZ, I. (2009), Soil Moisture Retrieval Using GNSS-R Techniques: Experimental Results Over a Bare Soil Field, *IEEE Trans. Geosci. Remote Sensing*, *47*(11), 3616–3624, doi:10.1109/TGRS.2009.2030672.

RODRIGUEZ-ITURBE, I. (2000), Ecohydrology: A hydrologic perspective of climate-soil-vegetation dynamies, *Water Resour. Res.*, *36*(1), 3–9, doi:10.1029/1999WR900210.

ROSOLEM, R., SHUTTLEWORTH, W. J., ZREDA, M., FRANZ, T. E., ZENG, X., AND KURC, S. A. (2013), The Effect of Atmospheric Water Vapor on Neutron Count in the Cosmic-Ray Soil Moisture Observing System, *Journal of Hydrometeorology*, *14*(5), 1659–1671, doi:10.1175/JHM-D-12-0120.1.

RUDOLPH, S., VAN DER KRUK, J., HEBEL, C. VON, ALI, M., HERBST, M., MONTZKA, C., PÄTZOLD, S., ROBINSON, D. A., VEREECKEN, H., AND WEIHERMÜLLER, L. (2015), Linking satellite derived LAI patterns with subsoil heterogeneity using large-scale ground-based electromagnetic induction measurements, *Geoderma*, *241-242*, 262–271, doi:10.1016/j.geoderma.2014.11.015.

SAKAKI, T., LIMSUWAT, A., SMITS, K. M., AND ILLANGASEKARE, T. H. (2008), Empirical two-point α -mixing model for calibrating the ECH 2 O EC-5 soil moisture sensor in sands, *Water Resour. Res.*, *44*(4), doi:10.1029/2008WR006870.

SALMINEN, R., BATISTA, M. J., BIDOVEC, M., DEMETRIADES, A., VIVO, B. de, VOS, W. de, DURIS, M., GILUCIS, A., GREGORAUSKIENE, V., HALAMIC, J., HEITZMANN, P., LIMA, A., JORDAN, G., KLAVER, G., KLEIN, P., LIS, J., LOCUTURA, J., MARSINA, K., MAZREKU, A., O'CONNOR, P. J., OLSSON, S., OTTESEN, R.-T., PETERSELL, V., PLANT, J. A., REEDER, S., SALPETEUR, I., SANDSTRÖM, H., SIEWERS, U., STEENFELT, A., AND TARVAINEN, T. (2005), *FOREGS Geochemical Atlas of Europe. Part 1 – Background Information and Maps.*, Geological survey of Finland Espoo.

SATO, T., AND NIITA, K. (2006), Analytical functions to predict cosmic-ray neutron spectra in the atmosphere, *Radiation research*, *166*(3), 544–555, doi:10.1667/RR0610.1.

SATO, T. (2015), Analytical Model for Estimating Terrestrial Cosmic Ray Fluxes Nearly Anytime and Anywhere in the World: Extension of PARMA/EXPACS, *PloS one*, *10*(12), e0144679, doi:10.1371/journal.pone.0144679.

SCHATTAN, P., BARONI, G., OSWALD, S. E., SCHÖBER, J., FEY, C., KORMANN, C., HUTTENLAU, M., AND ACHLEITNER, S. (2017), Continuous monitoring of snowpack dynamics in alpine terrain by aboveground neutron sensing, *Water Res*, *53*(5), 3615–3634, doi:10.1002/2016WR020234.

SCHATTAN, P., KÖHLI, M., SCHRÖN, M., BARONI, G., AND OSWALD, S. E. (2019), Sensing Area-Average Snow Water Equivalent with Cosmic-Ray Neutrons: The Influence of Fractional Snow Cover, *Water Resour. Res.*, *55*(12), 10796–10812, doi:10.1029/2019WR025647.

SCHEIFFELE, L. M., BARONI, G., FRANZ, T. E., JAKOBI, J., AND OSWALD, S. E. (2020), A profile shape correction to reduce the vertical sensitivity of cosmic-ray neutron sensing of soil moisture, *Vadose zone j.*, *19*(1), doi:10.1002/vzj2.20083.

SCHRÖN, M. (2017), Cosmic-ray neutron sensing and its applications to soil and land surface hydrology : on neutron physics, method development, and soil moisture estimation across scales.

SCHRÖN, M., KÖHLI, M., SCHEIFFELE, L., IWEMA, J., BOGENA, H. R., LV, L., MARTINI, E., BARONI, G., ROSOLEM, R., WEIMAR, J., MAI, J., CUNTZ, M., REBMANN, C., OSWALD, S. E., DIETRICH, P., SCHMIDT, U., AND ZACHARIAS, S. (2017), Improving calibration and validation of cosmic-ray neutron sensors in the light of spatial sensitivity, *Hydrol. Earth Syst. Sci.*, *21*(10), 5009–5030, doi:10.5194/hess-21-5009-2017.

SCHRÖN, M., ROSOLEM, R., KÖHLI, M., PIUSSI, L., SCHRÖTER, I., IWEMA, J., KÖGLER, S., OSWALD, S. E., WOLLSCHLÄGER, U., SAMANIEGO, L., DIETRICH, P., AND ZACHARIAS, S.

(2018a), Cosmic-ray Neutron Rover Surveys of Field Soil Moisture and the Influence of Roads, *Water Resour. Res.*, *54*(9), 6441–6459, doi:10.1029/2017WR021719.

SCHRÖN, M., ZACHARIAS, S., WOMACK, G., KÖHLI, M., DESILETS, D., OSWALD, S. E., BUMBERGER, J., MOLLENHAUER, H., KÖGLER, S., REMMLER, P., KASNER, M., DENK, A., AND DIETRICH, P. (2018b), Intercomparison of cosmic-ray neutron sensors and water balance monitoring in an urban environment, *Geosci. Instrum. Method. Data Syst.*, *7*(1), 83–99, doi:10.5194/gi-7-83-2018.

SCHRÖN, M., OSWALD, S. E., ZACHARIAS, S., KASNER, M., DIETRICH, P., AND ATTINGER, S. (2021), Neutrons on Rails: Transregional Monitoring of Soil Moisture and Snow Water Equivalent, *Geophys Res Lett*, *48*(24), doi:10.1029/2021GL093924.

SCHWINNING, S., AND SALA, O. E. (2004), Hierarchy of responses to resource pulses in arid and semi-arid ecosystems, *Oecologia*, *141*(2), 211–220, doi:10.1007/s00442-004-1520-8.

SEARS, V. F. (1992), Neutron scattering lengths and cross sections, *Neutron News*, *3*(3), 26–37, doi:10.1080/10448639208218770.

SENEVIRATNE, S. I., CORTI, T., DAVIN, E. L., HIRSCHI, M., JAEGER, E. B., LEHNER, I., ORLOWSKY, B., AND TEULING, A. J. (2010), Investigating soil moisture–climate interactions in a changing climate: A review, *Earth-Science Reviews*, *99*(3-4), 125–161, doi:10.1016/j.earscirev.2010.02.004.

SHEETS, K. R., AND HENDRICKX, J. M. H. (1995), Noninvasive Soil Water Content Measurement Using Electromagnetic Induction, *Water Resour. Res.*, *31*(10), 2401–2409, doi:10.1029/95WR01949.

SHIKLOMANOV, I. A. (1993), World fresh water resources, in *Water in Crisis: A Guide to the World's Fresh Water Resources*, edited by H. Gleick, pp. 13–24.

SIEBERT, S., DÖLL, P., HOOGEVEEN, J., FAURES, J.-M., FRENKEN, K., AND FEICK, S. (2005), Development and validation of the global map of irrigation areas, *Hydrol. Earth Syst. Sci.*, *9*(5), 535–547, doi:10.5194/hess-9-535-2005.

SIGOUIN, M. J., DYCK, M., SI, B. C., AND HU, W. (2016), Monitoring soil water content at a heterogeneous oil sand reclamation site using a cosmic-ray soil moisture probe, *Journal of Hydrology*, *543*, 510–522, doi:10.1016/j.jhydrol.2016.10.026.

SIGOUIN, M. J. P., AND SI, B. C. (2016), Calibration of a non-invasive cosmic-ray probe for wide area snow water equivalent measurement, *The Cryosphere*, *10*(3), 1181–1190, doi:10.5194/tc-10-1181-2016.

STEVANATO, L., BARONI, G., COHEN, Y., FONTANA, C. L., GATTO, S., LUNARDON, M., MARINELLO, F., MORETTO, S., AND MORSELLI, L. (2019), A Novel Cosmic-Ray Neutron Sensor for Soil Moisture Estimation over Large Areas, *Agriculture*, *9*(9), 202, doi:10.3390/agriculture9090202.

STRATI, V., ALBÉRI, M., ANCONELLI, S., BALDONCINI, M., BITTELLI, M., BOTTARDI, C., CHIARELLI, E., FABBRI, B., GUIDI, V., RAPTIS, K., SOLIMANDO, D., TOMEI, F., VILLANI, G., AND MANTOVANI, F. (2018), Modelling Soil Water Content in a Tomato Field: Proximal Gamma Ray Spectroscopy and Soil–Crop System Models, *Agriculture*, *8*(4), 60, doi:10.3390/agriculture8040060.

TIAN, Z., LI, Z., LIU, G., LI, B., AND REN, T. (2016), Soil water content determination with cosmic-ray neutron sensor: Correcting aboveground hydrogen effects with thermal/fast neutron ratio, *Journal of Hydrology*, *540*, 923–933, doi:10.1016/j.jhydrol.2016.07.004.

TOPP, G. C., DAVIS, J. L., AND ANNAN, A. P. (1980), Electromagnetic determination of soil water content: Measurements in coaxial transmission lines, *Water Resour. Res.*, *16*(3), 574–582, doi:10.1029/WR016i003p00574.

UNGER, P. W., AND JONES, O. R. (1998), Long-term tillage and cropping systems affect bulk density and penetration resistance of soil cropped to dryland wheat and grain sorghum, *Soil and Tillage Research*, *45*(1-2), 39–57, doi:10.1016/S0167-1987(97)00068-8.

UPADHYAYA, D. B., EVANS, J., MUDDU, S., TOMER, S. K., AL BITAR, A., YEGGINA, S., S, T., MORRISON, R., FRY, M., TRIPATHI, S. N., MUJUMDAR, M., GOSWAMI, M., GANESHI, N., NEMA, M. K., JAIN, S. K., ANGADI, S. S., AND YENAGI, B. S. (2021), The Indian COSMOS Network (ICON): Validating L-Band Remote Sensing and Modelled Soil Moisture Data Products, *Remote Sensing*, *13*(3), 537, doi:10.3390/rs13030537.

VATHER, T., EVERSON, C., AND FRANZ, T. E. (2019), Calibration and Validation of the Cosmic Ray Neutron Rover for Soil Water Mapping within Two South African Land Classes, *Hydrology*, *6*(3), 65, doi:10.3390/hydrology6030065.

VATHER, T., EVERSON, C. S., AND FRANZ, T. E. (2020), The Applicability of the Cosmic Ray Neutron Sensor to Simultaneously Monitor Soil Water Content and Biomass in an Acacia mearnsii Forest, *Hydrology*, *7*(3), 48, doi:10.3390/hydrology7030048.

VEREECKEN, H., HUISMAN, J. A., BOGENA, H., VANDERBORGHT, J., VRUGT, J. A., AND HOPMANS, J. W. (2008), On the value of soil moisture measurements in vadose zone hydrology: A review, *Water Resour. Res.*, *44*(4), doi:10.1029/2008WR006829.

VEREECKEN, H., HUISMAN, J. A., PACHEPSKY, Y., MONTZKA, C., VAN DER KRUK, J., BOGENA, H., WEIHERMÜLLER, L., HERBST, M., MARTINEZ, G., AND VANDERBORGHT, J.

(2014), On the spatio-temporal dynamics of soil moisture at the field scale, *Journal of Hydrology*, *516*, 76–96, doi:10.1016/j.jhydrol.2013.11.061.

VEREECKEN, H., HUISMAN, J. A., HENDRICKS FRANSSEN, H. J., BRÜGGEMANN, N., BOGENA, H. R., KOLLET, S., JAVAUX, M., VAN DER KRUK, J., AND VANDERBORGHT, J. (2015), Soil hydrology: Recent methodological advances, challenges, and perspectives, *Water Resour. Res.*, *51*(4), 2616–2633, doi:10.1002/2014WR016852.

WALSH, D. O., GRUNEWALD, E., TURNER, P., HINNELL, A., AND FERRE, P. (2011), Practical limitations and applications of short dead time surface NMR, *Near Surface Geophysics*, *9*(2), 103–113, doi:10.3997/1873-0604.2010073.

WANDERS, N., KARSSENBERG, D., ROO, A. DE, JONG, S. M. DE, AND BIERKENS, M. F. P. (2014), The suitability of remotely sensed soil moisture for improving operational flood forecasting, *Hydrol. Earth Syst. Sci.*, *18*(6), 2343–2357, doi:10.5194/hess-18-2343-2014.

WEIHERMÜLLER, L., HUISMAN, J. A., LAMBOT, S., HERBST, M., AND VEREECKEN, H. (2007), Mapping the spatial variation of soil water content at the field scale with different ground penetrating radar techniques, *Journal of Hydrology*, *340*(3-4), 205–216, doi:10.1016/j.jhydrol.2007.04.013.

WEIMAR, J., KÖHLI, M., BUDACH, C., AND SCHMIDT, U. (2020), Large-Scale Boron-Lined Neutron Detection Systems as a 3He Alternative for Cosmic Ray Neutron Sensing, *Front. Water*, *2*, doi:10.3389/frwa.2020.00016.

WEITZ, A. M., GRAUEL, W. T., KELLER, M., AND VELDKAMP, E. (1997), Calibration of time domain reflectometry technique using undisturbed soil samples from humid tropical soils of volcanic origin, *Water Resour. Res.*, *33*(6), 1241–1249, doi:10.1029/96WR03956.

WESTERN, A. W., GRAYSON, R. B., AND BLÖSCHL, G. (2002), Scaling of Soil Moisture: A Hydrologic Perspective, *Annu. Rev. Earth Planet. Sci.*, *30*(1), 149–180, doi:10.1146/annurev.earth.30.091201.140434.

WESTERN, A. W., ZHOU, S.-L., GRAYSON, R. B., MCMAHON, T. A., BLÖSCHL, G., AND WILSON, D. J. (2004), Spatial correlation of soil moisture in small catchments and its relationship to dominant spatial hydrological processes, *Journal of Hydrology*, *286*(1-4), 113–134, doi:10.1016/j.jhydrol.2003.09.014.

WOLF, B., CHWALA, C., FERSCH, B., GARVELMANN, J., JUNKERMANN, W., ZEEMAN, M. J., ANGERER, A., ADLER, B., BECK, C., BROSY, C., BRUGGER, P., EMEIS, S., DANNENMANN, M., ROO, F. DE, DIAZ-PINES, E., HAAS, E., HAGEN, M., HAJNSEK, I., JACOBEIT, J.,

JAGDHUBER, T., KALTHOFF, N., KIESE, R., KUNSTMANN, H., KOSAK, O., KRIEG, R., MALCHOW, C., MAUDER, M., MERZ, R., NOTARNICOLA, C., PHILIPP, A., REIF, W., REINEKE, S., RÖDIGER, T., RUEHR, N., SCHÄFER, K., SCHRÖN, M., SENATORE, A., SHUPE, H., VÖLKSCH, I., WANNINGER, C., ZACHARIAS, S., AND SCHMID, H. P. (2017), The SCALEX Campaign: Scale-Crossing Land Surface and Boundary Layer Processes in the TERENO-preAlpine Observatory, *Bulletin of the American Meteorological Society*, *98*(6), 1217–1234, doi:10.1175/BAMS-D-15-00277.1.

WU, K., RODRIGUEZ, G. A., ZAJC, M., JACQUEMIN, E., CLÉMENT, M., COSTER, A. DE, AND LAMBOT, S. (2019), A new drone-borne GPR for soil moisture mapping, *Remote Sensing of Environment*, *235*, 111456, doi:10.1016/j.rse.2019.111456.

ZACHARIAS, S., BOGENA, H., SAMANIEGO, L., MAUDER, M., FUß, R., PÜTZ, T., FRENZEL, M., SCHWANK, M., BAESSLER, C., BUTTERBACH-BAHL, K., BENS, O., BORG, E., BRAUER, A., DIETRICH, P., HAJNSEK, I., HELLE, G., KIESE, R., KUNSTMANN, H., KLOTZ, S., MUNCH, J. C., PAPEN, H., PRIESACK, E., SCHMID, H. P., STEINBRECHER, R., ROSENBAUM, U., TEUTSCH, G., AND VEREECKEN, H. (2011), A Network of Terrestrial Environmental Observatories in Germany, *Vadose Zone Journal*, *10*(3), 955–973, doi:10.2136/vzj2010.0139.

ZEHE, E., AND BLÖSCHL, G. (2004), Predictability of hydrologic response at the plot and catchment scales: Role of initial conditions, *Water Resour. Res.*, *40*(10), doi:10.1029/2003WR002869.

ZINK, M., SAMANIEGO, L., KUMAR, R., THOBER, S., MAI, J., SCHÄFER, D., AND MARX, A. (2016), The German drought monitor, *Environ. Res. Lett.*, *11*(7), 74002, doi:10.1088/1748-9326/11/7/074002.

ZREDA, M., DESILETS, D., FERRÉ, T. P. A., AND SCOTT, R. L. (2008), Measuring soil moisture content non-invasively at intermediate spatial scale using cosmic-ray neutrons, *Geophys. Res. Lett.*, *35*(21), doi:10.1029/2008GL035655.

ZREDA, M., SHUTTLEWORTH, W. J., ZENG, X., ZWECK, C., DESILETS, D., FRANZ, T., AND ROSOLEM, R. (2012), COSMOS: the COsmic-ray Soil Moisture Observing System, *Hydrol. Earth Syst. Sci.*, *16*(11), 4079–4099, doi:10.5194/hess-16-4079-2012.

ZWECK, C., ZREDA, M., AND DESILETS, D. (2013), Snow shielding factors for cosmogenic nuclide dating inferred from Monte Carlo neutron transport simulations, *Earth and Planetary Science Letters*, *379*, 64–71, doi:10.1016/j.epsl.2013.07.023.

Acknowledgements

General acknowledgments

First of all, I would like to thank my supervisors at Forschungszentrum Jülich, PD Dr. Heye Bogena and Prof. Dr. Johan Alexander “Sander” Huisman, for their continuous support in all phases of my academic development since the beginning of my work at IBG-3. I am grateful for all the opportunities you have given me and for the confidence you had in me. Most importantly you taught me what science is: think through and connect the dots – also a lecture for life. It was always a pleasure to work with you!

Bernd Schilling, Daniel Dolfus, and Ansgar Weuthen are thanked for always finding a quick solution and for the numerous hours spent on installations or rover surveys in the field. Dr.-Ing. Cosimo Brogi, Dr. Patrizia Ney, and Prof. Dr. Harry Vereecken are thanked for practical and intellectual support, fruitful discussions and the opening of new perspectives. Yasemin Bas, Justus Fiedler, and Manuel Schmidt are thanked for being patient with me as a supervisor. I would also like to thank numerous academic and non-academic (ex-)colleagues at IBG-3 who supported me during the work on this dissertation with ideas, skills, help for labor intensive work, institutes management, a nice talk, or an open ear for my problems: Nicole Adels, Dr. Roland Baatz, Prof. Dr. Nicolas Brüggemann, Ferdinand Engels, Odilia Esser, Hannah Fuchs, Nikhil Goodhechoore, Dr. Alexander Graf, Dr. Jannis Groh, Horst Hardelauf, Dipl.-Ing. Rainer Harms, Prof. Dr. Harrie-Jan Hendricks-Franssen, Dr. Michael Herbst, Dipl.-Ing. Normen Hermes, Dr. Frank Herrmann, Tobias Korf, Dipl.-Ing. Werner Küpper, Judith Mattes, David Mengen, Philipp Meulendick, Dr. Carsten Montzka, Prof. Dr. Youri Rothfuss, Marion Schlösser, Marius Schmidt, Sandy Schnober, Thomas Schuster, Lukas Strebel, Prof. Dr. Jan Vanderborght, Dr. Kathrin Vermöhlen, Claudia Walraf, and PD Dr. Lutz Weihermüller.

In addition, I would like to thank the members of the CosmicSense research group for critical questions and the opportunity to work in a stimulating team of cosmic ray neutron sensing enthusiasts. A special thanks goes to Dr. Martin Schrön and Dr. Markus Köhli, who always pushed me to my limits and found the right words in the right moments. I also want to thank my PhD colleagues form the CosmicSense team Veronika Döpper, Mandy Kasner, Daniel Rasche, Lena Scheiffele, and Jannis Weimar for clever ideas and for showing me that my problems are not unique. Furthermore, Sandra Sculz-Seyfried and Prof. Dr. Sascha

Oswald are thanked for the organization of the group and the mercator fellow Prof. Dr. Marek Zreda is thanked for valuable insights into neutron theory and fruitful discussions.

Prof. Dr. Julian Klaus is thanked for supporting my dissertation as second assessor and Prof. Dr. Andreas Kemna and Prof. Dr.-Ing. Jürgen Kusche are thanked for evaluating my dissertation as members of the PhD committee. Prof. Dr. Mariele Evers is thanked for being my interim second assessor and Prof. Dr. Bernd Diekkrüger is thanked for setting up my initial contact to Heye.

Last but not least I would like to thank my family and friends for enduring me. Mama, Papa, Oma, Pulheimer, Mehlbacher, Opa und Bonner – danke, Ihr seid die Besten! Danke Fred, Malu und Lina für besondere Geduld, Unterstützung und Freude. Ihr seid mindestens genauso viel die Besten! …50!

Specific acknowledgements for the Chapters 2 - 5 and Appendix V

Chapter 2

We thank Jingnuo Dong and Tyson Ochsner for making their dataset publicly available and for updating it for this work. Carsten Montzka, Bernd Schilling, Daniel Dolfus, and Ansgar Weuthen are thanked for supporting the reference measurements at the Selhausen test site and Benjamin Fersch is thanked for the organization of the measurement campaign at the Fendt test site. Furthermore, we thank the two reviewers for their constructive feedback and suggestions. This research was funded by the Deutsche Forschungsgemeinschaft (DFG, German Research Foundation)—project 357874777 of the research unit FOR 2694 Cosmic Sense. It also received supported from the MOSES (Modular Observation Solutions for Earth Systems) project funded by the Helmholtz-Gemeinschaft, which provided funding for the Jülich CRN rover. We also acknowledge the NMDB database funded by EU-FP7.

Chapter 3

We thank Jannis Weimar, Marek Zreda, and Martin Schrön for fruitful discussions. Furthermore, we thank David Bormann, one anonymous reviewer and the editor Harihar Rajaram for their constructive feedback and suggestions. The positions of Jannis Jakobi, Markus Köhli, and Daniel Rasche were funded by the Deutsche Forschungsgemeinschaft (DFG, German Research Foundation), project 357874777 of the research unit FOR 2694 Cosmic Sense. We also received support from the MOSES (Modular Observation Solutions for Earth Systems) project funded by the Helmholtz-Gemeinschaft, which allowed acquiring the Jülich CRN rover. We also acknowledge the NMDB database funded by EU-FP7. The rover data sets used in this study can be accessed through the TERENO (Terrestrial Environmental Observatories) Geoportal at https://doi.org/10.34731/1dg7-3x98%20.

Chapter 4

We thank Daniel Dolfus, Bernd Schilling, Ansgar Weuthen, Nicole Adels, Philip Pohlig, Yasemin Bas, and Odilia Esser for the technical support, the help during installations and the support with labor-intensive tasks such as soil and biomass measurements and sample processing. The position of Jannis Jakobi was funded by the Deutsche Forschungsgemeinschaft (DFG, German Research Foundation), project 357874777 of the research unit FOR 2694 Cosmic Sense. We also received support from SFB-TR32 Patterns

in Soil-Vegetation-Atmosphere Systems: Monitoring, Modelling and Data Assimilation funded by the Deutsche Forschungsgemeinschaft (DFG) and TERENO (TERrestrial Environmental Observatories) funded by the Helmholtz-Gemeinschaft. We also acknowledge the NMDB database funded by EU-FP7.

Chapter 5.2.1

Marius Schmidt, Daniel Dolfus, Nils Becker, Odilia Esser, Dr. Alexander Graf, Judith Mattes, Nicole Adels, Hannah Fuchs, and Martina Kettler are thanked for the plant height measurements. In addition, TERENO (TERrestrial Environmental Observatories) funded by the Helmholtz-Gemeinschaft and the NMDB database funded by EU-FP7 are acknowledged for the CRNS and neutron monitor data, respectively.

Chapter 5.2.2

The MOSES (Modular Observation Solutions for Earth Systems) project funded by the Helmholtz-Gemeinschaft is thanked for financing of the Jülich CRN rover. Furthemore, TERENO (TERrestrial Environmental Observatories) funded by the Helmholtz-Gemeinschaft and the NMDB database funded by EU-FP7 are acknowledged for the stationary CRNS data and neutron monitor data, respectively.

Appendix V

This research was funded by the Deutsche Forschungsgemeinschaft (DFG, German Research Foundation) – project 357874777 of the research unit FOR 2694 "Cosmic Sense". We also acknowledge the NMDB database funded by EU-FP7. We thank Jingnuo Dong and Tyson Ochsner for making their dataset publicly available and for updating it for this work.

Publications

First author peer reviewed journal publications

JAKOBI, J., HUISMAN, J. A., VEREECKEN, H., DIEKKRÜGER, B., AND BOGENA, H. R. (2018), Cosmic ray neutron sensing for simultaneous soil water content and biomass quantification in drought conditions, *Water Resour. Res.*, *54*(10), 7383-7402, doi: 10.1029/2018WR022692.

JAKOBI, J., HUISMAN, J. A., SCHRÖN, M., FIEDLER, J., BROGI, C., VEREECKEN, H., AND BOGENA, H. R. (2020), Error estimation for soil moisture measurements with cosmic ray neutron sensing and implications for rover surveys. *Front. water*, 2:10, doi: 10.3389/frwa.2020.00010.

JAKOBI, J., HUISMAN, J. A., AND BOGENA, H. R. (2020), Comment on Dong and Ochsner (2018):"Soil Texture Often Exerts Stronger Influence Than Precipitation on Mesoscale Soil Moisture Patterns". *Water Resources Research*, *57*(1), doi: 10.1029/2020WR027790.

JAKOBI, J., HUISMAN, J. A., KÖHLI, M., RASCHE, D., VEREECKEN, H., & BOGENA, H. R. (2021), The footprint characteristics of cosmic ray thermal neutrons, *Geophys. Res. Let.*, *48*(15), doi: 10.1029/2021GL094281.

First author conference contributions

JAKOBI, J., HUISMAN, J. A., VEREECKEN, H. AND BOGENA, H. R., (2018), Cosmic-ray neutron probes used for simultaneous soil moisture and biomass estimation. Poster presentation, TERENO Internal Conference 2018, Berlin.

JAKOBI, J., HUISMAN, J. A., SCHRÖN, M., ZACHARIAS, S. AND BOGENA, H. R. (2019), Simultaneous measurement of soil moisture and biomass pattern with a CRNS rover, Poster presentation, EGU General Assembly 2019, Vienna.

JAKOBI, J., HUISMAN, J. A., SCHRÖN, M., FIEDLER, J., BROGI, C., VEREECKEN, H., AND BOGENA, H. R. (2020), Error estimation for soil moisture measurements with cosmic-ray neutron sensing and implications for rover surveys, Poster presentation, EGU General Assembly 2020, Vienna.

JAKOBI, J., HUISMAN, J. A., SCHRÖN, M., FIEDLER, J., BROGI, C., VEREECKEN, H., AND BOGENA, H. R. (2020), Error estimation for soil moisture measurements with cosmic-ray neutron sensing and implications for rover surveys, Oral presentation, 6th international COSMOS workshop 2020, Heidelberg.

(Co-)supervisions

Bas, Y. (2018), Bachelor student, 3 month internship.

Fiedler, J. (2019), Master student, preparing master thesis: "Soil Moisture Estimation with a Cosmic-Ray Neutron Sensing Rover".

Schmidt, M. (2021), Master student, preparing master thesis: "Biomassebestimmung im Wüstebachtal / Hocheifel mittels allometrischer Funktionen und direkter Messungen".

Band / Volume 566
Cirrus clouds in the extratropical tropopause and lowermost stratosphere region
I. Bartolomé García (2022), iii, 155 pp
ISBN: 978-3-95806-610-6

Band / Volume 567
Stationary and Transient Behaviour of Polymer Electrolyte Fuel Cells
Y. Shi (2022), viii, 172 pp
ISBN: 978-3-95806-611-3

Band / Volume 568
14th Carolus Magnus Summer School on Plasma and Fusion Energy Physics
D. Reiser (Ed.), (2022), 207 pp
ISBN: 978-3-95806-613-7

Band / Volume 569
Spectral induced polarization of calcite precipitation in porous media
S. Izumoto (2022), xviii, 106 pp
ISBN: 978-3-95806-614-4

Band / Volume 570
Technische und ökonomische Bewertung der Polymer-Elektrolyt-Membran Elektrolyse
S. M. Saba (2022), IV, 263 pp
ISBN: 978-3-95806-615-1

Band / Volume 571
Advanced Sintering of Garnet-Based Ceramic Composite Cathodes for All-Solid-State Lithium Batteries
M. Ihrig (2022), VIII, 160 pp
ISBN: 978-3-95806-616-8

Band / Volume 572
Developing an integrated value-based institutional framework for analyzing nexus governance challenges – the case study of Germany
C. Märker (2022), 290 pp
ISBN: 978-3-95806-617-5

Band / Volume 573
Ecological sanitation via thermophilic co-composting of humanure and biochar as an approach to climate-smart agriculture
D. Castro Herrera (2022), XVIII, 127 pp
ISBN: 978-3-95806-622-9

Band / Volume 574
Towards 3D crosshole GPR full-waveform inversion
A. Mozaffari (2022), viii, 122 pp
ISBN: 978-3-95806-623-6

Band / Volume 575
Investigations of the atmospheric OH, HO2 and RO2 radical chemical budgets and their impact on tropospheric ozone formation in a rural area in West-Germany in the JULIAC 2019 campaign
C. Cho (2022), 182 pp
ISBN: 978-3-95806-625-0

Band / Volume 576
Thermochemische Beständigkeit von Carbonat-Keramik-Membranen für die CO_2-Abtrennung in Wassergas-Shift-Reaktoren
U. Gude (2022), X, 176, LXIII pp
ISBN: 978-3-95806-626-7

Band / Volume 577
Neue Ziele auf alten Wegen?
Strategien für eine treibhausgasneutrale Energieversorgung bis zum Jahr 2045
D. Stolten, P. Markewitz, T. Schöb, F. Kullmann, S. Risch, T. Groß, M. Hoffmann, D. Franzmann, T. Triesch, S. Kraus, R. Maier, B. Gillessen, H. Heinrichs, N. Pflugradt, T. Grube, J. Linssen, L. Kotzur (2022), VI, 81 pp
ISBN: 978-3-95806-627-4

Band / Volume 578
Improving stationary and mobile cosmic ray neutron soil moisture measurements
Assessment of the cosmic ray neutron uncertainty and the potential of the thermal neutron signal
J. C. Jakobi (2022), xxiii, 137 pp
ISBN: 978-3-95806-628-1

Energie & Umwelt / Energy & Environment
Band / Volume 578
ISBN 978-3-95806-628-1

Mitglied der Helmholtz-Gemeinschaft

JÜLICH
Forschungszentrum